STATIC AND MODAL ANALYSES OF LAMINATED COMPOSITE PLATES USING HIERARCHICAL FINITE ELEMENT METHOD

Karun Nayyar

A Thesis

in

The Department

Of

Mechanical and Industrial Engineering

Presented in Partial Fulfillment of the Requirements

for the Degree of Master of Applied Science at

Concordia University

Montreal, Quebec, Canada

March 2006

Your file Votre référence
ISBN: 978-0-494-16253-8
Our file Notre référence
ISBN: 978-0-494-16253-8

ABSTRACT

Static and Modal Analyses of Laminated Composite Plates using Hierarchical Finite Element Method

Karun Nayyar

Composite materials are widely being used in aircraft, automotive and robotic industries where the components under different loading conditions are subject to motion. There is a need for the accurate prediction of not only their static response but also their dynamic characteristics so that they can be designed against the failure due to various types of possible static and dynamic loads.

In the present thesis, static and vibration analyses of laminated plates are conducted using conventional and hierarchical finite element formulations based on First-order Shear Deformation Theory (FSDT). Conventional finite element formulation requires a large number of elements to obtain acceptable results. Besides, the necessity to satisfy internal C_0 or C_1 continuity across the elements' interfaces creates complexity even in simple structures. In order to overcome these limitations, the formulation based on Hierarchical Finite Element Method (HFEM) is developed in the present thesis for static and vibration analyses of laminated composite plates based on first-order shear deformation theory. Conventional finite element formulation is also developed based on FSDT. The developed formulations are applied to the analysis of various types of

laminated composite plates. The results are compared and the efficiency and accuracy of HFEM over conventional finite element method is explained. The efficiency and accuracy of the developed formulation is also established in comparison with approximate solutions based on Ritz method which are also developed for the cases under study. A detailed parametric study has been conducted on various types of laminated composite plates, all made of NCT-301 graphite/epoxy, in order to investigate the effects of boundary conditions, laminate configuration, aspect ratio values and elastic modulus to shear modulus (E/G) ratio.

ACKNOWLEDGMENTS

I would like to express my sincere gratitude to my supervisor, Dr. Rajamohan Ganesan for his invaluable guidance and financial support during my research at Concordia University. I would also like to thank my colleagues: Lin Chen, Daiying Liu and Wasim Arshad for their valuable discussions.

Here, I would also like to thank my parents, my sister and my brother-in-law without their support and encouragement this work would not have been possible.

CONTENTS

List of Figures

List of Tables

Nomenclature

w	Displacement in thickness direction
a	Length of the laminate
b	Width of the laminate
t	Time variable
u_o	Mid-plane displacement in x-direction
v_o	Mid-plane displacement in y-direction
σ_x	Stress in x-direction
ε_x	Strain in x-direction
σ_z	Stress in thickness direction
h	Thickness of the laminate
E	Modulus of elasticity
ρ_s	Translational inertia coefficient.
I	Rotary inertia coefficient
M_x	Bending moment per unit width
N_x	Axial force per unit width
A_{ij}	Coefficients of stretching stiffness matrix of composite beam

B_{ij} Coefficients of bending-stretching coupling matrix of composite beam

D_{ij} Coefficients of bending stiffness matrix of composite beam

k Shear correction factor

K_{ij}^{e} Coefficients of the element stiffness matrix

M_{ij}^{e} Coefficients of the element mass matrix

F_{i}^{e} Coefficients of the force vector

$[K]$ Stiffness matrix

$[M]$ Mass matrix

N_i Shape functions corresponding to i^{th} node of the finite element.

u_{0i} Mid-plane displacement in x-direction of the i^{th} node

$\hat{u}$ Generalized displacement variable containing nodal and hierarchical displacements

a_j Hierarchical displacement variable

R Aspect Ratio

λ Eigenvalue associated with the free vibration problem

κ_x Curvature of the beam in x-direction

ε_x^o Strain in x-direction of the reference point

U_0 Amplitude of vibrations in x-direction

G_{23} Out-of-plane shear modulus

G_{12} In-plane shear modulus

$\{d\}$ Matrix of nodal displacements

$[\ ]^{-1}$ Inverse of the matrix

$[\ ]^T$ Transpose of matrix

$N_{1,x}$ Derivative of shape function ' N_1 ' with respect to x

ν Poisson's ratio

E_1 Modulus of elasticity in fiber direction

E_2 Modulus of elasticity in transverse direction

$\bullet$ Differentiation with respect to time

ω Natural frequency of the laminate

ω_1 Lowest natural frequency of the laminate

Chapter 1

INTRODUCTION

1.1 Static and Modal Analysis in Mechanical Design

Linear static analysis allows engineers to test different load conditions and their resulting stresses and deformation. Knowing how a design will perform under different conditions allows engineers to make changes prior to physical prototyping, thus saving both time and money. Apart from static analysis, vibration analysis is also a critical component of design. Any physical system can vibrate. The frequencies at which vibration naturally occurs and the mode shapes which the vibrating system assumes are the properties of the system. An analyst must know these properties of the system in order to design it against the failure due to vibrations.

Inherent vibration modes in structural components or mechanical systems can shorten the equipment life and cause premature or completely unanticipated failure, often resulting in hazardous situations. Resonances are determined by the material properties (such as mass, stiffness, damping) and boundary conditions of the structure. If either the material properties or the boundary conditions of a structure change, its modes will

change. Modes are used as a simple and efficient means of characterizing resonant vibration, which makes a structure to vibrate with excessive, sustained oscillatory motion. Resonant vibration is caused by an interaction between the inertial and elastic properties of the material within the structure.

Detailed modal analysis determines the fundamental vibration mode shapes and corresponding frequencies. This can be relatively simple for the basic components of a simple system, and extremely complicated when qualifying a complex mechanical device or structure exposed to periodic loading. These systems require accurate determination of natural frequencies and mode shapes using techniques such as Finite Element Analysis.

1.2 Composite Materials and Structures in Mechanical Design

Over the last three decades, composites have found increasing application in engineering structures and in manufacturing industry. Broadly speaking, the word 'composites' means made of two or more different materials or phases. Each constituent material or phase has significantly different macroscopic behavior and a distinct interface exists between the constituent materials. Generally a composite material is a combination of two components of which one serves as the matrix and the other as fibers. Individual fiber is usually stiffer and stronger than the matrix. The fibers are the main load carrying agents and the matrix acts as a protecting agent and provides a means to distribute the load. The fibers and matrix are blended together under controlled temperature and pressure to give a new material called composite, with properties and performance

characteristics better than the constituent materials. Unlike isotropic materials, the most important aspect of composite materials is that composites can be optimized for strength, stiffness, fatigue, and heat and moisture resistance by changing the orientation of fibers. Composite materials have much higher strength to weight ratio than the conventional materials. The structural elements such as bars, beams and plates are made of stacking together many plies of fiber reinforced layers in different angles to achieve the desired properties. Currently thick laminates made of orthotropic layers find extensive application in fabricated plate and shell structures.

1.3 Finite Element Method in Mechanical Design

In the field of engineering design we come across many complex problems, the mathematical formulation of which is tedious and usually not possible to solve by analytical methods. The governing equations of motion are generally nonlinear partial differential equations, which are extremely difficult to solve in the closed form. At such instants we resort to the use of numerical techniques. The availability and sophistication of modern digital computers has made possible the extensive use of the finite element method for analyzing complex structures. Finite Element Method (FEM) is one of the most powerful numerical analysis tools in the engineering and physical sciences. The basic concept is that a body or structure may be divided into smaller elements of finite dimensions called as "Finite Elements". The original body or structure is then considered as an assemblage of these elements connected at a finite number of joints called as

"Nodes" or "Nodal Points". The properties of the elements are formulated and combined to obtain the properties of the entire body.

The equations of equilibrium for the entire structure or body are then obtained by combining the equilibrium equation of each element such that the continuity is ensured at each node. The necessary boundary conditions are then imposed and the equations of equilibrium are then solved to obtain the required variables such as Stress, Strain, Temperature Distribution or Velocity Flow depending on the application. Thus instead of solving the problem for the entire structure or body in one operation, in FEM attention is mainly devoted to the formulation of properties of the constituent elements. A common procedure is adopted for combining the elements, solution of equations and evaluation of the required variables in various disciplines of engineering. Further advancements in Finite element methodology have been made and Hierarchical Finite element Method (HFEM) has been developed. The HFEM provides us with critical advantages of using fewer elements and obtaining better accuracy in the calculation of natural frequencies, displacements and stresses of the component under study.

1.4 Literature Survey

In the following subsections, a comprehensive literature survey is presented on the free vibration analysis of laminated composite plates using higher order shear deformation theories and finite element methods. Important works done on the dynamic analysis of composite plates by analytical, experimental and finite element methodologies

have been chronicled. After a brief history of the hierarchical finite element method, works on the HFEM analysis of plates have been presented.

1.4.1 Dynamic Analysis of Composite Plates

A lot of attention has been given and extensive study has been done on linear dynamic behavior of isotropic rectangular plates. Leissa [3] gave accurate and comprehensive results for free vibrations of rectangular plates. Further improvements in the accuracy of solution and reduction in computational efforts has been done by works of Dickinson and Di Blasio [4], Bhat [5] and Liew et al [6]. All these authors used Rayleigh-Ritz discretization procedure with different choices of admissible displacements functions. On the dynamic behavior of composite laminated plates, most of the works have been published on the free vibration analysis. Lin and King [7] used classical laminated plate theory to compute the natural frequencies of un-symmetrically laminated rectangular plates.

The classical laminate theory which is an extension of classical plate theory to laminated plates ignores transverse stress components and models the plate as an equivalent single layer system. Transverse shear deformation and transverse normal stress are ignored in classical plate theory. Reissner [8] and Mindlin [9] improved the classical theory by including transverse shear deformations and rotary inertia effects.

In thick laminated systems, the components of stress and strain that are transverse to the plane of the laminate strongly influence the behavior. Thus the classical

laminate theory, which essentially ignores the effect of individual lamina across the thickness of the plate or shell, does not account for the effect of these stress and strain components. A number of shear deformation theories have been proposed till date. For laminated isotropic plates, such a theory was first proposed by Stavsky [10] and later generalized to laminated anisotropic plates by Yang, Norris and Stavsky [11].The Yang-Norris-Stavsky (YNS) theory was adequate for predicting the flexural vibration response of laminated anisotropic plates in the first few modes.

Ambartsumyan [12] developed a rather difficult approach to define transverse shear stresses that satisfy the required continuity conditions at the layer interfaces. This bending theory is limited to laminates consisting of orthotropic layers stacked symmetrically with respect to the mid-plane of the plate and having the axes of material symmetry coinciding with the plate co-ordinates axes. Yang et al [11] extended Mindlin's theory [9] for homogenous isotropic plates to thick laminates consisting of an arbitrary number of bonded anisotropic layers. The approach of Yang et al [11] was used by Whitney and Pagano [13] .Whitney [14] later concluded that the introduction of shear deformations can not improve the in-plane stress distributions as determined from classical plate theory. In the quest to obtain more accurate prediction of the behavior of composite plates, Lo et al [15] [16] and Kant et al [17] have proposed higher order theories in which the displacement assumptions are expressed in terms of a power series in the thickness variable. Whitney and Sun [18] and Nelson and Lorch [19] introduced quadratic variations and Lo et al [20] introduced cubic variations of in-plane displacements through the plate thickness. Reddy [21] obtained even higher order

variations by imposing the condition of vanishing transverse shear strains on the top and bottom surface of the plate. Higher order plate theory derived by Whitney and Sun was applied by Pagano [22] in the case of free edge boundary value problems with a plane of symmetry. Another class of approximate laminate theory was put forward by Srinivas [23] in which the number of field equations and boundary conditions do not depend upon the number of layers. Theoretical solutions of three dimensional elasticity theory were developed for the prediction of inter laminar stresses by Pagano [24] and Srinivas and Rao [25].These solutions were restricted to the special case of cross-ply laminates subjected to uniformity distributed loading and simply supported boundary conditions.

1.4.2 Hierarchical Finite Element Method (HFEM)

The idea of finite element method is to divide the domain of interest into smaller sub-domains called finite elements. The finite element method in general is a special case of Rayleigh-Ritz method, with the main difference between the two being the choice of interpolation functions used in the series representation of the solution. There are various procedures for the refinement of the finite element solutions. Broadly these fall into two categories. The first and most common procedure involves refining the mesh while keeping the degree of the polynomial approximation fixed. This is termed as h-version of the finite element method or simply finite element method. The second method involves keeping the mesh size constant and letting the degree of the approximating polynomial to tend to infinity [27], [28]. This approach is known as p-version of the finite element method or the Hierarchical Finite Element Method (HFEM).Though HFEM has much in common with the classical Rayleigh-Ritz method but the use of local

approximating displacement functions in HFEM results in greater versatility and improved rates of convergence.

While considerable effort has been made in the finite element vibration analysis of isotropic plates, only limited work has been done in the field of laminated anisotropic plates. Exploiting the symmetries exhibited by anisotropic plates, Noor and Mathers [29], [30] studied the effects of shear deformation and anisotropy on the accuracy and convergence of several shear-flexible displacement finite element models. The analysis was limited to symmetrically laminated cross-ply plates.

Hierarchical functions were initially introduced by Zienkiewicz et al [31]. Initial applications of HFEM were in the analysis of nuclear reactor vessels. [32]. After that, new and useful families of p-type elements were introduced by Peano [33] and Szabo et al [34], [35]. Adaptive refinements in the HFEM was put forward by Zienkiewicz et al [36]. Babuska et al [27] describes the mathematical aspect of the convergence of the finite element solution for the p-refinement. Szabo [37] showed that the uniform p-refinement allows the global energy norm error to be approximately extrapolated by three consecutive solutions. Kelly et al [38] and Gago et al [39] who initiated non-uniform p-refinement also dealt with error analysis and adaptive processes applied to finite element calculations.

The applications of HFEM at the commercial level took long time before its merits were recognized. Polynomial functions are more common in the finite element

analysis. With regards to HFEM, Legendre polynomials in the Rodrigues form are most popular. They have been applied to linear dynamic analysis of the plates using thin plate theory in references [40], [41] and to non-linear dynamic analysis of beams and plates in the frequency domain in references [42], [43].It has been shown that convergence is achieved with far fewer degrees of freedom in the HFEM than that in the h-version of the FEM. Bardell [44] used HFEM to determine the natural frequencies and modes of flat rectangular isotropic plates. Bardell et al [45] applied h-p method to study the linear vibrations of shells. Han et al [46] have extended Bardell's [41] model of HFEM for free vibration analysis of plates, to geometrically non-linear static analysis of symmetrically laminated rectangular plates.

1.5 Objectives of the Thesis

The objectives of the present thesis are, (1) to develop and apply the hierarchical finite element formulation based on First-order Shear Deformation Theory (FSDT) to static and modal analyses of laminated composite plates; (2) to show the superiority of the HFEM over conventional FEM by comparing the results from both the formulations for different laminates under various boundary conditions; and, (3) to conduct a detailed parametric study of laminated composite plates considering different laminate configurations, aspect ratios and E/G ratios.

Hierarchical finite element formulations are developed using polynomial functions. The developed methodology not only provides more accurate and better

convergence, but also, uses less number of elements as compared to the conventional FEM. Use of lesser number of elements results in lesser discontinuities in stress and strain distribution across element interfaces. Simple structures like rectangular plates can be analyzed using only one Hierarchical element thus completely eliminating the time and the cost involved in the meshing.

1.6 Layout of the Thesis

The present chapter is the first chapter and it provided a brief introduction and literature survey on static and dynamic analysis of rectangular isotropic and anisotropic plates using conventional and Hierarchical FEM. In chapter 2, the hierarchical finite element formulation is developed and applied to static analysis of laminated composite plates. Ritz method based on first order shear deformation theory is developed. Results are compared with conventional FEM and solutions available from various references.

In chapter 3, the hierarchical finite element formulation is developed and applied to modal analysis of laminated composite plates. Results are compared with conventional FEM based on first order shear deformation theory, and with Ritz method. In chapter 4, a detailed parametric study is performed which includes the effect of laminate configurations, boundary conditions, aspect ratio and E/G ratio on static deflection and natural frequencies of laminated composite plates. Chapter 5 brings the thesis to its end by providing the overall conclusions of the present work and recommendations for the future work.

Chapter 2

Static Analysis of Laminated Plates using Hierarchical Finite Element Formulation

2.1 Introduction

Engineering structures are generally designed on the basis of stress sustaining capacity of the structural components. Since weight is a crucial factor in the design of structures, the use of conventional isotropic material gives very little room for weight savings. Composite materials on the other hand have high strength to weight ratio and stiffness to weight ratio. Unlike the isotropic materials, the properties of composite materials can be tailored to have very high strength and yet being very light. A certain number of laminae with different fiber orientations are bonded together under a controlled environment with required heat and pressure to obtain a composite laminate with desired thickness and stiffness. The orientations of the fibers also depend upon the type of loadings the laminate undergoes. We can place fibers oriented perpendicular to each other for a laminate which is subjected to transverse loads and a laminate subjected to shear and tension may need fibers oriented at 45 degrees to resist the shear load and 0 and/or 90 degrees to resist the tensile load. Composite materials are being widely used in aircraft, automotive and robotic industries where the parts under different loading

conditions are subject to motion. There is therefore a need for the accurate prediction of not only their static but also their dynamic characteristics so that we can design them against the failure due to various types of possible static and dynamic loads.

In this chapter the static analysis of laminated plates is conducted using conventional and hierarchical finite element formulations based on First-order Shear Deformation Theory (FSDT). Section 2.2 discusses the plate theory employed and states the advantage of using the First-order Shear Deformation Theory over Classical Laminated Theory for the plate under study. In Section 2.4, Ritz solution for specially orthotropic plate has been provided. In Section 2.5, the finite element formulation for uniform laminated composite plates has been developed using FSDT. In Section 2.6, the formulation using the Hierarchical Finite Element Method (HFEM) is developed. The chapter ends with the comparison of results from conventional and hierarchical finite element formulations and summarizes the advantages of using HFEM over conventional finite element formulation for static analysis of laminated composite plates.

2.2 Plate Theory

When the thickness of the laminate is small as compared to the planar dimensions, laminate theories based on equivalent two-dimensional descriptions are used to analyze laminated composite structures. These two-dimensional theories, called as equivalent single layer theories are obtained from three dimensional elasticity theories. Some assumptions about the variations of displacements and stresses through the

thickness of laminate are made. Many theories with different assumptions have been developed over the years to accurately predict the response of laminated composite plates. The earliest plate theory suggested for the plates was the Kirchhoff plate theory or Classical Plate Theory (CPT). In this theory the normal of the plane is assumed to be straight and normal in the deformed configuration. The theory was extended to laminated plates and called as Classical Laminated Plate Theory (CLPT). The CLPT can be applied to a fine degree of accuracy to analyze the laminates whose thickness is small by two orders of magnitude as compared to the planar dimensions. Such an assumption neglects the transverse shear effects, which have significant impact on the behavior of laminated composite plates. This limits the usage of the theory for only thin laminates.

Since there are many structural applications using thick laminated composite plates with very high elasticity modulus to shear modulus ratios and are susceptible to thickness failures, the CLPT becomes inadequate. Although the transverse shear and normal stresses are an order of magnitude smaller than the in-plane stresses, the material strength allowable for the transverse stresses are also an order of magnitude smaller than the allowables for the in-plane stresses.

Mindlin further refined the CPT by including the transverse shear effects in his model and the theory when applied to composite laminates is called the First-order Shear Deformation Theory (FSDT). In this model, the normal of the plate is assumed to be straight but no longer normal in the deformed configuration thus allowing the independent rotations of the transverse normal as shown in Figure 2.1. This assumption

makes the transverse shear strains and stresses to be constant in the thickness direction of the laminated plate and thus requires the shear correction factor. The shear correction factor is a dimensionless quantity, which accounts for the difference between the constant state of shear strains and stresses in the First-order Shear Deformation Theory and the actual distribution of shear strains and stresses according to the elasticity theory. For composite laminates, the ply properties, lamination scheme, geometry of the structure and boundary conditions also affect the value of shear correction factor.

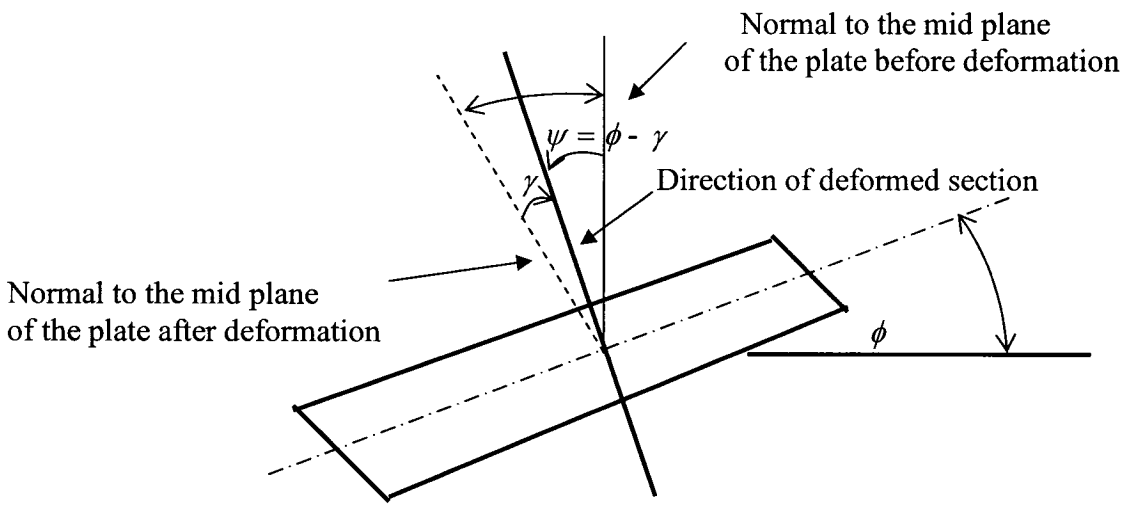

where ϕ is slope of the plate,
ψ is the actual rotation of the laminate, and
γ is the shear strain.

Figure 2.1 Deformation of the mid plane according to FSDT

2.3 Governing Equations

For a laminated plate of constant thickness "h" with different orientations of each layer with respect to a Cartesian co-ordinate system, the origin of the coordinate

system is located at the middle plane with z-axis being normal to the mid-plane. The material of each layer is assumed to have a plane of elastic symmetry parallel to the x-y plane. The assumed displacement field as per FSDT is as below

$$u(x,y,z) = u_0(x,y) + z\psi_x(x,y)$$

$$v(x,y,z) = v_0(x,y) + z\psi_y(x,y)$$

$$w(x,y,z) = w_0(x,y) \tag{2.1}$$

where u, v and w are the displacement components in x, y and z directions respectively, u_0, v_0 and w_0 are the corresponding mid-plane displacements in x, y and z directions, ψ_x and ψ_y are the rotations about x and y directions respectively, and z is the thickness variable in z-direction.

The corresponding strain field is given by

$$\varepsilon_{xx} = \frac{\partial u_0}{\partial x} + z\frac{\partial \psi_x}{\partial x}, \qquad \varepsilon_{yy} = \frac{\partial v_0}{\partial y} + z\frac{\partial \psi_y}{\partial y}, \qquad \varepsilon_{zz} = 0$$

$$\gamma_{xy} = \frac{\partial u_0}{\partial y} + \frac{\partial v_0}{\partial x} + z\left(\frac{\partial \psi_x}{\partial y} + \frac{\partial \psi_y}{\partial x}\right), \qquad \gamma_{xz} = \frac{\partial w_0}{\partial x} + \psi_x, \qquad \gamma_{yz} = \frac{\partial w_0}{\partial y} + \psi_y \tag{2.2}$$

The constitutive relation for any layer taking into consideration the plane of elastic symmetry is given by:

$$\begin{bmatrix} \sigma_x \\ \sigma_y \\ \tau_{xy} \\ \tau_{yz} \\ \tau_{xz} \end{bmatrix} = \begin{bmatrix} Q_{11} & Q_{12} & Q_{16} & 0 & 0 \\ Q_{12} & Q_{22} & Q_{26} & 0 & 0 \\ Q_{16} & Q_{26} & Q_{66} & 0 & 0 \\ 0 & 0 & 0 & Q_{44} & Q_{45} \\ 0 & 0 & 0 & Q_{45} & Q_{55} \end{bmatrix} \begin{bmatrix} \varepsilon_x \\ \varepsilon_y \\ \gamma_{xy} \\ \gamma_{yz} \\ \gamma_{xz} \end{bmatrix} \tag{2.3}$$

where, Q_{ij} (i, j = 1,2,6) are the plane stress reduced stiffness components and Q_{ij} (i, j = 4,5) are the transverse shear stiffness components of the layer material. We can introduce force and moment resultants per unit length as follows

$$(N_x, N_y, N_{xy}) = \int_{-h/2}^{h/2} (\sigma_x, \sigma_y, \tau_{xy}) dz, \qquad (Q_x, Q_y) = \int_{-h/2}^{h/2} (\tau_{xz}, \tau_{yz}) dz,$$

$$(M_x, M_y, M_{xy}) = \int_{-h/2}^{h/2} (\sigma_x, \sigma_y, \tau_{xy}) z dz \tag{2.4}$$

where N_x, N_y and N_{xy} are in plane force resultants,

Q_x and Q_y are transverse force resultants,

M_x and M_y are bending moment resultants, and

M_{xy} is the twisting moment resultant.

The constitutive equation of laminates according to FSDT associates the resultants and moments as follows:

$$\begin{bmatrix} N_x \\ N_y \\ N_{xy} \\ M_x \\ M_y \\ M_{xy} \\ Q_y \\ Q_x \end{bmatrix} = \begin{bmatrix} A_{11} & A_{12} & A_{16} & B_{11} & B_{12} & B_{16} & 0 & 0 \\ A_{12} & A_{22} & A_{26} & B_{12} & B_{22} & B_{26} & 0 & 0 \\ A_{16} & A_{26} & A_{66} & B_{16} & B_{26} & B_{66} & 0 & 0 \\ B_{11} & B_{12} & B_{16} & D_{11} & D_{12} & D_{16} & 0 & 0 \\ B_{12} & B_{22} & B_{26} & D_{12} & D_{22} & D_{26} & 0 & 0 \\ B_{16} & B_{26} & B_{66} & D_{16} & D_{26} & D_{66} & 0 & 0 \\ 0 & 0 & 0 & 0 & 0 & 0 & F_{44} & F_{45} \\ 0 & 0 & 0 & 0 & 0 & 0 & F_{45} & F_{55} \end{bmatrix} \begin{bmatrix} \partial u_0 / \partial x \\ \partial v_0 / \partial y \\ \partial u_0 / \partial y + \partial v_0 / \partial x \\ \partial \psi_x / \partial x \\ \partial \psi_y / \partial y \\ \partial \psi_x / \partial y + \partial \psi_y / \partial x \\ \partial w_0 / \partial y + \psi_y \\ \partial w_0 / \partial x + \psi_x \end{bmatrix} \tag{2.5}$$

where A_{ij}, B_{ij} and D_{ij} are given by

$$(A_{ij}, B_{ij}, D_{ij}) = \int_{-h/2}^{h/2} Q_{ij}^{(m)} (1, z, z^2) dz \qquad \text{i , j = 1,2,6} \tag{2.6a}$$

$$A_{ij} = k \int_{-h/2}^{h/2} Q_{ij}^{(m)} dz \qquad \text{i , j = 4,5} \tag{2.6b}$$

where $Q_{ij}^{(m)}$ are stiffness coefficients of the mth layer and

k is the shear correction factor.

Generally each lamina in the laminate can have its own material properties. The material properties of a lamina are known in their own coordinate system. They are first transformed into the plate coordinate system, using angle of orientation to obtain the stiffness coefficients, $Q_{ij}^{(m)}$ for each lamina. Then A_{ij}, B_{ij} and D_{ij} are obtained using Equation (2.6) where

$$A_{ij} = \int_{-h/2}^{h/2} Q_{ij}^{(m)} dz \qquad = \qquad \sum_{m=1}^{N_L} \int_{h_i}^{h_{i+1}} Q_{ij}^{(m)} dz \tag{2.7}$$

where h_i The distance of the lower surface of the m^{th} layer from the mid plane along the thickness coordinate and N_L is total number of layers of the laminate.

Once the A_{ij}, B_{ij} and D_{ij} are obtained the whole plate is analyzed as if made of a single material with characteristic constants A_{ij}, B_{ij} and D_{ij}.In the absence of body forces and shear stresses on the faces of laminate, the equations of plates are [1]

$$\partial N_x / \partial x + \partial N_{xy} / \partial y = \rho_s \partial^2 u / \partial t^2, \qquad \partial N_{xy} / \partial x + \partial N_y / \partial y = \rho_s \partial^2 v / \partial t^2$$

$$\partial Q_x / \partial x + \partial Q_y / \partial y = \rho_s \partial^2 w / \partial t^2, \qquad \partial M_x / \partial x + \partial M_{xy} / \partial y - Q_x = I \partial^2 \psi_x / \partial t^2$$

$$\partial M_{xy} / \partial x + \partial M_y / \partial y - Q_y = I \partial^2 \psi_y / \partial t^2 \tag{2.8}$$

where ρ_s is the translational inertia coefficient and I is the rotary inertia coefficient.

In case of static problems the right hand side of Equations (2.8) reduces to zero.

Strain energy of the laminate is given by

$$U = \frac{1}{2} \iiint (\sigma_x \varepsilon_x + \sigma_y \varepsilon_y + \sigma_z \varepsilon_z + \tau_{yz} \gamma_{yz} + \tau_{xz} \gamma_{xz} + \tau_{xy} \gamma_{xy}) dx dy dz \tag{2.9}$$

Now substituting the values from Equations (2.2), (2.3), (2.5) into Equation (2.8), we can express strain energy in terms of displacements and slope functions as follows

$$U =$$

$$\frac{1}{2}\{A_{11}\left(\frac{\partial u_0}{\partial x}\right)^2 + 2A_{16}\frac{\partial u_0}{\partial x}\frac{\partial u_0}{\partial y} + A_{66}\left(\frac{\partial u_0}{\partial y}\right)^2 + \frac{\partial u_0}{\partial x}\left(A_{12}\frac{\partial v_0}{\partial y} + A_{16}\frac{\partial v_0}{\partial x}\right)$$
$$+ \frac{\partial v_0}{\partial y}\left(A_{12}\frac{\partial u_0}{\partial x} + A_{26}\frac{\partial u_0}{\partial y}\right) + \frac{\partial u_0}{\partial y}\left(A_{26}\frac{\partial v_0}{\partial y} + A_{66}\frac{\partial v_0}{\partial x}\right) + \frac{\partial v_0}{\partial x}\left(A_{16}\frac{\partial u_0}{\partial x} + A_{66}\frac{\partial u_0}{\partial y}\right)$$
$$+ A_{22}\left(\frac{\partial v_0}{\partial y}\right)^2 + 2A_{26}\frac{\partial v_0}{\partial y}\frac{\partial v_0}{\partial x} + A_{66}\left(\frac{\partial v_0}{\partial x}\right)^2$$
$$+ \frac{\partial u_0}{\partial x}\left(B_{11}\frac{\partial \psi_x}{\partial x} + B_{16}\frac{\partial \psi_x}{\partial y} + B_{12}\frac{\partial \psi_y}{\partial y} + B_{16}\frac{\partial \psi_y}{\partial x}\right)$$
$$+ \left(\frac{\partial u_0}{\partial y} + \frac{\partial v_0}{\partial x}\right)\times\left(B_{16}\frac{\partial \psi_x}{\partial x} + B_{66}\frac{\partial \psi_x}{\partial y} + B_{26}\frac{\partial \psi_y}{\partial y} + B_{66}\frac{\partial \psi_y}{\partial x}\right)$$

$$+ \frac{\partial v_0}{\partial y}\times\left(B_{12}\frac{\partial \psi_x}{\partial x} + B_{26}\frac{\partial \psi_x}{\partial y} + B_{22}\frac{\partial \psi_y}{\partial y} + B_{26}\frac{\partial \psi_y}{\partial x}\right)$$
$$+ \frac{\partial \psi_x}{\partial x}\left(B_{11}\frac{\partial u_0}{\partial x} + B_{16}\frac{\partial u_0}{\partial y} + B_{12}\frac{\partial v_0}{\partial y} + B_{16}\frac{\partial v_0}{\partial x}\right)$$
$$+ \left(\frac{\partial \psi_x}{\partial y} + \frac{\partial \psi_y}{\partial x}\right)\left(B_{16}\frac{\partial u_0}{\partial x} + B_{66}\frac{\partial u_0}{\partial y} + B_{26}\frac{\partial v_0}{\partial y} + B_{66}\frac{\partial v_0}{\partial x}\right)$$
$$+ \frac{\partial \psi_y}{\partial y}\left(B_{12}\frac{\partial u_0}{\partial x} + B_{26}\frac{\partial u_0}{\partial y} + B_{22}\frac{\partial v_0}{\partial y} + B_{26}\frac{\partial v_0}{\partial x}\right)$$

$$+ A_{44}\left(\frac{\partial w}{\partial y}\right)^2 + 2A_{45}\frac{\partial w}{\partial x}\frac{\partial w}{\partial y} + A_{55}\left(\frac{\partial w}{\partial x}\right)^2 + \frac{\partial w}{\partial y}\left(A_{44}\psi_y + A_{45}\psi_x\right)$$
$$+ \frac{\partial w}{\partial x}\left(A_{45}\psi_y + A_{55}\psi_x\right) + \psi_x\left(A_{45}\frac{\partial w}{\partial y} + A_{55}\frac{\partial w}{\partial x}\right) + \psi_y\left(A_{44}\frac{\partial w}{\partial y} + A_{45}\frac{\partial w}{\partial x}\right)$$

$$+ D_{11}\left(\frac{\partial \psi_x}{\partial x}\right)^2 + 2D_{16}\frac{\partial \psi_x}{\partial x}\frac{\partial \psi_x}{\partial y} + D_{66}\left(\frac{\partial \psi_x}{\partial y}\right)^2 + A_{55}{\psi_x}^2$$

$$+\frac{\partial \psi_x}{\partial x}\left(D_{12}\frac{\partial \psi_y}{\partial y}+2D_{16}\frac{\partial \psi_y}{\partial x}\right)+\frac{\partial \psi_y}{\partial y}\left(D_{12}\frac{\partial \psi_x}{\partial x}+2D_{26}\frac{\partial \psi_x}{\partial y}\right)$$
$$+2D_{66}\frac{\partial \psi_x}{\partial y}\frac{\partial \psi_y}{\partial x}+2A_{45}\psi_x\psi_y+D_{22}\left(\frac{\partial \psi_y}{\partial y}\right)^2+2D_{26}\frac{\partial \psi_y}{\partial x}\frac{\partial \psi_y}{\partial y} \tag{2.10}$$
$$+D_{66}\left(\frac{\partial \psi_y}{\partial x}\right)^2+A_{44}{\psi_y}^2\}dA$$

2.4 Ritz Solution for Specially Orthotropic Symmetric Laminate

In this Section the approximate solution using Ritz method is discussed. In the case of pure bending of specially orthotropic and symmetric composite laminate using FSDT, the strain energy equation is given by

$$U_d=\frac{1}{2}\iint\{D_{11}\left(\frac{\partial \psi_x}{\partial x}\right)^2+D_{22}\left(\frac{\partial \psi_y}{\partial y}\right)^2+D_{66}\left(\frac{\partial \psi_x}{\partial y}\right)^2+D_{66}\left(\frac{\partial \psi_y}{\partial x}\right)^2+2D_{12}\frac{\partial \psi_x}{\partial x}\frac{\partial \psi_y}{\partial y}$$
$$+2D_{66}\frac{\partial \psi_x}{\partial y}\frac{\partial \psi_y}{\partial x}+A_{44}\left(\frac{\partial w}{\partial y}\right)^2+A_{55}\left(\frac{\partial w}{\partial x}\right)^2+A_{44}(\psi_y)^2+A_{55}(\psi_x)^2+2A_{45}\frac{\partial w}{\partial x}\frac{\partial w}{\partial y}$$
$$+2A_{45}\frac{\partial w}{\partial y}\psi_x+2A_{44}\frac{\partial w}{\partial y}\psi_y+2A_{45}\frac{\partial w}{\partial x}\psi_y+2A_{55}\frac{\partial w}{\partial x}\psi_x+2A_{45}\psi_x\psi_y\}dA \tag{2.11}$$

The potential energy related with the uniformly distributed transverse load q(x,y) is

$$W_f=\int_{x=0}^{a}\int_{y=0}^{b}q(x,y)w_o(x,y)dxdy \tag{2.12}$$

The load $q(x,y)$ can be expanded as Fourier series as follows

$$q(x,y) = \sum_{i=1}^{M}\sum_{j=1}^{N} q_{ij} \sin\left(\frac{i\pi x}{a}\right)\sin\left(\frac{j\pi y}{b}\right) \tag{2.13}$$

In the case of uniform loading distributed over the surface of plate,

$$q_{ij} = \frac{16q_0}{\pi^2 ij} \quad \text{If M and N are odd i.e. i,j = 1,3,5,7 .....}$$

$$q_{ij} = 0 \quad \text{If M and N are even i.e. i,j = 2,4,6,8.....} \tag{2.14}$$

In the general case the load can be rewritten as

$$q(x,y) = \sum_{i=1}^{I}\sum_{j=1}^{J} \frac{16q_0}{\pi^2(2i-1)(2j-1)} \sin\left(\frac{(2i-1)\pi x}{a}\right)\sin\left(\frac{(2j-1)\pi y}{b}\right) \quad \text{i, j = 1,2,3.....} \tag{2.15}$$

The approximated solution is expanded in a double series as below

$$w_o(x,y) = \sum_{m=1}^{M}\sum_{n=1}^{N} A_{mn} X_m(x) Y_n(y) \tag{2.16a}$$

$$\psi_x(x,y) = \sum_{m=1}^{M}\sum_{n=1}^{N} B_{mn} P_m(x) Q_n(y) \tag{2.16b}$$

$$\psi_y(x,y) = \sum_{m=1}^{M}\sum_{n=1}^{N} C_{mn} S_m(x) T_n(y) \tag{2.16c}$$

The expression for potential energy (2.12) after substituting the expression for q(x, y) from Equation (2.15) and $w_o(x,y)$ from Equation (2.16) becomes as follows:

$$W_f = \int_{x=0}^{a}\int_{y=0}^{b} \sum_{i=1}^{I}\sum_{j=1}^{J} \frac{16q_0}{\pi^2(2i-1)(2j-1)} \sin\left(\frac{(2i-1)\pi x}{a}\right)\sin\left(\frac{(2j-1)\pi y}{b}\right) \sum_{m=1}^{M}\sum_{n=1}^{N} A_{mn} X_m(x) Y_n(y) dxdy$$

(2.17)

The functions $X_m(x)$ and $Y_n(y)$ are chosen so as to satisfy the boundary conditions. These functions could be polynomials, trigonometric functions, etc. The coefficients A_{mn}, B_{mn}, C_{mn} are determined by stationarity condition which can be written as

$$\frac{\partial \widetilde{U}_d}{\partial A_{mn}} = \frac{\partial \widetilde{W}_f}{\partial A_{mn}} \tag{2.18a}$$

$$\frac{\partial \widetilde{U}_d}{\partial B_{mn}} = \frac{\partial \widetilde{W}_f}{\partial B_{mn}} \tag{2.18b}$$

$$\frac{\partial \widetilde{U}_d}{\partial C_{mn}} = \frac{\partial \widetilde{W}_f}{\partial C_{mn}} \tag{2.18c}$$

where $\widetilde{U}_d$ and $\widetilde{W}_f$ are the strain energy and the potential energy because of transverse load, obtained by substituting the approximate expression (2.16) for the deflection into the Equations (2.11) and (2.12). We can calculate the terms corresponding to potential energy and strain energy by taking the partial derivatives of strain energy and potential energy with respect to A_{mn}, B_{mn}, C_{mn} as given below.

The right hand side of Equation (2.18a) can be solved to give the resulting expression as follows

$$\int_{x=0}^{a}\int_{y=0}^{b}\sum_{i=1}^{I}\sum_{j=1}^{J}\frac{16q_0}{\pi^2(2i-1)(2j-1)}\sin\left(\frac{(2i-1)\pi x}{a}\right)\sin\left(\frac{(2j-1)\pi y}{b}\right)X_m(x)Y_n(y)dxdy \tag{2.19}$$

Note: The right hand sides of Equations (2.18b) and (2.18c) are zero.

The expression for the strain energy (2.11) contains 16 terms added inside the integral. The integral of the various terms in the expression of strain energy can be written as sum of integrals of individual terms. The left hand sides of Equations (2.18a), (2.18b), (2.18c) can be obtained by substituting the assumed solutions from Equation (2.16), into each of these 16 terms, taking their partial derivatives with respect to constants A_{mn}, B_{mn}, C_{mn} and then taking the integral of the resulting terms as given below.

First 4 terms are calculated here, the calculation of remaining 12 terms can be found in Appendix-I

Term 1

$$D_{11}\left(\frac{\partial \psi_x}{\partial x}\right)^2$$

After substituting the assumed solutions from Equation (2.16)

$$\text{Term 1} = D_{11}\sum_{m=1}^{M}\sum_{n=1}^{N}\sum_{i=1}^{M}\sum_{j=1}^{N} B_{mn}B_{ij}\frac{dP_m}{dx}\frac{dP_i}{dx}Q_nQ_j$$

and

$$\frac{1}{2}\frac{\partial}{\partial A_{mn}}(Term1) = 0 \tag{2.20a}$$

$$\frac{1}{2}\frac{\partial}{\partial B_{mn}}(Term1) = D_{11}\sum_{i=1}^{M}\sum_{j=1}^{N} B_{ij}\frac{dP_m}{dx}\frac{dP_i}{dx}Q_nQ_j \tag{2.20b}$$

$$\frac{1}{2}\frac{\partial}{\partial C_{mn}}(Term1) = 0 \tag{2.20c}$$

Integration of non zero term yields

$$\frac{1}{2}\int_{x=0}^{a}\int_{y=0}^{b}\frac{\partial}{\partial B_{mn}}(Term1)dxdy = D_{11}\sum_{i=1}^{M}\sum_{j=1}^{N}B_{ij}\int_{x=0}^{a}\frac{dP_m}{dx}\frac{dP_i}{dx}dx\int_{y=0}^{b}Q_nQ_jdy \tag{2.21}$$

Term 2

$$D_{22}\left(\frac{\partial\psi_y}{\partial y}\right)^2$$

After substituting the assumed solutions from Equation (2.16)

$$\text{Term 2} = D_{22}\sum_{m=1}^{M}\sum_{n=1}^{N}\sum_{i=1}^{M}\sum_{j=1}^{N}C_{mn}C_{ij}\ \frac{dT_m}{dy}\frac{dT_i}{dy}S_nS_j$$

and

$$\frac{1}{2}\frac{\partial}{\partial A_{mn}}(Term2)=0 \tag{2.22a}$$

$$\frac{1}{2}\frac{\partial}{\partial B_{mn}}(Term2)=0 \tag{2.22b}$$

$$\frac{1}{2}\frac{\partial}{\partial C_{mn}}(Term2)=D_{22}\sum_{i=1}^{M}\sum_{j=1}^{N}C_{ij}\frac{dT_n}{dy}\frac{dT_j}{dy}S_mS_i \tag{2.22c}$$

Integration of non zero term yields

$$\frac{1}{2}\int_{x=0}^{a}\int_{y=0}^{b}\frac{\partial}{\partial C_{mn}}(Term2)dxdy = D_{22}\sum_{i=1}^{M}\sum_{j=1}^{N}C_{ij}\int_{x=0}^{a}S_mS_idx\int_{y=0}^{b}\frac{dT_n}{dy}\frac{dT_j}{dy}dy \tag{2.23}$$

Term 3

$$D_{66}\left(\frac{\partial\psi_x}{\partial y}\right)^2$$

After substituting the assumed solutions from Equation (2.16)

$$\text{Term 3} = D_{66}\sum_{m=1}^{M}\sum_{n=1}^{N}\sum_{i=1}^{M}\sum_{j=1}^{N}B_{mn}B_{ij}\ \frac{dQ_n}{dy}\frac{dQ_j}{dy}P_mP_i$$

$$\frac{1}{2}\frac{\partial}{\partial A_{mn}}(Term3)=0 \tag{2.24a}$$

$$\frac{1}{2}\frac{\partial}{\partial B_{mn}}(Term3)=D_{66}\sum_{i=1}^{M}\sum_{j=1}^{N}B_{ij}\frac{dQ_n}{dy}\frac{dQ_j}{dy}P_mP_i \tag{2.24b}$$

$$\frac{1}{2}\frac{\partial}{\partial C_{mn}}(Term3)=0 \tag{2.24c}$$

Integration of non zero term yields

$$\frac{1}{2}\int_{x=0}^{a}\int_{y=0}^{b}\frac{\partial}{\partial B_{mn}}(Term3)dxdy = D_{66}\sum_{i=1}^{M}\sum_{j=1}^{N}B_{ij}\int_{x=0}^{a}P_mP_i dx\int_{y=0}^{b}\frac{dQ_n}{dy}\frac{dQ_j}{dy}dy \tag{2.25}$$

Term 4

$$D_{66}\left(\frac{\partial\psi_y}{\partial x}\right)^2$$

After substituting the assumed solutions from Equation (2.16)

$$\text{Term 4} = D_{66}\sum_{m=1}^{M}\sum_{n=1}^{N}\sum_{i=1}^{M}\sum_{j=1}^{N}C_{mn}C_{ij}\frac{dS_m}{dx}\frac{dS_i}{dx}T_nT_j$$

$$\frac{1}{2}\frac{\partial}{\partial A_{mn}}(Term4)=0 \tag{2.26a}$$

$$\frac{1}{2}\frac{\partial}{\partial B_{mn}}(Term4)=0 \tag{2.26b}$$

$$\frac{1}{2}\frac{\partial}{\partial C_{mn}}(Term4)=D_{66}\sum_{i=1}^{M}\sum_{j=1}^{N}C_{ij}\frac{dS_m}{dx}\frac{dS_i}{dx}T_nT_j \tag{2.26c}$$

Integration of non zero term yields

$$\frac{1}{2}\int_{x=0}^{a}\int_{y=0}^{b}\frac{\partial}{\partial C_{mn}}(Term4)dxdy = D_{66}\sum_{i=1}^{M}\sum_{j=1}^{N}C_{ij}\int_{x=0}^{a}\frac{dS_m}{dx}\frac{dS_i}{dx}dx\int_{y=0}^{b}T_nT_j dy \tag{2.27}$$

After substituting the 4 terms as calculated above and the remaining 12 terms from Appendix-I, the Equation (2.18) can be written in the matrix form as given in equation (2.28), to solve for the three constants. The number of equations and hence the related constants differ as the values of m and n (number of terms used in approximation functions of the solutions) increases.

In case where m=n=1 the system of equations becomes

$$\begin{bmatrix} a_{11} & b_{11} & c_{11} \\ a_{21} & b_{21} & c_{21} \\ a_{31} & c_{31} & c_{31} \end{bmatrix} \begin{bmatrix} A_1 \\ B_1 \\ C_1 \end{bmatrix} = \begin{Bmatrix} F_1 \\ 0 \\ 0 \end{Bmatrix} \tag{2.28}$$

First matrix on the left hand side contains the terms of strain energy. The second matrix on the left hand side consists of the vector of constants which are to be determined. The matrix on the right hand side contains the terms of potential energy. F_1 denotes the potential energy due to transverse load corresponding to transverse displacement. As there is no external moment applied, so the terms of the potential energy corresponding to rotations ψ_x and ψ_y are zero.

In the case where $m = n = 2$ the system of Equations (2.18a), (2.18b), (2.18c) becomes

$$\begin{bmatrix} a_{11} & a_{12} & b_{11} & b_{12} & c_{11} & c_{12} \\ a_{21} & a_{22} & b_{21} & b_{22} & c_{21} & c_{22} \\ a_{31} & a_{32} & b_{31} & b_{32} & c_{31} & c_{32} \\ a_{41} & a_{42} & b_{41} & b_{42} & c_{41} & c_{42} \\ a_{51} & a_{52} & b_{51} & b_{52} & c_{51} & c_{52} \\ a_{61} & a_{62} & b_{61} & b_{62} & c_{61} & c_{62} \end{bmatrix} \begin{bmatrix} A_1 \\ A_2 \\ B_1 \\ B_2 \\ C_1 \\ C_2 \end{bmatrix} = \begin{Bmatrix} F_1 \\ F_2 \\ 0 \\ 0 \\ 0 \\ 0 \end{Bmatrix} \tag{2.29}$$

The set of Equations (2.29) can be written in the concise form as below

$$[abc]\{ABC\} = \{F\} \tag{2.30}$$

The constants can be determined as below

$$\{ABC\} = [abc]^{-1}\{F\} \tag{2.31}$$

The values of A_1 and A_2 are substituted in Equation (2.16a) to calculate transverse deflection 'w'. The value of maximum transverse deflection is found by finding the displacement at x = a/2 and y = b/2.

2.4.1 Validation of Ritz Solution

The results obtained using Ritz method based on FSDT for simply supported boundary conditions (SSSS) are compared with the exact solution based on CLPT that is available in reference [1].

Example 2.1

The correctness of the program is checked by considering the bending analysis of $[0/90]_{24s}$ laminate which is a 96 ply symmetric cross-ply rectangular laminate of dimensions 0.55 by 0.55 meters and subjected to a uniform surface load of 1MPa with all sides simply supported. The composite material is NCT-301 graphite/epoxy. The material properties are given below in Table 2.1.

E_1	144 GPa
E_2, E_3	12.14 GPa
ν_{21}, ν_{31}	0.017
ν_{23}	0.458
G_{12}, G_{13}	4.48 GPa
G_{23}	3.2 GPa
ρ	1660.8 kg/m^3

Table 2.1 Material properties of NCT-301 graphite/epoxy [47]

Exact Solution using CLPT [1] : The maximum transverse displacement $w_{0\max}$ is given by

$$w_{0\max} = \frac{16 q_0 a^4}{\pi^6} \alpha \tag{2.32}$$

where, $q_0 = 1.0 \times 10^6$, $a = 0.55$ meters, b = 0.55 meters, R = a/b,

$$\alpha = \sum_{m=1}^{\infty} \sum_{n=1}^{\infty} \alpha_{mn} \tag{2.33}$$

$$\alpha_{mn} = \frac{(-1)^{m+n-2}}{(2m-1)(2n-1) D_{2m-1,2n-1}} \tag{2.34}$$

where

$$D_{mn} = D_{11} m^4 + 2(D_{12} + 2D_{66})(mnR)^2 + D_{22}(nR)^4 \tag{2.35}$$

After substituting the values from Equation (2.33) and values of respective bending stiffness coefficients into Equation (2.32) the value of transverse deflection at the centre of the plate is

$$w_{0\max} = 0.05798 \text{ meters}$$

Ritz Solution based on FSDT

The values of transverse deflection for different values of M and N as in Equation (2.16) using Ritz Method are given in Table 2.2 The results show an improvement in the transverse deflection as we increase the values of M and N in the displacement function.

Value of M	Value of N	Center Deflection (meters)
1	1	.060961645
2	2	.060961721
3	3	.061051270
4	4	.061051271

Table 2.2 Ritz Solution for $[0/90]_{24s}$ Laminate for SSSS Boundary Condition

The approximate value for the transverse deflection is obtained for M = N = 4 which is

$$w_{0\max} = 0.06105 \text{ meters}$$

2.5 Formulation using Conventional Finite Element Method

2.5.1 Interpolation Functions

In the present analysis of the plate a Mindlin finite element is employed using nine node rectangular element. The resulting element stiffness matrix is of the order of 45 by 45.

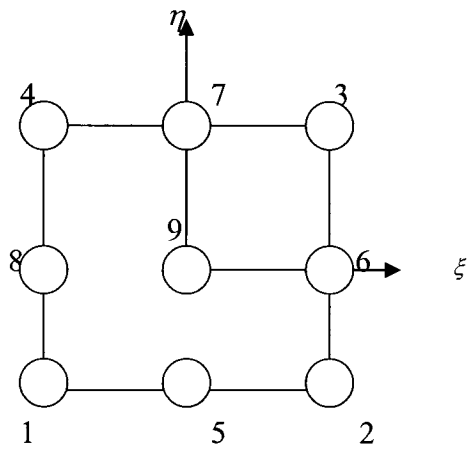

Figure 2.2 Nine node rectangular element

The corresponding shape functions are

$$N_1 = \frac{1}{4}(\xi^2 - \xi)(\eta^2 - \eta) \qquad N_5 = \frac{1}{2}(1-\xi^2)(\eta^2 - \eta)$$

$$N_2 = \frac{1}{4}(\xi^2 + \xi)(\eta^2 - \eta) \qquad N_6 = \frac{1}{2}(\xi^2 + \xi)(1-\eta^2)$$

$$N_3 = \frac{1}{4}(\xi^2 + \xi)(\eta^2 + \eta) \qquad N_7 = \frac{1}{2}(1-\xi^2)(\eta^2 + \eta)$$

$$N_4 = \frac{1}{4}(\xi^2 - \xi)(\eta^2 + \eta) \qquad N_8 = \frac{1}{2}(\xi^2 - \xi)(1-\eta^2)$$

$$N_9 = (1-\xi^2)(1-\eta^2) \tag{2.36}$$

2.5.2 Stiffness Matrix for Composite Laminate

Displacements can be expressed in terms of interpolation functions as follows

$$u_o = \sum_{i=1}^{9} N_i u_{oi};\ v_o = \sum_{i=1}^{9} N_i v_{oi};\ w_o = \sum_{i=1}^{9} N_i w_{oi};\ \psi_x = \sum_{i=1}^{9} N_i \psi_{xi};\ \psi_y = \sum_{i=1}^{9} N_i \psi_{yi}$$

Thus,

$$\begin{bmatrix} u_o \\ v_o \\ w_o \\ \psi_x \\ \psi_y \end{bmatrix} = \sum_{i=1}^{9} \begin{bmatrix} N_i & 0 & 0 & 0 & 0 \\ 0 & N_i & 0 & 0 & 0 \\ 0 & 0 & N_i & 0 & 0 \\ 0 & 0 & 0 & N_i & 0 \\ 0 & 0 & 0 & 0 & N_i \end{bmatrix} \begin{bmatrix} u_{oi} \\ v_{oi} \\ w_{oi} \\ \psi_{xi} \\ \psi_{yi} \end{bmatrix} \tag{2.37}$$

which is of the form,

$$\{u\} = [N]\{d\} \tag{2.38}$$

where

$$\{d\} = \lfloor u_1 \; v_1 \; w_1 \; \psi_{x1} \; \psi_{y1} \ldots\ldots\ldots u_9 \; v_9 \; w_9 \; \psi_{x9} \; \psi_{y9} \rfloor^T \tag{2.39}$$

Strain-displacement matrix [B] can be expressed as,

$$[B]_{8x45} = [\partial]_{8x5} [N]_{5x45} \tag{2.40}$$

where

$$[\partial] = \begin{bmatrix} \frac{\partial}{\partial x} & 0 & 0 & 0 & 0 \\ 0 & \frac{\partial}{\partial y} & 0 & 0 & 0 \\ \frac{\partial}{\partial y} & \frac{\partial}{\partial x} & 0 & 0 & 0 \\ 0 & 0 & 0 & \frac{\partial}{\partial x} & 0 \\ 0 & 0 & 0 & 0 & \frac{\partial}{\partial y} \\ 0 & 0 & 0 & \frac{\partial}{\partial y} & \frac{\partial}{\partial x} \\ 0 & 0 & \frac{\partial}{\partial y} & 0 & -1 \\ 0 & 0 & \frac{\partial}{\partial x} & -1 & 0 \end{bmatrix} \tag{2.41}$$

Thus the matrix [B] is given by:

$$[B]=\begin{bmatrix} N_{1,x} & 0 & 0 & 0 & 0 & . & . & N_{9,x} & 0 & 0 & 0 & 0 \\ 0 & N_{1,y} & 0 & 0 & 0 & . & . & 0 & N_{9,y} & 0 & 0 & 0 \\ N_{1,y} & N_{1,x} & 0 & 0 & 0 & . & . & N_{9,y} & N_{9,x} & 0 & 0 & 0 \\ 0 & 0 & 0 & N_{1,x} & 0 & . & . & 0 & 0 & 0 & N_{9,x} & 0 \\ 0 & 0 & 0 & 0 & N_{1,y} & . & . & 0 & 0 & 0 & 0 & N_{9,y} \\ 0 & 0 & 0 & N_{1,y} & N_{1,x} & . & . & 0 & 0 & 0 & N_{9,y} & N_{9,x} \\ 0 & 0 & N_{1,y} & 0 & -N_1 & . & . & 0 & 0 & N_{9,y} & 0 & -N_9 \\ 0 & 0 & N_{1,x} & -N_1 & 0 & . & . & 0 & 0 & N_{9,x} & -N_9 & 0 \end{bmatrix} \tag{2.42}$$

The element stiffness matrix can be written as

$$[K]=\int_A [B]^T{}_{8\times 45}\ [E]_{8\times 8}[B]_{8\times 45}\,dA \tag{2.43}$$

where [E] is the elasticity matrix from the right hand side of Equation (2.5) and [B] is the strain displacement matrix from Equation (2.42).

2.5.3 Validation of Conventional Finite Element Formulation

The correctness of the formulation and program is checked by considering the bending analysis of a 96 ply symmetric cross-ply rectangular laminate $[0/90]_{24s}$ of dimensions 0.55 by 0.55 meters and subjected to a uniform surface load of 1MPa with all sides simply supported. The composite material is NCT-301 graphite/epoxy.

The approximate solution for maximum transverse deflection obtained using the Ritz method based on FSDT from Example 2.1 is

$$w_{0\max} = .06105 \text{ meters}$$

The value of transverse deflection at the centre of the plate using a mesh of 10×10 elements in Conventional FEM is

$$w_{0\max} = 0.05855 \text{ meters}$$

2.5.4 Convergence Check for the Conventional Finite Element Formulation

The convergence is checked and the results obtained are as given in Table 2.3 for plates of different laminate configurations and different boundary conditions. Maximum Transverse Displacement ($w_{0\max}$) of laminated composite plate described in Example 2.1, with all sides simply supported (SSSS) is determined using conventional finite element method based on FSDT for different laminate configurations.

Mesh / Laminate Configuration	2by2 ($w_{0\max}$)	3by3 ($w_{0\max}$)	4by4 ($w_{0\max}$)	5by5 ($w_{0\max}$)	6by6 ($w_{0\max}$)
$[0/90]_{24s}$	0.04969	0.05595	0.05724	0.05792	0.05820
$[0/90/+\text{-}45]_{12s}$	0.03904	0.04259	0.04327	0.04369	0.04392
$[+\text{-}45]_{24s}$	0.03174	0.03380	0.03429	0.03461	0.03484
$[+\text{-}45]_{48}$	0.03174	0.03379	0.03428	0.03460	0.03483

7by7 ($w_{0\max}$)	8by8 ($w_{0\max}$)	9by9 ($w_{0\max}$)	10by10 ($w_{0\max}$)
0.05836	0.05845	0.05851	0.05855
0.04408	0.04420	0.04429	0.04437
0.03501	0.03514	0.03524	0.03532
0.03500	0.03513	0.03523	0.03531

Table 2.3 Convergence of maximum transverse displacement of laminated composite plates with all sides simply supported (SSSS)

Note: 2by2 represents a mesh of 2 elements in each direction. Similar meaning applies for 3by3, 4by4, etc.

Example 2.2

The correctness of the formulation and program is checked by considering the bending analysis of a 96 ply symmetric cross-ply rectangular laminate $[0/90]_{24s}$ of dimensions 0.55 by 0.55 meters and subjected to a uniform surface load of q_0= 1MPa with all sides fully clamped (CCCC).

The approximate solution using the beam functions [1] in the Ritz Method based on CLPT is given by

$$w_{0\max} = 0.00348 \frac{q_0 a^4}{D_{11} + 0.6047(D_{12} + 2D_{66})R^2 + D_{22}R^4} \tag{2.44}$$

Substituting the given values of dimensions and loadings and the values of bending stiffness coefficients for 96 ply symmetric cross-ply laminate the deflection at the centre is calculated :

$$w_{0\max} = 0.01350 \text{ meters}$$

Conventional FEM

The value of transverse deflection at the centre of the plate using a mesh of 15 by 15 conventional elements is:

$$w_{0\max} = 0.01337 \text{ meters}$$

The convergence is checked and the results obtained are as given below for plates of different laminate configurations and different boundary conditions. Maximum transverse displacement ($w_{0\max}$) of laminated composite plate described in Example 2.1 with all sides clamped (CCCC) is determined using conventional finite element method based on FSDT for different laminate configurations as given in Table 2.4.

Mesh / Laminate Configuration	2by2 ($w_{0\max}$)	3by3 ($w_{0\max}$)	4by4 ($w_{0\max}$)	5by5 ($w_{0\max}$)	6by6 ($w_{0\max}$)
$[0/90]_{24s}$	0.00301	0.01015	0.01176	0.01258	0.01292
$[0/90/+\text{-}45]_{12s}$	0.00302	0.01027	0.01190	0.01272	0.01308
$[+\text{-}45]_{24s}$	0.00304	0.01049	0.01217	0.01298	0.01340
$[+\text{-}45]_{48}$	0.00304	0.01049	0.01217	0.01298	0.01340

7by7 ($w_{0\max}$)	8by8 ($w_{0\max}$)	9by9 ($w_{0\max}$)	10by10 ($w_{0\max}$)
0.01311	0.01321	0.01327	0.01330
0.01328	0.01340	0.01346	0.01350
0.01364	0.01377	0.01386	0.01391
0.01363	0.01377	0.01386	0.01391

Table 2.4 Convergence of maximum transverse displacement of laminated composite plates with all sides clamped (CCCC)

2.6 Hierarchical Finite Element Formulation

Contrary to h version of finite element formulation, in p version or hierarchical finite element formulation, the mesh is left unchanged; instead, the order of polynomial

of interpolation functions is increased to refine the solution. The Hierarchical Finite Element is a special form of Classical Rayleigh-Ritz method. The only difference in the two is in the choice of interpolation function used for interpolating the solution. In the conventional Finite Element Method the domain of interest is divided into a number of smaller, not necessarily identical but convex sub domains, which are called finite elements. The solution is then approximated by locally admissible polynomial functions, which are piece-wise continuous over each sub domain. The degree of these polynomials is generally of the order of one, two or maximum three.

The accuracy of the finite element approximation can be improved by two means. Either by increasing the number of sub domains called as finite elements, keeping the degree of interpolating polynomial constant or by keeping the mesh size constant and by letting the degree of interpolating polynomial functions to go to infinity. The latter approach is known as p-version of finite element method or better known as Hierarchical Finite Element Method (HFEM). Clearly the HFEM and Rayleigh-Ritz method have much in common. In HFEM the admissible displacement interpolation functions are local unlike the global functions as in Rayleigh-Ritz method. This results in greater versatility and better convergence rates. The HFEM has many advantages over conventional FEM. First of all, in HFEM the accuracy of the solution is improved by increasing the degree of polynomial without disturbing the mesh size and number of nodes. Secondly, when the order of Hierarchical Mode is increased the size of element stiffness and mass matrices are also increased and the original element and mass matrices are embedded in the new ones. Now because of this embedding property the computed eigen values always

approach their actual values asymptotically and always are upper bound to their actual values. Thirdly for eigen values of equal order the HFEM always gives better approximation as compared to conventional FEM and last but not least in HFEM it is possible to model the simple structures like a plate as just one hierarchical finite element. This helps in avoiding the necessity to satisfy internal C_0 or C_1 continuity across the elements' interfaces.

2.6.1 Hierarchical Shape Functions

The hierarchical shape functions can be selected from a variety of polynomial or trigonometric functions provided the chosen set is complete. In this thesis we have chosen the polynomial functions. The best suitable polynomials would be the ones, which have the property that the set of functions corresponding to an approximation of lower order constitutes a subset of set of functions corresponding to a higher order approximation. The set of functions used in present work has been derived from Rodrigues form of Legendre Polynomials. The element stiffness matrix will always involve integral of product of derivatives of the interpolation functions. If those derivatives were orthogonal then they would result in diagonal square matrix. It is well known that the Legendre Polynomials are orthogonal. So we chose our hierarchical shape functions as integrals of Legendre Polynomials so that their derivatives are Legendre polynomials.

We obtain shape functions for 2 dimensional p-elements as a tensor product of simple one-dimensional shape functions. P-degrees of freedom are associated with

directional derivatives at midpoints of element edges and with mixed derivatives at the center point of the element.

In one dimension we can write displacements as

$$u = N_1 u_1 + N_2 u_2 + \sum_{i=2}^{p} N_{hi} u_{hi} \tag{2.45}$$

where $i = 2,.....p$ is the order of hierarchical polynomial.

Extending this concept to 2-dimensions and knowing that shape functions in 2-dimensions are tensor product of shape functions in one dimension, we can write displacement as

$$u = N_1 u_1 + N_2 u_2 + N_3 u_3 + N_4 u_4 + \sum_{i=2}^{p} N_{hi} u_{hi} \tag{2.46}$$

where N_1, N_2, N_3, N_4 are conventional shape functions.

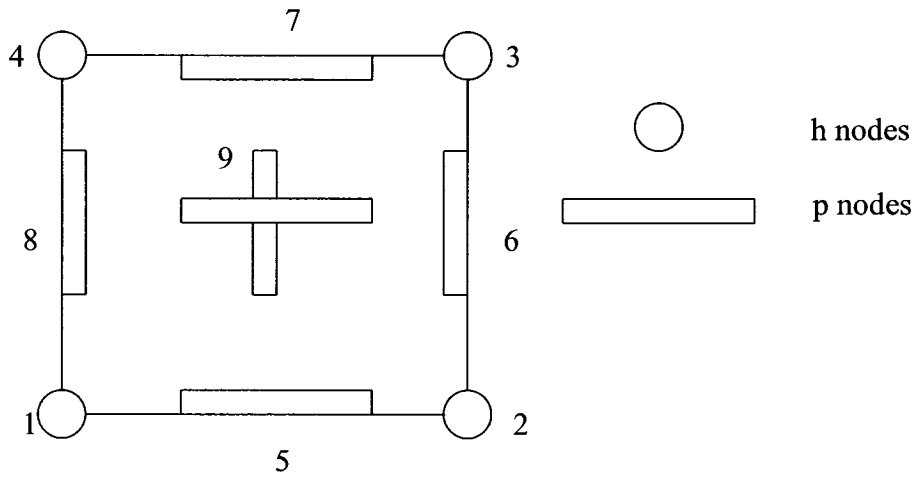

Figure 2.3 Location of p and h nodes for two-dimensional element

The h degrees of freedom in our case are $(u, v, w, \psi_x, \psi_y)$ and p degrees of freedom are associated with the directional derivative at midpoint of element edges and with mixed derivative at the center point of the element as shown in Figure 2.3.

We will first derive shape functions in one dimension.

$$N_1(\xi) = (1-\xi)/2$$

$$N_2(\xi) = (1+\xi)/2$$

$$N_i(\xi) = \varphi_{i-1}(\xi) \qquad i = 3,4,\ldots\ldots\ldots\ldots\text{p+1}$$

where

$$\varphi_j(\xi) = \sqrt{\frac{2j-1}{2}}\int_{-1}^{\xi} P_{j-1}(t)dt$$

$$= \frac{1}{\sqrt{4j-2}}(P_j(\xi) - P_{j-2}(\xi)) \qquad \text{j} = 2,3,\ldots\ldots\ldots\ldots \qquad (2.47)$$

and $P_k(\xi)$ are well known Legendre Polynomials

$$P_k(\xi) = \frac{1}{2^k k!}\frac{d^k}{d\xi^k}(\xi^2 - 1)^k \qquad \text{k} = 0,1\ldots\ldots\ldots\ldots\ldots\ldots \qquad (2.48)$$

Shape functions for 2 dimensional cases can now be easily constructed by taking tensor

product. When one hierarchical shape function is added and the tensor product is taken, we get the resulting set of hierarchical shape functions as below:

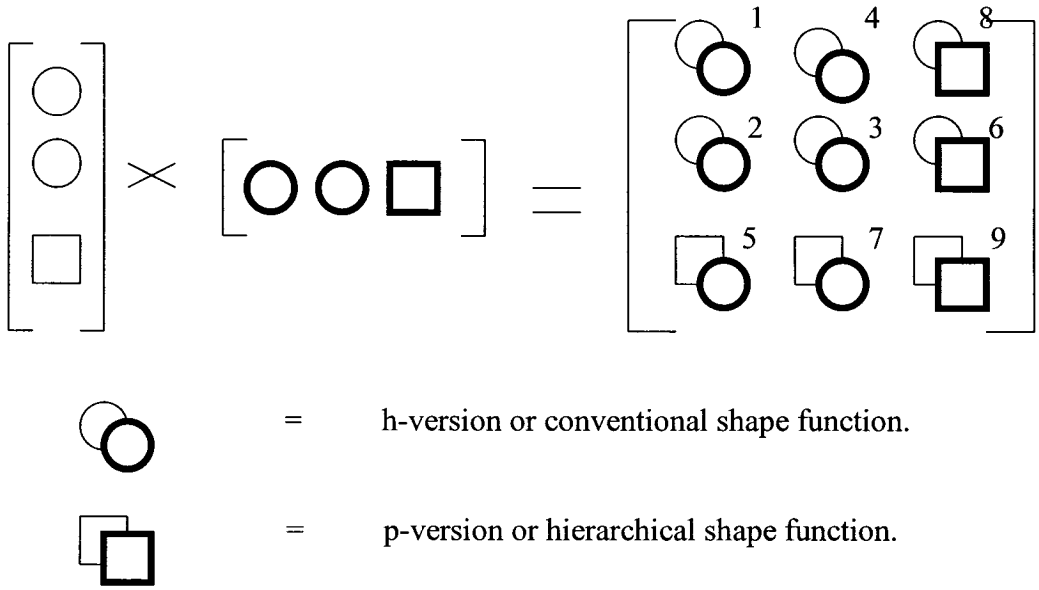

Figure 2.4 Visualization of hierarchical shape functions

The first four hierarchical shape functions in one dimension as derived from Equation (2.47) are as given below

$$
\begin{aligned}
N_{h1} &= \frac{3(s^2-1)}{2\sqrt{6}} \\
N_{h2} &= \frac{\sqrt{10}(s^3-s)}{4} \\
N_{h3} &= \frac{(35s^4-30s^2+7)}{8\sqrt{14}} \\
N_{h4} &= \frac{(63s^5-90s^3+27s)}{24\sqrt{2}}
\end{aligned}
\tag{2.49}
$$

When one hierarchical shape function ($N_{h1} = \frac{3(s^2-1)}{2\sqrt{6}}$) is added and the tensor product is taken as shown in Figure 2.4 the resulting two dimensional shape functions are given by

$$\begin{bmatrix} \frac{(1-s)}{2} \\ \frac{(1+s)}{2} \\ \frac{3(s^2-1)}{2\sqrt{6}} \end{bmatrix} X \begin{bmatrix} \frac{(1-t)}{2} & \frac{(1+t)}{2} & \frac{3(t^2-1)}{2\sqrt{6}} \end{bmatrix} = \begin{bmatrix} \frac{(1-s)}{2}\frac{(1-t)}{2} & \frac{(1-s)}{2}\frac{(1+t)}{2} & \frac{(1-s)}{2}\frac{3(t^2-1)}{2\sqrt{6}} \\ \frac{(1+s)}{2}\frac{(1-t)}{2} & \frac{(1+s)}{2}\frac{(1+t)}{2} & \frac{(1+s)}{2}\frac{3(t^2-1)}{2\sqrt{6}} \\ \frac{3(s^2-1)}{2\sqrt{6}}\frac{(1-t)}{2} & \frac{3(s^2-1)}{2\sqrt{6}}\frac{(1+t)}{2} & \frac{3(s^2-1)}{2\sqrt{6}}\frac{3(t^2-1)}{2\sqrt{6}} \end{bmatrix} \tag{2.50}$$

The 2-dimensional hierarchical shape functions obtained after tensor product are arranged in a row vector according to a set pattern as per the numbering shown in figure above. The resulting shape function row vector as per the numbering shown in Figure 2.4 will contain

N = [Four conventional shape functions represented by numbers 1,2,3,4 corresponding to four corner nodes, Shape functions represented by 5,6,7,8 corresponding to four edges, Shape functions represented by number 9 corresponding to inner domain of the element].

2.6.2 The Development of Hierarchical Finite element Method

The displacement u of the hierarchical composite element is defined by nodal displacement u_i and hierarchical displacement variable a_j

$$u = N_i u_i + N_j a_j = \hat{N}\hat{u} \tag{2.51}$$

where, the matrix $\hat{N}$ contains the nodal shape functions N_i (i = 1,..,4) and hierarchical shape functions N_j (j= 5,..,n), where 'n' represents the number of all hierarchical shape functions. The vector $\hat{u}$ contains the nodal displacements u_i (i = 1,..,4) and hierarchical displacement variable a_j (j= 5,..,n) where 'n' represents the number of all hierarchical shape functions.

The element equations can be derived by using the principal of virtual work

$$\delta U_\varepsilon - \delta W = 0 \tag{2.52}$$

The external virtual work is given by

$$\delta W = \delta u^T F^i + \int_V \delta u^T F^B dV + \int_S \delta u^T F^S dS \tag{2.53}$$

where F^i, F^B and F^S are the vectors of nodal forces, body forces and surface forces respectively.

The internal virtual work is given by

$$\delta U_\varepsilon = \int_V \delta \varepsilon^T \sigma dV \tag{2.54}$$

where σ is the stress tensor.

The virtual displacement and strains are defined as follows

$$\begin{aligned} \delta u &= \hat{N} \delta \hat{u} \\ \delta \varepsilon &= \hat{B} \delta \hat{u} \end{aligned} \tag{2.55}$$

where $\hat{B}$ represents the strain displacement matrix

$$\hat{B}=\begin{bmatrix} N_{1,x} & 0 & 0 & 0 & 0 & . & . & N_{9,x} & 0 & 0 & 0 & 0 \\ 0 & N_{1,y} & 0 & 0 & 0 & . & . & 0 & N_{9,y} & 0 & 0 & 0 \\ N_{1,y} & N_{1,x} & 0 & 0 & 0 & . & . & N_{9,y} & N_{9,x} & 0 & 0 & 0 \\ 0 & 0 & 0 & N_{1,x} & 0 & . & . & 0 & 0 & 0 & N_{9,x} & 0 \\ 0 & 0 & 0 & 0 & N_{1,y} & . & . & 0 & 0 & 0 & 0 & N_{9,y} \\ 0 & 0 & 0 & N_{1,y} & N_{1,x} & . & . & 0 & 0 & 0 & N_{9,y} & N_{9,x} \\ 0 & 0 & N_{1,y} & 0 & -N_1 & . & . & 0 & 0 & N_{9,y} & 0 & -N_9 \\ 0 & 0 & N_{1,x} & -N_1 & 0 & . & . & 0 & 0 & N_{9,x} & -N_9 & 0 \end{bmatrix}$$

Substituting Equation (2.55) into Equation (2.52), the principal of virtual work becomes

$$F^i + \int_V \hat{N}^T F^B dV + \int_S \hat{N}^T F^S dS = \int_V \hat{B}^T C \hat{B} dV \hat{u} \tag{2.56}$$

In the absence of body forces and nodal concentrated forces, when there is only surface forces Equation (2.56) becomes

$$\int_S \delta u^T F^S dS = \int_V \hat{B}^T C \hat{B} dV \hat{u} \tag{2.57}$$

The element stiffness matrix

$$\mathrm{K} = \int_V \hat{B}^T C \hat{B} dV \tag{2.58}$$

2.7 Validation of Hierarchical Finite Element Formulation

Example 2.3

The correctness of the formulation and program is checked by considering the bending analysis of a 96 ply symmetric cross-ply rectangular laminate $[0/90]_{24s}$ with dimensions

0.55 by 0.55 meters and subjected to a uniform surface load of 100 Pa with one side (x = 0) fully clamped and other sides free (CFFF).The material used is NCT-301 graphite/ epoxy.

Since in Section 2.5.3 we have verified the correctness of the conventional FEM program for CCCC and SSSS boundary conditions, so using that program this time for CFFF boundary conditions, the results of transverse deflection at the top right corner node of the plate given in Example 2.3 are compared with the results of HFEM.

The results obtained using conventional FEM

The value of transverse deflection at the top right corner node of the laminated plate as described in Example 2.3, using a mesh of 10 by 10 elements of conventional FEM is

$$w_0 = \quad 9.9048 \times 10^{-5} \quad \text{meters}$$

The results obtained using HFEM

The value of transverse deflection at the top right corner node of the laminated plate as described in Example 2.3, using one element with four hierarchical shape functions is given as

$$w_0 = \quad 9.9172 \times 10^{-5} \quad \text{meters}$$

Example 2.4

The correctness of the formulation and program is checked by considering the bending analysis of a 96 ply symmetric cross-ply rectangular laminate $[0/90]_{24s}$ of dimensions 0.55 by 0.55 meters and subjected to a uniform surface load of 1KPa with one side fully clamped (CFFC). The material used is NCT-301 graphite/epoxy.

Again using the Conventional FEM program as verified in Section 2.5.3, this time for CFFC boundary conditions, the results of transverse deflection at the top right corner node of the plate given in Example 2.3 are compared with the results of HFEM.

The results obtained using Conventional FEM

The value of transverse deflection at the top right corner node of the laminated plate as described in Example 2.4, using a mesh of 100 elements with 10 in each direction, in the conventional FEM is

$$w_0 = \quad 6.3186 \times 10^{-4} \quad \text{meters}$$

The results obtained using HFEM

The value of transverse deflection at the top right corner node of the laminated plate as described in Example 2.4, using one element with four hierarchical shape functions is given as

$$w_0 = \quad 6.2769 \times 10^{-4} \quad \text{meters}$$

2.8 Conclusions

Hierarchical FEM has been applied for static analysis of laminated composite plates. The results are compared with that of the conventional FEM and Ritz solutions based on classical laminate theory as well as first order shear deformation theory. Four hierarchical shape functions are included corresponding to each of the x and y directions. Tensor product of the vectors in two directions gives 36 shape functions, out of which 4 shape functions corresponding to four corner nodes are the conventional shape functions. The remaining 32 shape functions are distributed as 4 along each side and 16 inside the element. The static deflection at a desired node obtained using HFEM with one element having (36 × 5 =) 180 degrees of freedom gives approximately the same value as that obtained using conventional FEM with 10 elements in each x and y directions, with each element having 9 nodes, which gives 21 nodes in each direction and each node having 5 degrees of freedom, which gives (441 × 5 =) 2205 degrees of freedom. In conventional FEM, the continuity of displacement and slope is enforced at the common nodes across the elements' interface. The stresses in a plate are directly proportional to the rate of change of slope of the plate. The continuity of the rate of change of slope is not enforced across the elements' interface in the conventional FEM. As the number of elements are increased in the mesh to refine the solution, more and more discontinuities result in the model across the elements' interfaces. In hierarchical FEM, not only the displacement and slope continuity is satisfied but also the number of element interfaces are significantly reduced which helps to avoid the discontinuities in the values of stresses in the finite element model.

Chapter 3

Modal Analysis of Laminated Plates using Hierarchical Finite Element Formulation

3.1 Introduction

It is very essential to know the behavior of a composite plate under dynamic loading because it can cause serious damage in composite plates e.g. matrix cracking, fiber cracking and delamination. Many researchers have carried out extensive study of dynamic response of isotropic plates. Only a few have carried out investigations on laminated composite plates. Most of the studies provide analytical and semi-analytical solutions, which are based on classical laminate plate theory neglecting the effects of shear deformation and rotary inertia. As a result the free vibration frequencies calculated by using the thin plate theory are higher than those obtained by Mindlin Plate Theory (in which the transverse shear and rotary inertia effects are included). The deviation increases with increasing mode number. Therefore, in order to get the reliable prediction of natural frequencies of high modulus laminated composite plates, shear deformable theories become necessary to use. A number of shear deformable theories have been used till date. In the present study, the FSDT has been employed in the vibration analysis of the laminated composite plates.

3.2 Equations of Motion

When time is taken into account, the general displacement field at a point (x,y,z) at the instant t, for the First-order Shear Deformation Theory becomes

$$u(x,y,z,t) = u_0(x,y,t) + z\psi_x(x,y,t) \tag{3.1a}$$

$$v(x,y,z,t) = v_0(x,y,t) + z\psi_y(x,y,t) \tag{3.1b}$$

$$w(x,y,z,t) = w_0(x,y,t) \tag{3.1c}$$

The displacement field can further be written in the form as given below where ω is the angular frequency of the plate's vibration.

$$u_0(x,y,t) = U_0(x,y)e^{i\omega t} \tag{3.2a}$$

$$v_0(x,y,t) = V_0(x,y)e^{i\omega t} \tag{3.2b}$$

$$w_0(x,y,t) = W_0(x,y)e^{i\omega t} \tag{3.2c}$$

$$\psi_x(x,y,t) = \Psi_x(x,y)e^{i\omega t} \tag{3.2d}$$

$$\psi_y(x,y,t) = \Psi_y(x,y)e^{i\omega t} \tag{3.2e}$$

Corresponding strain field and the constitutive relations are as given in Equation (2.2) and (2.3) respectively. In the absence of body forces, the equations of motion associated with the given plate are [26]

$$\partial N_x / \partial x + \partial N_{xy} / \partial y = \rho_s \partial^2 u / \partial t^2 \tag{3.3a}$$

$$\partial N_{xy} / \partial x + \partial N_y / \partial y = \rho_s \partial^2 v / \partial t^2 \tag{3.3b}$$

$$\partial Q_x / \partial x + \partial Q_y / \partial y = \rho_s \partial^2 w / \partial t^2 \tag{3.3c}$$

$$\partial M_x / \partial x + \partial M_{xy} / \partial y - Q_x = I \partial^2 \psi_x / \partial t^2 \tag{3.3d}$$

$$\partial M_{xy} / \partial x + \partial M_y / \partial y - Q_y = I \partial^2 \psi_y / \partial t^2 \tag{3.3e}$$

where (N_x, N_y, N_{xy}) and (M_x, M_y, M_{xy}) are Force and Moment resultants as given in Equation (2.4) in Chapter 2 and Translational Inertia (ρ_s) and Rotary Inertia (I) coefficients are as given in Equation (3.4).

$$(\rho_s, I) = \int_{-h/2}^{h/2} (1, z^2) \rho^m dz \tag{3.4}$$

where ρ^m is the material density of the layer 'm'.

For the finite element formulation, the variational form of Equation (3.3) is required. So one needs to find the Strain Energy and Kinetic Energy associated with the plate under study.

3.3 Approximate Solution for Specially Orthotropic Symmetric Composite Laminate by Ritz Method.

In this section the approximate solution in conjunction with Ritz method is discussed. In the case of specially orthotropic and symmetric composite laminate, using FSDT, the strain energy is as given in Equation (3.5).

$$U_d = \frac{1}{2}\iint\{D_{11}\left(\frac{\partial \psi_x}{\partial x}\right)^2 + D_{22}\left(\frac{\partial \psi_y}{\partial y}\right)^2 + D_{66}\left(\frac{\partial \psi_x}{\partial y}\right)^2 + D_{66}\left(\frac{\partial \psi_y}{\partial x}\right)^2 + 2D_{12}\frac{\partial \psi_x}{\partial x}\frac{\partial \psi_y}{\partial y}$$
$$+ 2D_{66}\frac{\partial \psi_x}{\partial y}\frac{\partial \psi_y}{\partial x} + A_{44}\left(\frac{\partial w}{\partial y}\right)^2 + A_{55}\left(\frac{\partial w}{\partial x}\right)^2 + A_{44}(\psi_y)^2 + A_{55}(\psi_x)^2 + 2A_{45}\frac{\partial w}{\partial x}\frac{\partial w}{\partial y}$$
$$+ 2A_{45}\frac{\partial w}{\partial y}\psi_x + 2A_{44}\frac{\partial w}{\partial y}\psi_y + 2A_{45}\frac{\partial w}{\partial x}\psi_y + 2A_{55}\frac{\partial w}{\partial x}\psi_x + 2A_{45}\psi_x\psi_y\}dA$$

(3.5)

The kinetic energy for the specially orthotropic and symmetric composite laminate, considering the shear deformation and rotary inertia effect is as given in Equation (3.6).

$$T = \frac{1}{2}\int_{\Omega}\left\{\rho_s\left[\left(\frac{\partial u}{dt}\right)^2 + \left(\frac{\partial v}{dt}\right)^2 + \left(\frac{\partial w}{dt}\right)^2\right] + I\left[\left(\frac{\partial \psi_x}{dt}\right)^2 + \left(\frac{\partial \psi_y}{dt}\right)^2\right]\right\}dAdt \tag{3.6}$$

$$= \frac{1}{2}\int_{\Omega}\left\{\rho_s\left[\left(\frac{\partial u_0}{dt} + z\frac{\partial \psi_x}{dt}\right)^2 + \left(\frac{\partial v_0}{dt} + z\frac{\partial \psi_y}{dt}\right)^2 + \left(\frac{\partial w_0}{dt}\right)^2\right] + I\left[\left(\frac{\partial \psi_x}{dt}\right)^2 + \left(\frac{\partial \psi_y}{dt}\right)^2\right]\right\}dAdt$$

(3.7)

The term inside the integral becomes

$$\left[\rho_s\left(\frac{\partial u_0}{dt}\right)^2 + \rho_s z^2\left(\frac{\partial \psi_x}{dt}\right)^2 + \rho_s 2z\frac{\partial u_0}{dt}\frac{\partial \psi_x}{dt} + \rho_s\left(\frac{\partial v_0}{dt}\right)^2 + \rho_s z^2\left(\frac{\partial \psi_y}{dt}\right)^2 + \rho_s 2z\frac{\partial v_0}{dt}\frac{\partial \psi_y}{dt} + \rho_s\left(\frac{\partial w_0}{dt}\right)^2\right]$$
$$+ I\left[\left(\frac{\partial \psi_x}{dt}\right)^2 + \left(\frac{\partial \psi_y}{dt}\right)^2\right]$$

(3.8)

which can also be written as:

$$\rho_s\left(\frac{\partial u_0}{dt}\right)^2+\rho_s z^2\left(\frac{\partial \psi_x}{dt}\right)^2+\rho_s 2z\frac{\partial u_0}{dt}\frac{d\psi_x}{dt}+\rho_s\left(\frac{\partial v_0}{dt}\right)^2+\rho_s z^2\left(\frac{\partial \psi_y}{dt}\right)^2+\rho_s 2z\frac{\partial v_0}{dt}\frac{\partial \psi_y}{dt}+\rho_s\left(\frac{\partial w_0}{dt}\right)^2$$

$$+I\left(\frac{\partial \psi_x}{dt}\right)^2+I\left(\frac{\partial \psi_y}{dt}\right)^2 \tag{3.9}$$

Finally the expression for kinetic energy neglecting in-plane velocities becomes

$$T=\frac{1}{2}\int_{\Omega}\left\{-e^{2iwt}\rho_s\omega^2\left(z^2{\psi_x}^2+z^2{\psi_y}^2+{w_o}^2\right)-Ie^{2iwt}\omega^2\left({\psi_x}^2+{\psi_y}^2\right)\right\}dA \tag{3.10}$$

Maximum kinetic energy is given by

$$T_{\max}=\frac{1}{2}\int_{\Omega}\left\{\rho_s\omega^2\left(z^2{\psi_x}^2+z^2{\psi_y}^2+{w_o}^2\right)-I\omega^2\left({\psi_x}^2+{\psi_y}^2\right)\right\}dA \tag{3.11}$$

$$T_{\max}=\frac{1}{2}\int_{\Omega}\left\{\omega^2(I+\rho_s z^2){\psi_x}^2+\omega^2(I+\rho_s z^2){\psi_y}^2+\rho_s\omega^2{w_0}^2\right\}dA \tag{3.12}$$

In the absence of transverse loads, the maximum energy function reduces to

$$U_{d\max} - T_{\max} = \frac{1}{2}\int_{x=0}^{a}\int_{y=0}^{b}[\{D_{11}\left(\frac{\partial\psi_x}{\partial x}\right)^2 + D_{22}\left(\frac{\partial\psi_y}{\partial y}\right)^2 + D_{66}\left(\frac{\partial\psi_x}{\partial y}\right)^2 + D_{66}\left(\frac{\partial\psi_y}{\partial x}\right)^2$$
$$+ 2D_{12}\frac{\partial\psi_x}{\partial x}\frac{\partial\psi_y}{\partial y} + 2D_{66}\frac{\partial\psi_x}{\partial y}\frac{\partial\psi_y}{\partial x} + A_{44}\left(\frac{\partial w}{\partial y}\right)^2 + A_{55}\left(\frac{\partial w}{\partial x}\right)^2 + A_{44}(\psi_y)^2 + A_{55}(\psi_x)^2$$
$$+ 2A_{45}\frac{\partial w}{\partial x}\frac{\partial w}{\partial y} + 2A_{45}\frac{\partial w}{\partial y}\psi_x + 2A_{44}\frac{\partial w}{\partial y}\psi_y + 2A_{45}\frac{\partial w}{\partial x}\psi_y + 2A_{55}\frac{\partial w}{\partial x}\psi_x + 2A_{45}\psi_x\psi_y\}$$
$$- \{\omega^2(I + \rho_s z^2){\psi_x}^2 + \omega^2(I + \rho_s z^2){\psi_y}^2 + \rho_s\omega^2{w_0}^2\}]dA$$

(3.13)

The approximate solutions are sought in the usual form of a double series.

$$w_o(x,y) = \sum_{m=1}^{M}\sum_{n=1}^{N} A_{mn}X_m(x)Y_n(y) \tag{3.14a}$$

$$\psi_x(x,y) = \sum_{m=1}^{M}\sum_{n=1}^{N} B_{mn}P_m(x)Q_n(y) \tag{3.14b}$$

$$\psi_y(x,y) = \sum_{m=1}^{M}\sum_{n=1}^{N} C_{mn}S_m(x)T_n(y) \tag{3.14c}$$

where the functions $X_m, Y_n, P_m, Q_n, S_m, T_n$ are chosen so as to satisfy the boundary conditions along the edges x = 0, x=a and y=0, y=b. The coefficients A_{mn}, B_{mn}, C_{mn} are determined by stationarity condition which can be written as

$$\frac{\partial}{\partial A_{mn}}\left[\tilde{U}_{d\max} - \tilde{T}_{\max}\right] = 0 \quad \text{or} \quad \frac{\partial\tilde{U}_{d\max}}{\partial A_{mn}} = \frac{\partial\tilde{T}_{\max}}{\partial A_{mn}} \tag{3.15a}$$

$$\frac{\partial}{\partial B_{mn}}\left[\tilde{U}_{d\max} - \tilde{T}_{\max}\right] = 0 \quad \text{or} \quad \frac{\partial\tilde{U}_{d\max}}{\partial B_{mn}} = \frac{\partial\tilde{T}_{\max}}{\partial B_{mn}} \tag{3.15b}$$

$$\frac{\partial}{\partial C_{mn}}\left[\tilde{U}_{d\max} - \tilde{T}_{\max}\right] = 0 \quad \text{or} \quad \frac{\partial\tilde{U}_{d\max}}{\partial C_{mn}} = \frac{\partial\tilde{T}_{\max}}{\partial C_{mn}} \tag{3.15c}$$

where $\widetilde{U}_{d\max}$ and $\widetilde{T}_{\max}$ are the maximum strain energy and the maximum kinetic energy associated with the laminate under study, obtained by substituting the approximate expression (3.13) for the deflection into the Equations (3.4) and (3.11). We can calculate the terms corresponding to kinetic energy and strain energy by taking the partial derivative of kinetic energy and strain energy with respect to A_{mn}, B_{mn}, C_{mn}.

Terms corresponding to strain energy

There are 16 terms added inside the integral in the expression of strain energy. The integral of the various terms in the expression of the strain energy can be written as sum of the integrals of the individual terms. The left hand side of the Equations (3.14a), (3.14b) and (3.14c) can be obtained by substituting the assumed solutions from Equation (3.13), into each of these 16 terms, taking their partial derivative with respect to constants A_{mn}, B_{mn}, C_{mn} and then taking the integral of the resulting terms as calculated in Section 2.4.

After substituting the 16 terms the left hand side of the Equation (3.14) can be written in the matrix form as below to solve for the three constants. The number of equations and hence the related constants differ as the values of m and n (number of terms used in approximation functions of the solutions) increases.

In case where m=n=1 the left hand side of Equation (3.15) becomes

$$\begin{bmatrix} a_{11} & b_{11} & c_{11} \\ a_{21} & b_{21} & c_{21} \\ a_{31} & b_{31} & c_{31} \end{bmatrix} \begin{bmatrix} A_1 \\ B_1 \\ C_1 \end{bmatrix} \tag{3.16}$$

In the case where $m = n = 2$ the left hand side of Equation (3.15) becomes

$$\begin{bmatrix} a_{11} & a_{12} & b_{11} & b_{12} & c_{11} & c_{12} \\ a_{21} & a_{22} & b_{21} & b_{22} & c_{21} & c_{22} \\ a_{31} & a_{32} & b_{31} & b_{32} & c_{31} & c_{32} \\ a_{41} & a_{42} & b_{41} & b_{42} & c_{41} & c_{42} \\ a_{51} & a_{52} & b_{51} & b_{52} & c_{51} & c_{52} \\ a_{61} & a_{62} & b_{61} & b_{62} & c_{61} & c_{62} \end{bmatrix} \begin{bmatrix} A_1 \\ A_2 \\ B_1 \\ B_2 \\ C_1 \\ C_2 \end{bmatrix} \tag{3.17}$$

The above matrices can be written in the concise form as below

$$[abc]\{ABC\} \tag{3.18}$$

Terms corresponding to kinetic energy

There are 3 terms added inside the integral in the expression of the kinetic energy. The integral of the various terms in the expression of the strain energy can be written as sum of the integrals of the individual terms. The right hand side of the Equations (3.15a), (3.15b) and (3.15c) can be obtained by substituting the assumed solutions from Equation (3.14), into each of these 16 terms, taking their partial derivative with respect to constants A_{mn}, B_{mn}, C_{mn} and then taking the integral of the resulting terms as in the following.

Term 1

$$\omega^2(I+\rho_s z^2)\psi_x{}^2$$

After substituting the assumed solutions from Equation (3.14)

$$\text{Term 1} = \omega^2(I+\rho_s z^2)\sum_{m=1}^{M}\sum_{n=1}^{N}\sum_{i=1}^{M}\sum_{j=1}^{N}B_{mn}B_{ij}P_mQ_nP_iQ_j$$

and

$$\frac{1}{2}\frac{\partial}{\partial A_{mn}}(Term1) = 0 \tag{3.19a}$$

$$\frac{1}{2}\frac{\partial}{\partial B_{mn}}(Term1) = \omega^2(I+\rho_s z^2)\sum_{i=1}^{M}\sum_{j=1}^{N}B_{ij}P_mQ_nP_iQ_j \tag{3.19b}$$

$$\frac{1}{2}\frac{\partial}{\partial C_{mn}}(Term1) = 0 \tag{3.19c}$$

Integration of non zero term yields

$$\frac{1}{2}\int_{x=0}^{a}\int_{y=0}^{b}\frac{\partial}{\partial B_{mn}}(Term1)dxdy = \omega^2(I+\rho_s z^2)\sum_{i=1}^{M}\sum_{j=1}^{N}B_{ij}\int_{x=0}^{a}P_mP_i dx\int_{y=0}^{b}Q_nQ_j dy \tag{3.20}$$

Term 2

$$\omega^2(I+\rho_s z^2)\psi_y{}^2$$

After substituting the assumed solutions from Equation (3.14)

$$\text{Term 2} = \omega^2(I+\rho_s z^2)\sum_{m=1}^{M}\sum_{n=1}^{N}\sum_{i=1}^{M}\sum_{j=1}^{N}C_{mn}C_{ij}S_mT_nS_iT_j$$

and

$$\frac{1}{2}\frac{\partial}{\partial A_{mn}}(Term2) = 0 \tag{3.21a}$$

$$\frac{1}{2}\frac{\partial}{\partial B_{mn}}(Term2)=0 \tag{3.21b}$$

$$\frac{1}{2}\frac{\partial}{\partial C_{mn}}(Term2)=\omega^2(I+\rho_s z^2)\sum_{i=1}^{M}\sum_{j=1}^{N}C_{ij}S_mT_nS_iT_j \tag{3.21c}$$

Integration of non zero term yields

$$\frac{1}{2}\int_{x=0}^{a}\int_{y=0}^{b}\frac{\partial}{\partial C_{mn}}(Term2)dxdy = \omega^2(I+\rho_s z^2)\sum_{i=1}^{M}\sum_{j=1}^{N}C_{ij}\int_{x=0}^{a}S_mS_i dx\int_{y=0}^{b}T_nT_j dy \tag{3.22}$$

Term 3

$\rho_s\omega^2 w_0{}^2$

After substituting the assumed solutions from Equation (3.14)

$$\text{Term 3} = \rho_s\omega^2\sum_{m=1}^{M}\sum_{n=1}^{N}\sum_{i=1}^{M}\sum_{j=1}^{N}A_{mn}A_{ij}X_mY_nX_iY_j$$

and

$$\frac{1}{2}\frac{\partial}{\partial A_{mn}}(Term3) = \rho_s\omega^2\sum_{i=1}^{M}\sum_{j=1}^{N}A_{ij}X_mY_nX_iY_j \tag{3.23a}$$

$$\frac{1}{2}\frac{\partial}{\partial B_{mn}}(Term3)=0 \tag{3.23b}$$

$$\frac{1}{2}\frac{\partial}{\partial C_{mn}}(Term3)=0 \tag{3.23c}$$

Integration of non zero term yields

$$\frac{1}{2}\int_{x=0}^{a}\int_{y=0}^{b}\frac{\partial}{\partial A_{mn}}(Term3)dxdy = \rho_s\omega^2\sum_{i=1}^{M}\sum_{j=1}^{N}A_{ij}\int_{x=0}^{a}X_mX_i dx\int_{y=0}^{b}Y_nY_j dy \tag{3.24}$$

After substituting the 3 terms as calculated above, the right hand side of Equation (3.15)

can be written in the matrix form as below to solve for the three constants. The number of equations and hence the related constants differ as the values of m and n (number of terms used in approximation functions of the solutions) increases.

In case where m=n=1 the right hand side of Equation (3.15) becomes

$$\begin{bmatrix} \alpha_{11} & 0 & 0 \\ 0 & \beta_{22} & 0 \\ 0 & 0 & \chi_{33} \end{bmatrix} \begin{bmatrix} A_1 \\ B_1 \\ C_1 \end{bmatrix} \tag{3.25}$$

First matrix contains the terms of kinetic energy. The second matrix consists of the vector of constants which are to be determined.

In the case where $m = n = 2$ the right hand side of Equation (3.15) becomes

$$\begin{bmatrix} \alpha_{11} & \alpha_{12} & 0 & 0 & 0 & 0 \\ \alpha_{21} & \alpha_{22} & 0 & 0 & 0 & 0 \\ 0 & 0 & \beta_{11} & \beta_{12} & 0 & 0 \\ 0 & 0 & \beta_{21} & \beta_{22} & 0 & 0 \\ 0 & 0 & 0 & 0 & \chi_{11} & \chi_{12} \\ 0 & 0 & 0 & 0 & \chi_{21} & \chi_{22} \end{bmatrix} \begin{bmatrix} A_1 \\ A_2 \\ B_1 \\ B_2 \\ C_1 \\ C_2 \end{bmatrix} \tag{3.26}$$

The above matrices can be written in the concise form as below

$$[\alpha\beta\chi]\{ABC\} \tag{3.27}$$

From Equations (3.18) and (3.27), the Equation (3.15) can be written as

$$\{[abc] - [\alpha\beta\chi]\}\{ABC\} = 0 \tag{3.28}$$

Now the system of Equations (3.28) is homogenous and a non-zero solution is obtained when the determinant of the system is zero, i.e.

$$\text{Determinant}\left(\{[abc]-[\alpha\beta\chi]\}\right)=0 \tag{3.29}$$

The above condition leads to an equation whose solutions are the natural frequencies of flexural vibration of the plate. The lowest value of natural frequency is important from the structural design point of view.

3.3.1 Validation of Ritz Solution

The results from Ritz Method using FSDT for simply supported boundary conditions (SSSS) are compared with the solutions based on CLPT given in reference [1].

Example 3.1

The correctness of the formulation and program is checked by considering the modal analysis of $[0/90]_{24s}$ laminate which is a 96 ply symmetric cross-ply rectangular laminate of dimensions 0.55 by 0.55 meters with all sides simply supported. The composite material is NCT-301 graphite/epoxy. The material properties are given below in Table 3.1.

E_1	144 GPa
E_2, E_3	12.14 GPa
ν_{21}, ν_{31}	0.017
ν_{23}	0.458
G_{12}, G_{13}	4.48 GPa
G_{23}	3.2 GPa
ρ	1660.8 kg/m^3

Table 3.1 Material properties of NCT-301 graphite/epoxy [47]

Approximate solution by Ritz method using CLPT

$$\omega_{mn} = \frac{1}{a^2}\sqrt{\frac{D_{11}}{\rho_s}}\sqrt{c_1^{\,4} + 2(\alpha_{12} + 2\alpha_{66})R^2 c_2 + \alpha_{22}R^4 c_3^{\,4}} \tag{3.30}$$

where

$$\alpha_{12} = D_{12}/D_{11}, \qquad \alpha_{22} = D_{22}/D_{11}, \qquad \alpha_{66} = D_{66}/D_{11} \tag{3.31}$$

$$c_1 = \pi, \quad c_2 = \pi^4, \quad c_3 = \pi \tag{3.32}$$

$$a = 0.55, R = 1 \tag{3.33}$$

and

$$\rho_s = 1660.8 \times (\text{Thickness of laminate})$$

$$= 1660.8 \times (\text{Thickness of each layer} \times \text{Number of layers of the laminate})$$

$$= 1660.8 \times (1.25 \times 10^{-4}) \times 96 \tag{3.34}$$

After substituting the values from Equations (3.31), (3.32), (3.33) and (3.34) in the Equation (3.30) the value of the first (lowest) natural frequency of the plate under study is

$$\omega_{mn} = 1.1750 \times 10^3 \text{ rad/s}$$

Ritz solution using FSDT

The value of the lowest natural frequency of the simply supported (SSSS) laminated rectangular plate under study for M = N = 4 using Ritz method based on FSDT is:

$$\omega_{mn} = 1.1487 \times 10^3 \text{ rad/s}$$

3.4 Analysis using Conventional Finite Element Formulation

3.4.1 Interpolation Functions

The first variation of the Lagrangian L (= T - V) i.e. Hamilton's principle leads to the equation of motion (3.3) expressed in terms of the displacements and slope functions. Here V denotes the total potential energy which is sum of the strain energy and the energy due to applied loads of the plate. This variational form is convenient for the finite element formulation. Since the primary interest here is in the free vibration analysis, the potential energy due to applied loads is zero.

Let the domain Ω be divided into a set of finite elements. The restriction of the Lagrangian functional 'L' to the finite element Ω_e is denoted by L_e.

$$L = \sum_{e=1}^{N} L_e\left(u_0^{\,e}, v_0^{\,e}, w^e, \psi_x^{\,e}, \psi_y^{\,e}\right) \tag{3.35}$$

where, N is the total number of finite element in the mesh.

$$u_o = \sum_{i=1}^{9} N_i u_{oi};\ v_o = \sum_{i=1}^{9} N_i v_{oi};\ w_o = \sum_{i=1}^{9} N_i w_{oi};\ \psi_x = \sum_{i=1}^{9} N_i \psi_{xi};\ \psi_y = \sum_{i=1}^{9} N_i \psi_{yi} \tag{3.36}$$

$$\begin{bmatrix} u_o \\ v_o \\ w_o \\ \psi_x \\ \psi_y \end{bmatrix} = \sum_{i=1}^{9} \begin{bmatrix} N_i & 0 & 0 & 0 & 0 \\ 0 & N_i & 0 & 0 & 0 \\ 0 & 0 & N_i & 0 & 0 \\ 0 & 0 & 0 & N_i & 0 \\ 0 & 0 & 0 & 0 & N_i \end{bmatrix} \begin{bmatrix} u_{oi} \\ v_{oi} \\ w_{oi} \\ \psi_{xi} \\ \psi_{yi} \end{bmatrix} \tag{3.37}$$

which is of the form,

$$\{u\} = [N]\{d\} \tag{3.38}$$

where

$$\{d\} = [u_1\ v_1\ w_1\ \psi_{x1}\ \psi_{y1} \ldots\ldots\ldots u_9\ v_9\ w_9\ \psi_{x9}\ \psi_{y9}]^T \tag{3.39}$$

where $N_i(x,y)$ are the finite element shape functions. In the present analysis of the plate under study a Mindlin finite element is employed using nine node rectangular elements with the nine shape functions as given in Equation (2.28) in Chapter 2. The resulting element stiffness matrix and mass matrix are of the order of 45 by 45. The same interpolations are employed for all the five fields. Substitution of Equation (3.10) into the first variation δL_e of L_e gives the following set of equations for a typical element Ω_e.

$$[M]\{\ddot{\Delta}\} + [K]\{\Delta\} = \{0\} \tag{3.40}$$

where,

$$\{\Delta\} = \left[\{u_i\}^T, \{v_i\}^T, \{w_i\}^T, \{\psi_{xi}\}^T, \{\psi_{yi}\}^T\right] \tag{3.41}$$

$$[M] = \int_A \rho h [N]^T [N] dA \tag{3.42}$$

$$[K] = \int_A [B]^T [E][B] dA \tag{3.43}$$

where ' ρ ' is the density and 'h' is the thickness of the laminate.

Matrix [B] can be expressed as,

$$[B]_{8x45} = [\partial]_{8x5} [N]_{5x45} \tag{3.44}$$

$$[B]=\begin{bmatrix} N_{1,x} & 0 & 0 & 0 & 0 & . & . & N_{9,x} & 0 & 0 & 0 & 0 \\ 0 & N_{1,y} & 0 & 0 & 0 & . & . & 0 & N_{9,y} & 0 & 0 & 0 \\ N_{1,y} & N_{1,x} & 0 & 0 & 0 & . & . & N_{9,y} & N_{9,x} & 0 & 0 & 0 \\ 0 & 0 & 0 & N_{1,x} & 0 & . & . & 0 & 0 & 0 & N_{9,x} & 0 \\ 0 & 0 & 0 & 0 & N_{1,y} & . & . & 0 & 0 & 0 & 0 & N_{9,y} \\ 0 & 0 & 0 & N_{1,y} & N_{1,x} & . & . & 0 & 0 & 0 & N_{9,y} & N_{9,x} \\ 0 & 0 & N_{1,y} & 0 & -N_1 & . & . & 0 & 0 & N_{9,y} & 0 & -N_9 \\ 0 & 0 & N_{1,x} & -N_1 & 0 & . & . & 0 & 0 & N_{9,x} & -N_9 & 0 \end{bmatrix}$$

3.4.2 Validation of Conventional Finite Element Formulation

Example 3.2

The correctness of the formulation and program is checked by considering the modal analysis of $[0/90]_{24s}$ laminate which is a 96 ply symmetric cross ply rectangular laminate of dimensions 0.55 by 0.55 meters with all sides simply supported. The composite material is NCT-301 graphite/epoxy.

The material properties are given below in Table 3.1.The approximate solution using the Ritz method based on FSDT is as given in Example 3.1

$$\omega = 1.1487\times 10^3 \text{ rad/s}$$

Conventional FEM

The value of first natural frequency of the plate under study using a mesh of 10×10 elements of conventional FEM is

$$\omega = 1.3168\times 10^3 \text{ rad/s}$$

Example 3.3

The correctness of the formulation and program is checked by considering the modal analysis of $[0/90]_{24s}$ laminate which is a 96 ply symmetric cross ply rectangular laminate of dimensions 0.55 by 0.55 meters with all sides clamped. The composite material is NCT-301 graphite/epoxy.

Material Properties of NCT-301 are taken from Table 3.1 given in example 3.1. The approximate solution using the Ritz method is

$$\omega = 2.5427 \times 10^3 \text{ rad/s}$$

Conventional FEM

The value of first natural frequency of the plate under study using a mesh of 10×10 elements in conventional FEM is

$$\omega = 2.532 \times 10^3 \text{ rad/s}$$

Convergence Check for the Conventional Finite Element Solution

The convergence of the solution is checked and the results obtained are as given below for plates of different laminate configurations and different boundary conditions. The lowest natural frequency (ω_{mn}) of laminated composite plate described in Example 3.1 with all sides simply supported (SSSS) is calculated using conventional finite element method based on FSDT for different laminate configurations as given in Table 3.2.

Mesh / Laminate Configuration	2by2 (ω_1)	3by3 (ω_1)	4by4 (ω_1)	5by5 (ω_1)	6by6 (ω_1)
$[0/90]_{24s}$	1.4176×10^3	1.3541×10^3	1.3337×10^3	1.3254×10^3	1.3214×10^3
$[0/90/\pm45]_{12s}$	1.5992×10^3	1.5487×10^3	1.5309×10^3	1.5223×10^3	1.5172×10^3
$[\pm45]_{24s}$	1.7728×10^3	1.7312×10^3	1.7134×10^3	1.7028×10^3	1.6957×10^3
$[\pm45]_{48}$	1.7730×10^3	1.7314×10^3	1.7137×10^3	1.7031×10^3	1.6960×10^3

7by7 (ω_1)	8by8 (ω_1)	9by9 (ω_1)	10by10 (ω_1)
1.3193×10^3	1.3181×10^3	1.3173×10^3	1.3168×10^3
1.5138×10^3	1.5114×10^3	1.5096×10^3	1.5083×10^3
1.6907×10^3	1.6870×10^3	1.6842×10^3	1.6821×10^3
1.6909×10^3	1.6872×10^3	1.6844×10^3	1.6823×10^3

Table 3.2 Convergence of the lowest natural frequency of laminated composite plates with all sides simply supported (SSSS)

The lowest natural frequency (ω_1) of laminated composite plate described in Example 3.1 with all sides clamped (CCCC) is calculated using conventional finite element method based on FSDT for different laminate configurations as given in Table 3.3.

Mesh / Laminate Configuration	2by2 (ω_1)	3by3 (ω_1)	4by4 (ω_1)	5by5 (ω_1)	6by6 (ω_1)
$[0/90]_{24s}$	6179.94	2831.53	2667.48	2598.42	2566.32
$[0/90/\pm 45]_{12s}$	6158.30	2809.48	2648.15	2583.48	2553.33
$[\pm 45]_{24s}$	6131.34	2768.83	2612.05	2551.88	2523.46
$[\pm 45]_{48}$	6131.39	2769.02	2612.33	2552.20	2523.82

7by7 (ω_1)	8by8 (ω_1)	9by9 (ω_1)	10by10 (ω_1)
2549.92	2540.91	2535.66	2532.45
2537.75	2529.06	2523.94	2520.76
2508.39	2499.75	2494.52	2491.20
2508.75	2500.12	2494.89	2491.58

Table 3.3 Convergence of the lowest natural frequency of laminated composite plates with all sides clamped (CCCC)

Mode Shapes

Mode shapes are plotted using surf (P) command in MATLAB, where P is the m × n matrix generated out of eigenvector corresponding to the lowest eigenvalue and hence the lowest natural frequency. In our case a mesh of (10×10 =) 100 elements is used. Since a 9-node rectangular element is used in meshing, the mesh contains (21 × 21 =) 441 nodes. The size of eigenvector is (441×5 =) 2205. The node numbers 1 to 21 which are numbered along the edge x = 0, contribute to the first set of (21×5=) 105 values of eigenvector, node numbers 22 to 42 contribute to the 2nd set of 21 values and so

on. Finally node numbers 421 to 441 contribute to the 21st set of 21 values. Altogether it gives (105×21 =) 2205 values of eigenvector. The eigenvector comprises of the values corresponding to all the five degrees of freedom. In order to plot the mode shapes, first we separate the values corresponding to the 3rd degree of freedom which is the transverse displacement in z-direction. The resulting vector is of size (2205/5 =) 441. It comprises of 21 sets of 21 values. Now these 21 sets of 21 values are arranged in the form of matrix with first set of 21 values becoming the first vector, 2nd set of 21values becoming the 2nd vector and so on. Finally we get a matrix of size 21×21. This is the matrix P used in surf (P) command in MATLAB. Surf (P) creates a 3-dimensional shaded surface from the z-component in matrix P using x = 1: n and y = 1: m where [m, n] = size (P). The surface height specified by P is a single valued function defined over a geometrically rectangular grid.

In all of the following mode shapes in Figures 3.1 and 3.2, the x-axis ranges from 1 to 21 and y-axis ranges from 1 to 21 corresponding to [m, n] which is the size of matrix (P), as explained above. The z-axis gives the surface height in meters.

Mode shapes for CCCC and CFFF boundary conditions

Mode shapes of first six modes of $[0/90]_{24s}$ laminated plate with dimensions given in Example 3.1 and with all sides clamped (CCCC) are as given in Fig.3.1. Mode shapes of first six modes of $[0/90]_{24s}$ laminated plate with dimensions given in Example 3.1 and with one side clamped and others free (CFFF) are as given in Fig 3.2.

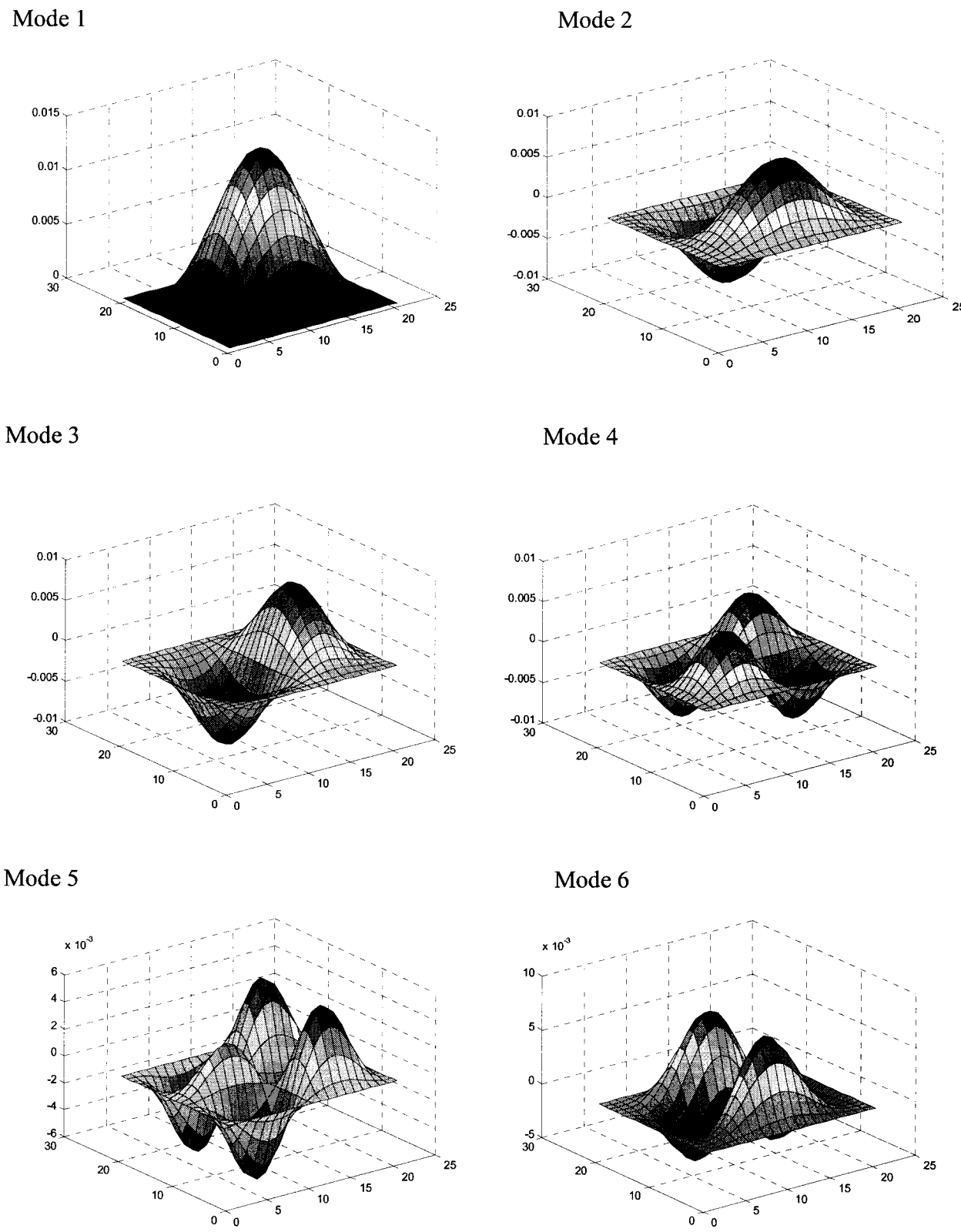

Fig 3.1 First six mode shapes of $[0/90]_{24s}$ laminated plate with all sides clamped

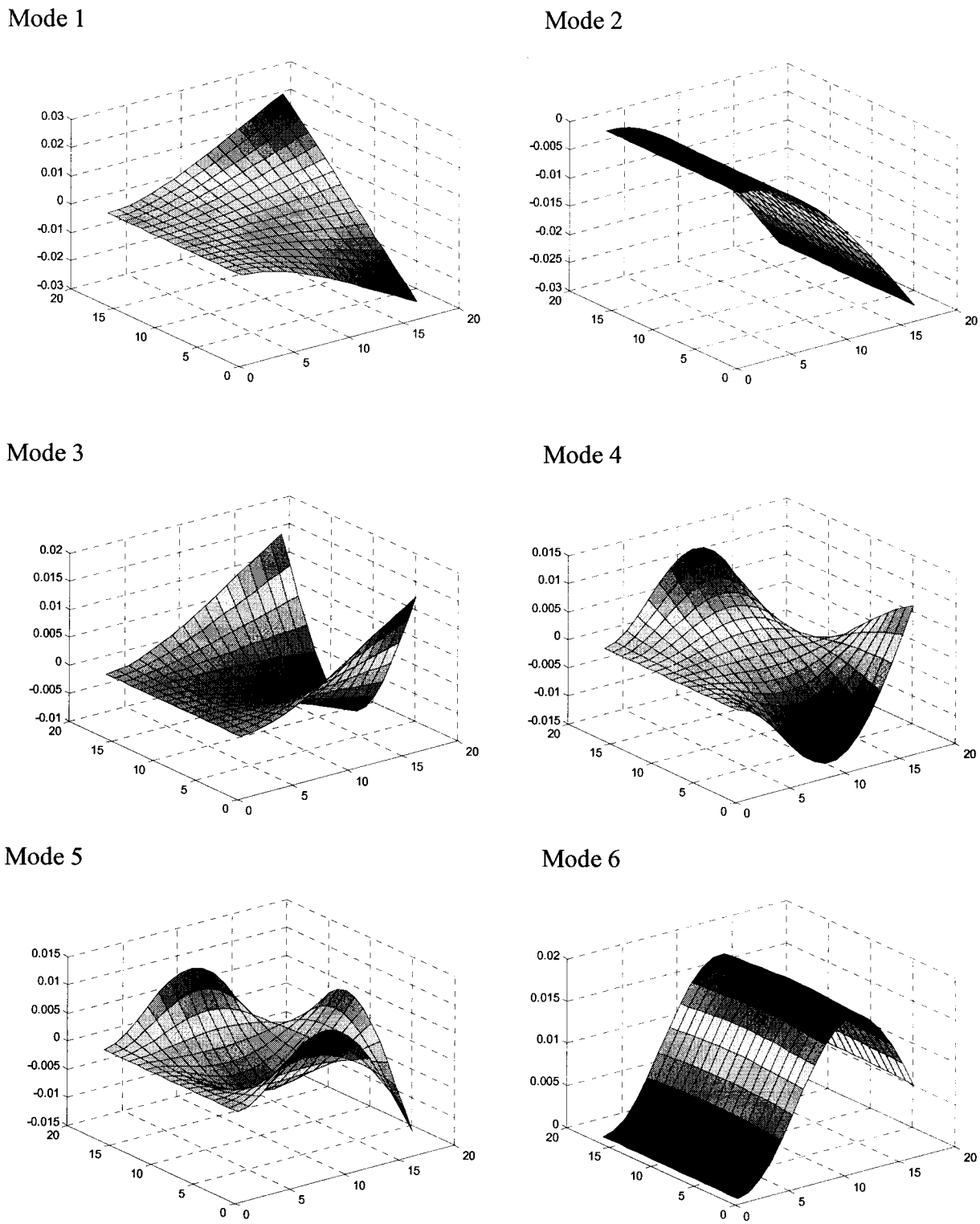

Fig 3.2 First six mode shapes of $[0/90]_{24s}$ laminated plate with CFFF boundary condition

3.5 Hierarchical Finite Element Formulation

In this section, the HFEM developed in Chapter 2 is applied to free vibration analysis of laminated rectangular plates. A fully clamped rectangular symmetric laminated plate is considered. Since very high order polynomials are used as displacement functions, the plate is modeled as only one finite element. The stiffness and mass matrices in the equations of motion are evaluated using symbolic integration in MATLAB environment. The convergence of natural frequencies with increasing number of hierarchical shape functions is analyzed. The natural frequencies obtained using HFEM are compared with those obtained using conventional FEM in Section 3.2. First-order shear deformation theory is employed which takes into account shear deformation and rotary inertia effects.

3.5.1 Stiffness and Mass Matrices

A flat specially orthotropic laminated rectangular plate is considered with edges of the plate as x=0, x =a, y=0, y=b. The displacement fields can be expanded in terms of hierarchical shape functions as below.

$$
\begin{aligned}
u &= N_1 u_1 + N_2 u_2 + N_3 u_3 + N_4 u_4 + \sum_{i=1}^{p} N_{hi} u_{hi} \\
v &= N_1 v_1 + N_2 v_2 + N_3 v_3 + N_4 v_4 + \sum_{i=1}^{p} N_{hi} v_{hi} \\
w &= N_1 w_1 + N_2 w_2 + N_3 w_3 + N_4 w_4 + \sum_{i=1}^{p} N_{hi} w_{hi} \\
\psi_x &= N_1 \psi_{x1} + N_2 \psi_{x2} + N_3 \psi_{x3} + N_4 \psi_{x4} + \sum_{i=1}^{p} N_{hi} \psi_{xhi} \\
\psi_y &= N_1 \psi_{y1} + N_2 \psi_{y2} + N_3 \psi_{y3} + N_4 \psi_{y4} + \sum_{i=1}^{p} N_{hi} \psi_{yhi}
\end{aligned}
\tag{3.45}
$$

Where N_1, N_2, N_3 and N_4 are the conventional shape functions for 4 node finite element, Nh_i are the hierarchical shape functions. Equation (3.45) can be written in precise form as

$$\{u\} = [N]\{q\} \tag{3.46}$$

where [N] is the shape function matrix, and {q} is the generalized displacements matrix.

The equations of motion of the plate are obtained by substituting Equation (3.46) into the expressions for the strain energy and kinetic energy and then employing Lagrange's equations.

Substituting Equation (3.46) into Equation (3.5), which is the expression for strain energy and Equation (3.12), which is the expression for kinetic energy, and making use of Lagrange's equations [40], the following equations of motion are obtained.

$$[M]\{\ddot{q}\} + [K]\{q\} = 0 \tag{3.47}$$

$$[M] = \int_A \rho h [N]^T [N] dA \tag{3.48}$$

$$[K] = \int_A [B]^T [E][B] dA \tag{3.49}$$

where M is the mass matrix and K is the stiffness matrix The integrals in mass matrix and stiffness matrix are evaluated using symbolic integration.

3.5.2 Validation of Hierarchical Finite Element Formulation

Example 3.4

The correctness of the formulation and program is checked by considering the modal analysis of a 96 ply symmetric cross ply rectangular laminate of dimensions 0.30 by 0.30 meters and with all sides fully clamped (CCCC). The composite material is NCT-301 graphite/epoxy. Material Properties of NCT-301 are taken from Table 3.1 given in Example 3.1

The results obtained using Ritz method based on CLPT

The approximate value of first natural frequency of the laminated plate under study, using Ritz Method based on CLPT is given by

$$\omega_{mn} = \frac{1}{a^2}\sqrt{\frac{D_{11}}{\rho_s}}\sqrt{c_1^{\,4} + 2(\alpha_{12} + 2\alpha_{66})R^2 c_2 + \alpha_{22}R^4 c_3^{\,4}} \tag{3.50}$$

where

$$\alpha_{12} = D_{12}/D_{11}, \qquad \alpha_{22} = D_{22}/D_{11}, \qquad \alpha_{66} = D_{66}/D_{11} \tag{3.51}$$

$$c_1 = 4.730, \quad c_2 = 151.30, \quad c_3 = 4.730 \tag{3.52}$$

$$a = 0.30,\ R = 1 \tag{3.53}$$

and

$$\rho_s = 1660.8 \times (\text{Thickness of laminate})$$

$$= 1660.8 \times (\text{Thickness of each layer} \times \text{Number of layers of the laminate})$$

$$= 1660.8 \times (1.25 \times 10^{-4}) \times 96 \tag{3.54}$$

Substituting the values from Equations (3.51), (3.52), (3.53) and (3.54) into Equation (3.50) the lowest natural frequency is

$$\omega_{mn} = 8.5462 \times 10^3$$

The results obtained using HFEM

The value of lowest natural frequency of the laminated plate under study, using 4 Hierarchical shape functions is given as below.

$$\omega_{mn} = 8.3714 \times 10^3$$

3.6 Conclusions

Conventional finite element formulation has been developed using first order shear deformation theory for free vibration analysis and the values of lowest natural frequencies have been determined. The results are compared with that of the Ritz method. Hierarchical finite element formulation has also been developed and applied for modal analysis of rectangular laminated plates. The values of lowest natural frequencies are determined using hierarchical finite element method and the results are compared with that of the Ritz method. The accuracy of HFEM with one element having 180 degrees of freedom as explained in Section 2.8 is approximately the same as that of the conventional FEM with 100 elements having 2205 degrees of freedom. So less number of degrees of freedom is required using HFEM than using conventional FEM for providing almost the same results.

Chapter 4

Parametric Study of Composite Laminates

4.1 Introduction

In the previous chapters, the conventional and hierarchical finite element formulations for static and modal analyses of laminated rectangular composite plates have been developed. The HFEM was applied first to conduct the static analysis and then the modal analysis.

We will now conduct a comprehensive parametric study of the static and dynamic response of laminated composite plates using conventional and hierarchical finite element analyses. Parametric study is conducted on NCT-301 graphite/epoxy rectangular laminated plate. The properties are listed in Table 4.1. The specifications of composite laminate and the geometric properties are detailed in individual cases of parametric study. All the problems are solved using both conventional and hierarchical finite element formulations.

4.2 Parametric Study on Static Response of Rectangular Laminated Plate

Problem Description: A rectangular laminated composite plate has the following geometric properties: Length (a) = width (b) = 0.55 m, Thickness of each ply = 0.125 mm, Number of plies= 96.

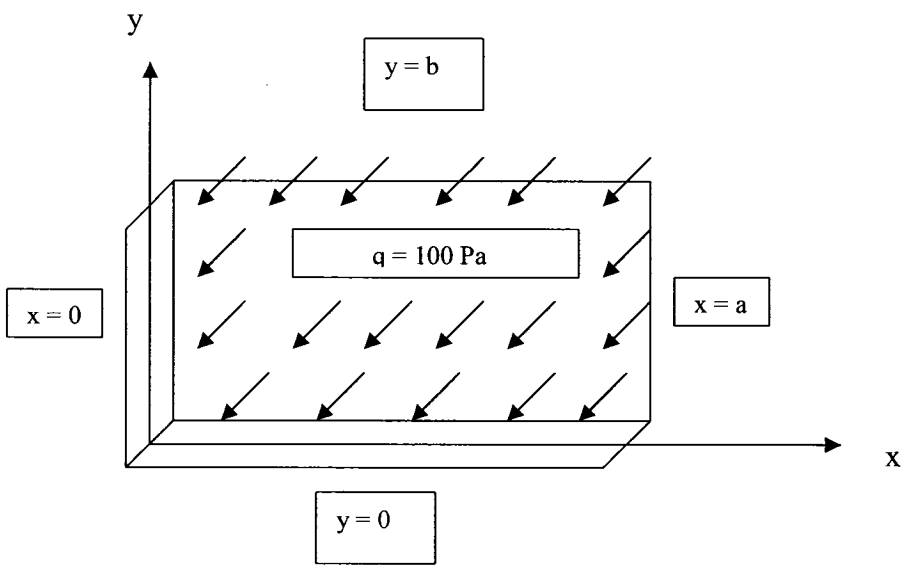

Figure 4.1 Rectangular laminated NCT-301 graphite/epoxy composite plate

Uniformly distributed load is applied on the rectangular plate and central deflection is determined for all possible changes that can be performed on the composite plates such as, the change in the boundary conditions, the change in the laminate configurations, the change in aspect ratio, and the change in elastic modulus to shear modulus (E/G) ratio. The static analysis is performed using both the formulations,

conventional and hierarchical as described in the previous chapters. Tables and Figures are provided for comparison and commenting purposes.

Density ($\rho, kg/m^3$)	1660.80
Longitudinal Modulus E_1 (GPa)	144
Transverse Modulus E_2 (GPa)	12.14
E_3	$(=E_2)$
In Plane Shear Modulus G_{12} (GPa)	4.48
Shear Modulus G_{13} (GPa)	$(=G_{12})$
Out of Plane Shear Modulus G_{23} (GPa)	3.20
Poisson's Ratio (ν_{12})	0.21
ν_{21}	0.017

Table 4.1 Mechanical properties of NCT-301 graphite/epoxy composite material [47]

4.2.1 The Effect of Boundary Conditions on Static Deflection

To consider the effects of different boundary conditions on the static deflection of the laminated plate shown in Figure 4.1, different laminate configurations under CCCC and SSSS boundary conditions are taken and the values of the maximum central deflection are obtained under 100 Pa uniformly distributed load using the hierarchical finite element formulation.

Laminate Configuration	Central Deflection (m) CCCC	Central Deflection (m) SSSS
$[0/90]_{24s}$	1.9089×10^{-5}	2.5694×10^{-4}
$[0/90/\pm45]_{12s}$	1.8588×10^{-5}	1.2881×10^{-4}
$[\pm10]_{24s}$	1.9922×10^{-5}	4.9498×10^{-4}
$[\pm20]_{24s}$	1.9341×10^{-5}	4.2510×10^{-4}
$[\pm30]_{24s}$	1.8746×10^{-5}	3.3491×10^{-4}
$[\pm45]_{24s}$	1.8206×10^{-5}	1.0777×10^{-4}
$[\pm45]_{48}$	1.8200×10^{-5}	1.0774×10^{-4}

Table 4.2 Central deflection of CCCC (fully clamped) and SSSS (simply supported) laminates with different laminate configurations using hierarchical finite element formulation

It is observed that the fully clamped plate (CCCC) and simply supported plate (SSSS) behave in a similar manner for different laminate configurations, except that the values are different for each laminate configuration. For both the cases i.e. CCCC and SSSS boundary conditions, different laminate configurations behave as below.

The static deflection of symmetric cross-ply laminate $[0/90]_{24s}$ is more than that of quasi-isotropic laminate$[0/90/\pm45]_{12s}$. For angle-ply laminates the deflection decreases as the angle of fiber orientation increases i.e. central deflection of $[\pm10]_{24s}$ laminate is greater than that of $[\pm20]_{24s}$ laminate which is greater than that of $[\pm30]_{24s}$ and which in turn is greater than that of $[\pm45]_{24s}$ laminate.

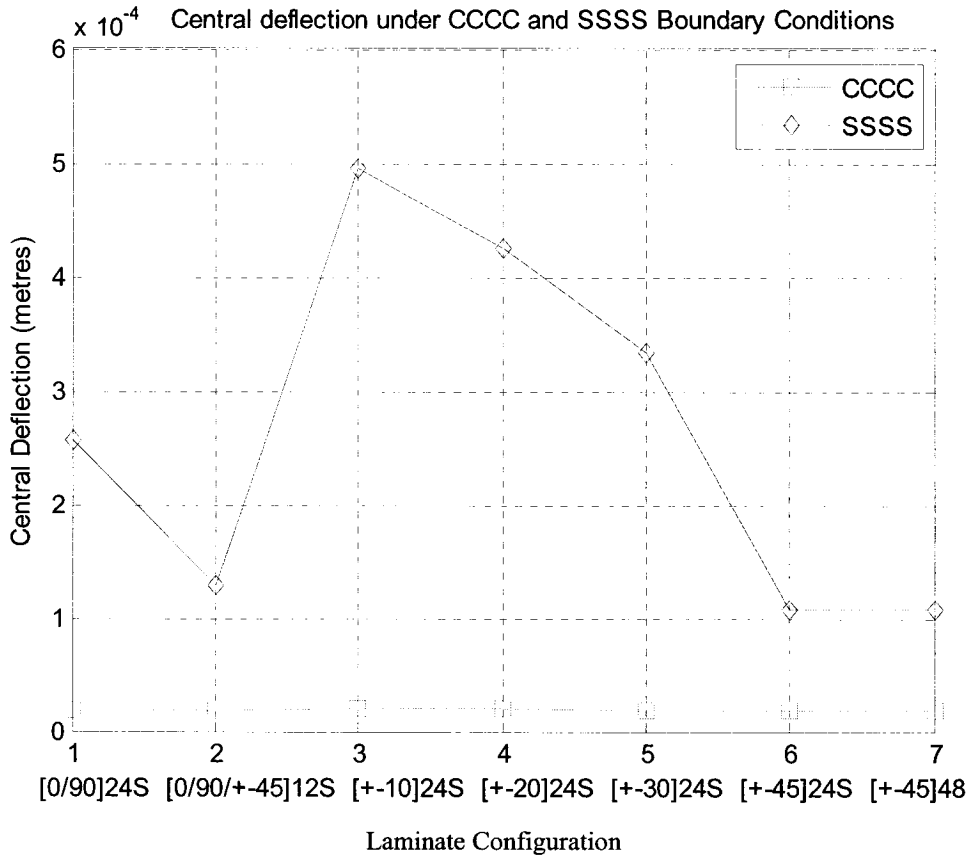

Figure 4.2a Variation of central deflection of different laminate configurations under CCCC and SSSS boundary conditions

Out of symmetric laminate $[\pm 45]_{24s}$ and anti-symmetric laminate $[\pm 45]_{48}$ the central deflection is more for symmetric laminate though the difference is very less. This implies that out of the laminate configurations under study, $[\pm 45]_{48}$ laminate has greatest stiffness and $[\pm 10]_{24s}$ has least stiffness. The variation of central deflection of different laminate configurations under CCCC boundary conditions is plotted at a smaller scale as shown in Figure 4.2b

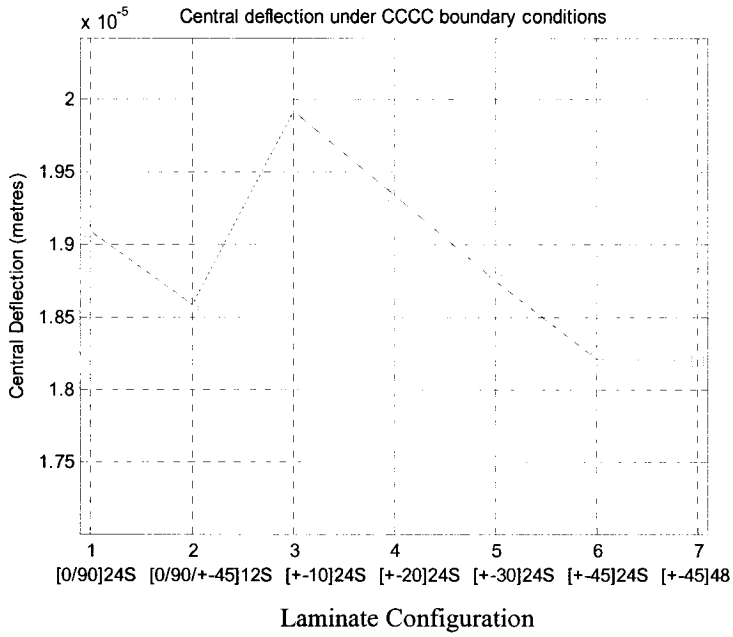

Figure 4.2b Variation of central deflection of different laminate configurations under CCCC boundary conditions

4.2.2 The Effect of Aspect Ratio on Static Deflection

To consider the effect of aspect ratio on the static deflection, different laminate configurations under CCCC boundary conditions are analyzed under 100 Pa uniformly distributed load.

Laminate Configuration	Aspect Ratio				
	R=0.25	R=0.5	R=1	R=2	R=4
$[0/90]_{24s}$	2.1797×10^{-5}	3.3488×10^{-5}	1.9089×10^{-5}	3.5279×10^{-5}	2.3833×10^{-5}
$[0/90/\pm45]_{12s}$	2.9783×10^{-5}	3.7774×10^{-5}	1.8588×10^{-5}	3.8933×10^{-5}	3.1357×10^{-5}
$[\pm45]_{24s}$	4.5079×10^{-5}	4.4673×10^{-5}	1.8206×10^{-5}	4.4673×10^{-5}	4.5079×10^{-5}

Table 4.3 Effect of aspect ratio on central deflection of CCCC (fully clamped) laminate using hierarchical finite element formulation

Effect of aspect ratio on static deflection is determined in two parts. First, $[0/90]_{24s}$, $[0/90/\pm 45]_{12s}$ and $[\pm 45]_{24s}$ laminates are analyzed.

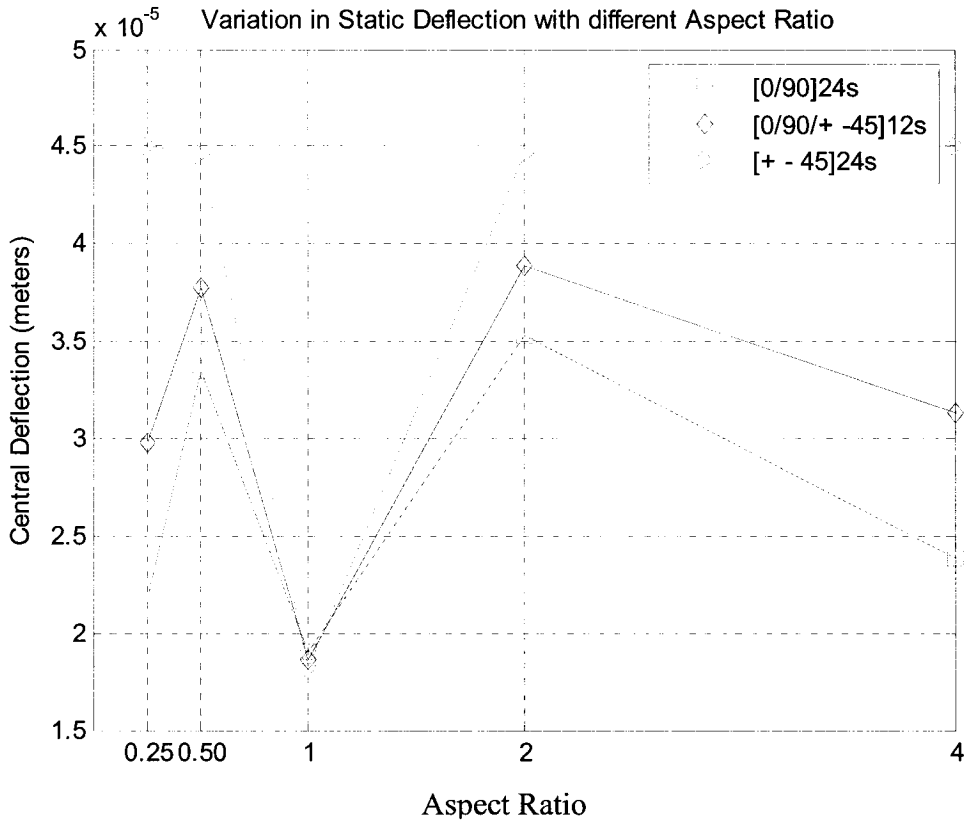

Figure 4.3 Variation of central deflection of CCCC laminate for different aspect ratio values

It is observed that as the aspect ratio is increased beyond 1.0, the central deflection also increases. When aspect ratio is decreased to 0.5, the central deflection increases and when aspect ratio is decreased further to 0.25, the central deflection decreases. When aspect ratio is increased beyond one, the laminates behave exactly the same for aspect ratio values of 2.0 and 4.0 as shown in Figure 4.3.In the second part, laminates with configurations $[\pm 10]_{24s}$, $[\pm 20]_{24s}$, $[\pm 30]_{24s}$ are analyzed. It is observed that for aspect ratio value less than 1.0, the central deflection is greatest for $[\pm 30]_{24s}$ and

lowest for $[\pm 10]_{24s}$ but as the aspect ratio increases more than 1.0, the deflection for $[\pm 10]_{24s}$ becomes greatest followed by $[\pm 20]_{24s}$,which is further followed by $[\pm 30]_{24s}$.

Laminate Configuration	Aspect Ratio				
	R=0.25	R=0.5	R=1	R=2	R=4
$[\pm 10]_{24s}$	5.8277×10^{-6}	1.7781×10^{-5}	1.9922×10^{-5}	1.34661 e-4	2.2708×10^{-4}
$[\pm 20]_{24s}$	8.1416×10^{-6}	2.0694×10^{-5}	1.9341×10^{-5}	1.10748 e-4	1.8511×10^{-4}
$[\pm 30]_{24s}$	1.6014×10^{-5}	2.6523×10^{-5}	1.8746×10^{-5}	8.0423×10^{-5}	1.1804×10^{-4}

Table 4.4 Effect of aspect ratio on central deflection of CCCC (fully clamped) angle-ply laminates using hierarchical finite element formulation

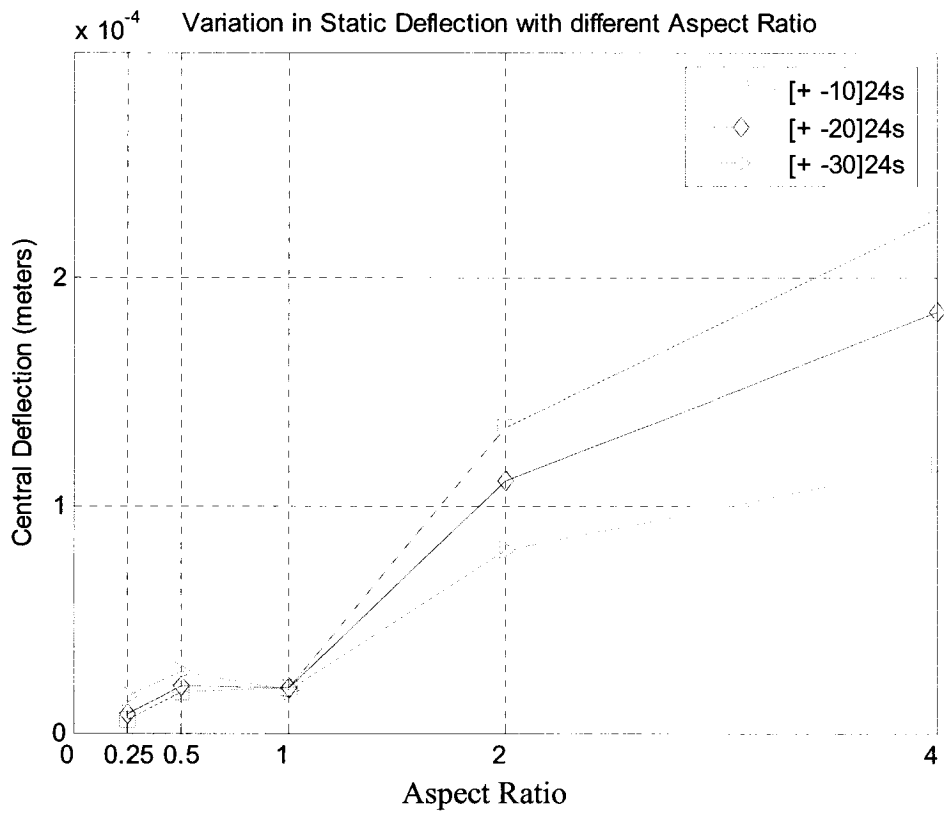

Figure 4.4 Variation of central deflection of CCCC laminates for different aspect ratio values

The effect of laminate configuration on the static deflection is explained as below. We already know from Table 4.2 that the static deflection for $[\pm 10]_{24s}$ laminate is greater than that of $[\pm 20]_{24s}$ which is greater than that of $[\pm 30]_{24s}$ for a square plate. As the aspect ratio is lowered below 1, the laminate looks as below in Figure 4.5

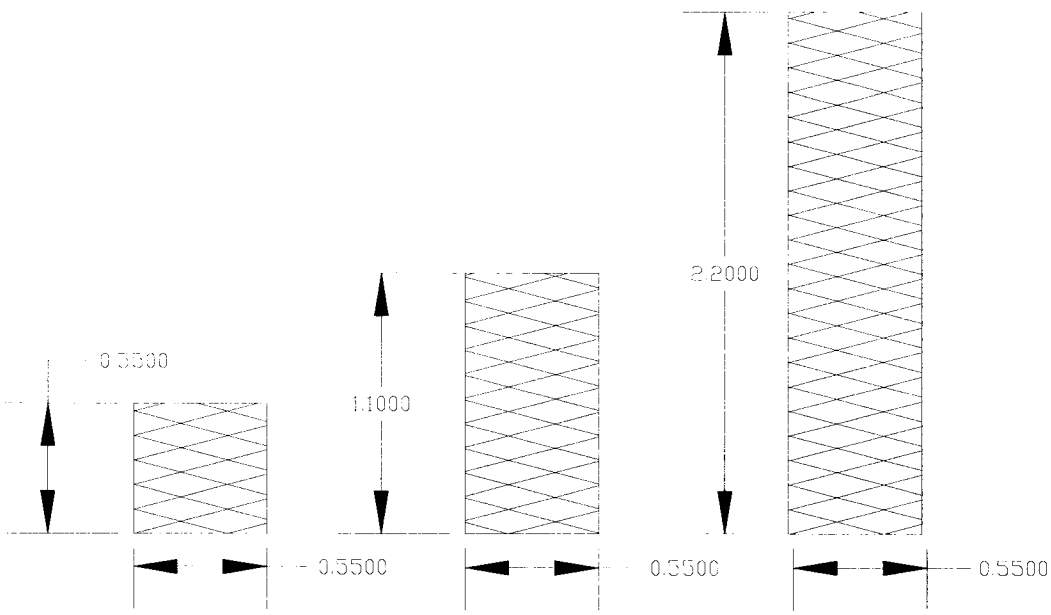

Aspect Ratio = 1 Aspect Ratio = 0.5 Aspect Ratio = 0.25

Figure 4.5 Laminates with aspect ratio less than or equal to 1.0

We observe that as the aspect ratio is lowered than 1.0, y-axis becomes the major axis of the laminate. The fiber angle with respect to major axis (in this case y axis) is changed from θ to (360- θ). This causes the reversal of behavior of angle-ply laminates than the one shown in Table 4.2.

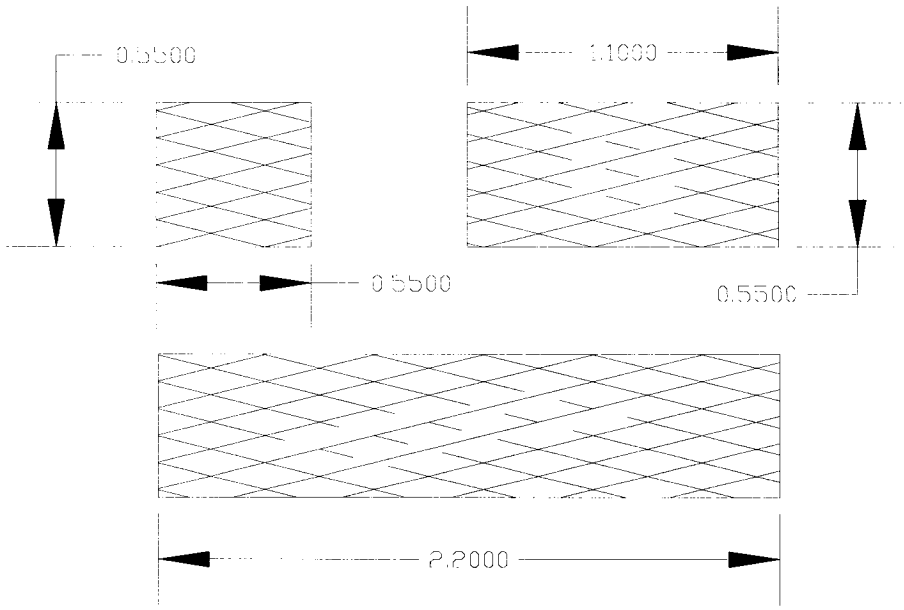

Aspect Ratio = 1 Aspect Ratio = 2 Aspect Ratio = 4

Figure 4.6 Laminates with aspect ratio greater than or equal to 1.0

In the case when the aspect ratio is increased beyond 1.0, the major axis of the laminate is x-axis so the angle of fibers with respect to major axis is still the same, and so the angle-ply laminates preserve their behavior as shown for a square plate given in Table 4.2.

4.2.3 The Effect of Elastic Modulus to Shear Modulus (E/G) Ratio on Static Deflection

The effect of change in the ratio of Elastic Modulus in transverse direction (E_2) to shear modulus (G) is analyzed in this section. Keeping elastic modulus constant the shear modulus is changed and the changing central deflection value is analyzed.

Laminate Configuration	E/G Ratio				
	E/G=1/0.4	E/G=1/0.5	E/G=1/0.6	E/G=1/0.7	E/G=1/0.8
$[\pm 10]_{24s}$	1.9847×10^{-5}	1.9607×10^{-5}	1.9372×10^{-5}	1.9142×10^{-5}	1.8916×10^{-5}
$[\pm 20]_{24s}$	1.9272×10^{-5}	1.9052×10^{-5}	1.8837×10^{-5}	1.8625×10^{-5}	1.8418×10^{-5}
$[\pm 30]_{24s}$	1.8682×10^{-5}	1.8477×10^{-5}	1.8276×10^{-5}	1.8080×10^{-5}	1.7888×10^{-5}
$[0/90]_{24s}$	1.9018×10^{-5}	1.8789×10^{-5}	1.8566×10^{-5}	1.8347×10^{-5}	1.8132×10^{-5}
$[0/90/\pm 45]_{12s}$	1.8523×10^{-5}	1.8318×10^{-5}	1.8117×10^{-5}	1.7920×10^{-5}	1.7727×10^{-5}
$[\pm 45]_{24s}$	1.8144×10^{-5}	1.7948×10^{-5}	1.7757×10^{-5}	1.7571×10^{-5}	1.7388×10^{-5}

Table 4.5 Central deflection (in meters) for different E/G ratios for different laminate configurations with CCCC boundary conditions

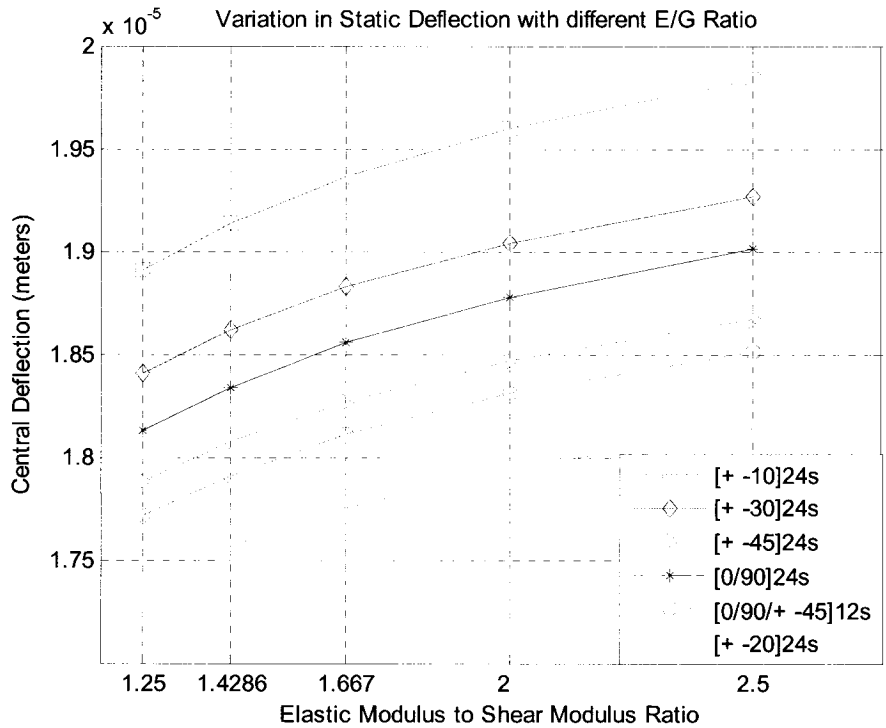

Figure 4.7 Central deflection (in meters) for different E/G ratios for different laminate configurations with CCCC boundary conditions

We observe that as the E/G ratio is decreased the central deflection decreases for all the laminate configurations. The behavior of different laminate configurations for changing E/G ratio can be seen in Figure 4.7.

4.3 Parametric Study on Free Vibration Response of Rectangular Laminated Plate

The lowest 4 natural frequencies are determined for all possible changes that can be performed on the composite plates such as, the change in the boundary conditions, the change in the laminate configurations, the change in aspect ratio, and the change in E/G ratio. The natural frequencies are obtained using both the formulations, conventional and hierarchical as described in the previous chapters. Tables and Figures are provided for comparison and commenting purposes.

4.3.1 The Effect of Boundary Conditions on Natural Frequencies

To consider the effects of different boundary conditions on the natural frequencies of the laminated plate, the laminate with configuration of $[0/90]_{24s}$ is taken and the values of the lowest four natural frequencies are obtained using the hierarchical finite element formulation.

Mode	CCCC	SSSS	CFFC	CFFF
1	2578.262	908.920	680.656	479.044
2	3508.950	925.980	1401.795	611.379
3	3575.024	1203.932	1593.991	1244.64
4	3847.203	1235.984	1884.468	1422.337

Table 4.6 First four frequencies (rad/s) of $[0/90]_{24s}$ laminate subjected to different boundary conditions using hierarchical finite element formulation

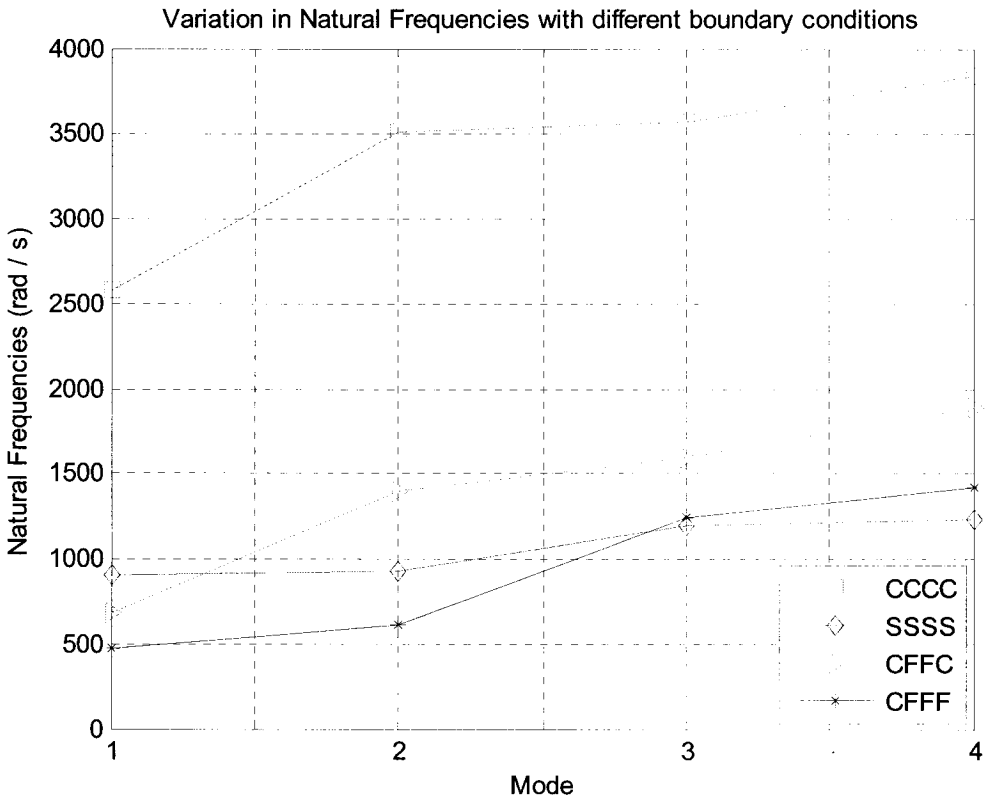

Figure 4.8 Natural frequencies of $[0/90]_{24s}$ laminate with different boundary conditions

Table 4.1 gives us the detailed results for the lowest four natural frequencies with different boundary conditions for the $[0/90]_{24s}$ plate. One hierarchical element with four

internal hierarchical degrees of freedom each in x and y directions respectively are used to model the plate. The total internal degrees of freedom are 16 which are obtained by taking the tensor product of degrees of freedom in each direction. It may be noted that the frequencies and the modes are not continuous in a finite element model. However the frequencies are plotted as continuous functions in Figure 4.8 and in similar figures that follow, in order to observe the laminate behavior at a glance.

As expected, there is a considerable variation in the values of the frequencies for different boundary conditions. We observe that relaxing the degrees of freedom along the edges of the plate significantly reduces the initial frequencies. In Figure 4.1 the clamped-clamped (CCCC) type of support gives the highest value of natural frequencies, whereas the CFFF type gives the lowest value (The frequency of the first mode of the fully clamped plate is nearly 6 times that of the plate with only one edge clamped). The simply supported type (SSSS) comes as the second highest followed by CFFC as third highest in terms of values of first natural frequency.

4.3.2 Hierarchical FEM vs. Conventional FEM

One hierarchical element with 4 internal degrees of freedom in each direction gives the same results as that of a 64 elements mesh in conventional FEM. The hierarchical element has 4 h-nodes, 4 p-nodes on each edge in between the h-nodes and 16 internal p-nodes as shown in Figure 2.3. In total there are 4 h-nodes and 32 p-nodes in the hierarchical element chosen. The results from hierarchical and conventional finite

element formulations are compared for 1st four natural frequencies of $[0/90]_{24s}$ laminate with CCCC and CFFC boundary conditions, as given in Tables 4.7 and 4.8.

Mode	CCCC Conventional FEM	CCCC Hierarchical FEM	Percentage Change (%)
1	2540.919	2578.262	1.47
2	3404.098	3508.950	3.08
3	3465.386	3575.024	3.16
4	3730.352	3847.203	3.13

Table 4.7 Comparison of frequencies obtained using conventional and hierarchical finite elements for $[0/90]_{24s}$ laminate with CCCC boundary conditions

Mode	CFFC Conventional FEM	CFFC Hierarchical FEM	Percentage Change (%)
1	678.389	680.656	0.33
2	1399.003	1401.795	0.20
3	1586.772	1593.991	0.45
4	1887.669	1884.468	0.17

Table 4.8 Comparison of frequencies obtained using conventional and hierarchical finite elements for $[0/90]_{24s}$ laminate with CFFC boundary conditions

From Tables 4.7 and 4.8, we find that percentage change in the natural frequency calculated using Hierarchical FEM from that of the Conventional FEM is less than 5 % in all the cases.

4.3.3 Mode shapes

In this section the first four mode shapes of $[0/90]_{24s}$ laminated plate with boundary conditions of all sides fully clamped are plotted. The mode shapes for boundary conditions SSSS (all sides simply supported), CFFC (sides x=0, y =b are fully clamped and sides x=a, y =0 are free), CFFF (side x=0 fully clamped and other sides are free) are plotted in Appendix-II. The mode shapes are generated using conventional finite element method with a mesh of 64 elements. As explained in Section 3.4.2, since a mesh of 8 × 8 elements is used, the x-axis ranges from 1 to 17 and y-axis ranges from 1 to 17 corresponding to [m, n] which is the size of matrix (P), as explained above. The z-axis gives the surface height in meters.

Comparing the mode shapes as given in Figure 4.9 and Figure 4.9.1 in Appendix –II, clearly the effect of the constraint on the degrees of freedom on the edges of plate under CCCC and SSSS boundary conditions is reflected in different mode shapes in both the cases. It is also interesting to observe the mode shapes under CFFC and CFFF boundary conditions, which are given in Appendix –II.

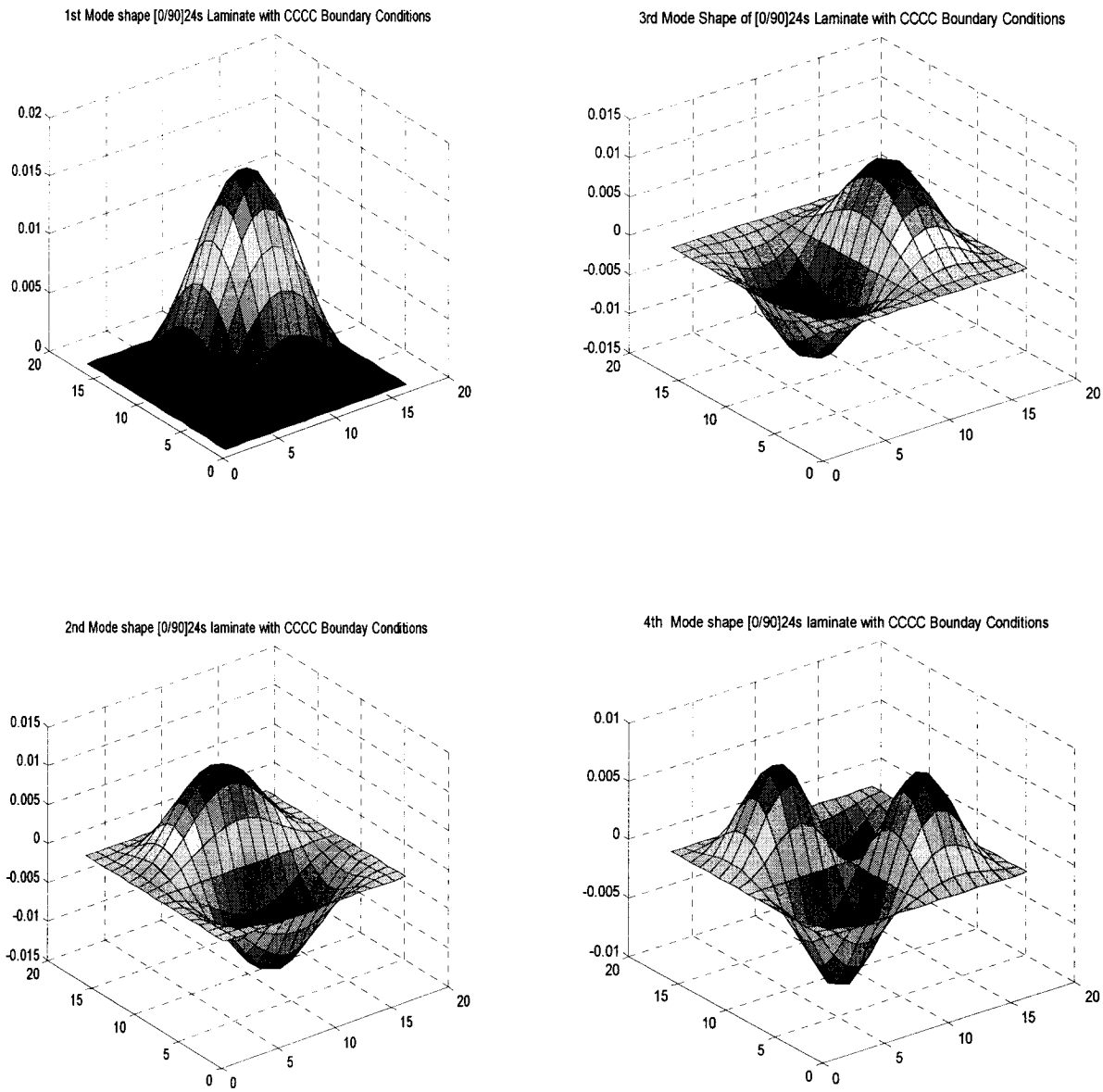

Figure 4.9 First four mode shapes of $[0/90]_{24s}$ laminate with CCCC boundary conditions

Swapping the boundary conditions: Another observation is made by swapping the boundary conditions of clamped and free edges, and by observing the difference in the values of first four natural frequencies. In CFCF, sides x= 0 and x=a are clamped and y = 0 and y = b are free and reversing the boundary conditions it becomes FCFC, with sides x=0 and x=a free and y=0 and y=b clamped .The frequencies are calculated using Conventional FEM.

Mode	CFCF	FCFC
1	182.719	183.017
2	195.144	191.636
3	273.921	266.852
4	280.251	283.919

Table 4.9 First four frequencies of $[0/90]_{24s}$ laminate with CFCF and FCFC boundary conditions

We can see that the natural frequency differs when the boundary conditions are swapped which is because of the anisotropic behavior of $[0/90]_{24s}$ laminate. The corresponding mode shapes for both the boundary conditions discussed are plotted in Figure 4.10 and Figure 4.11. In these figures, we can see the symmetric changes in the mode shapes upon swapping the boundary conditions.

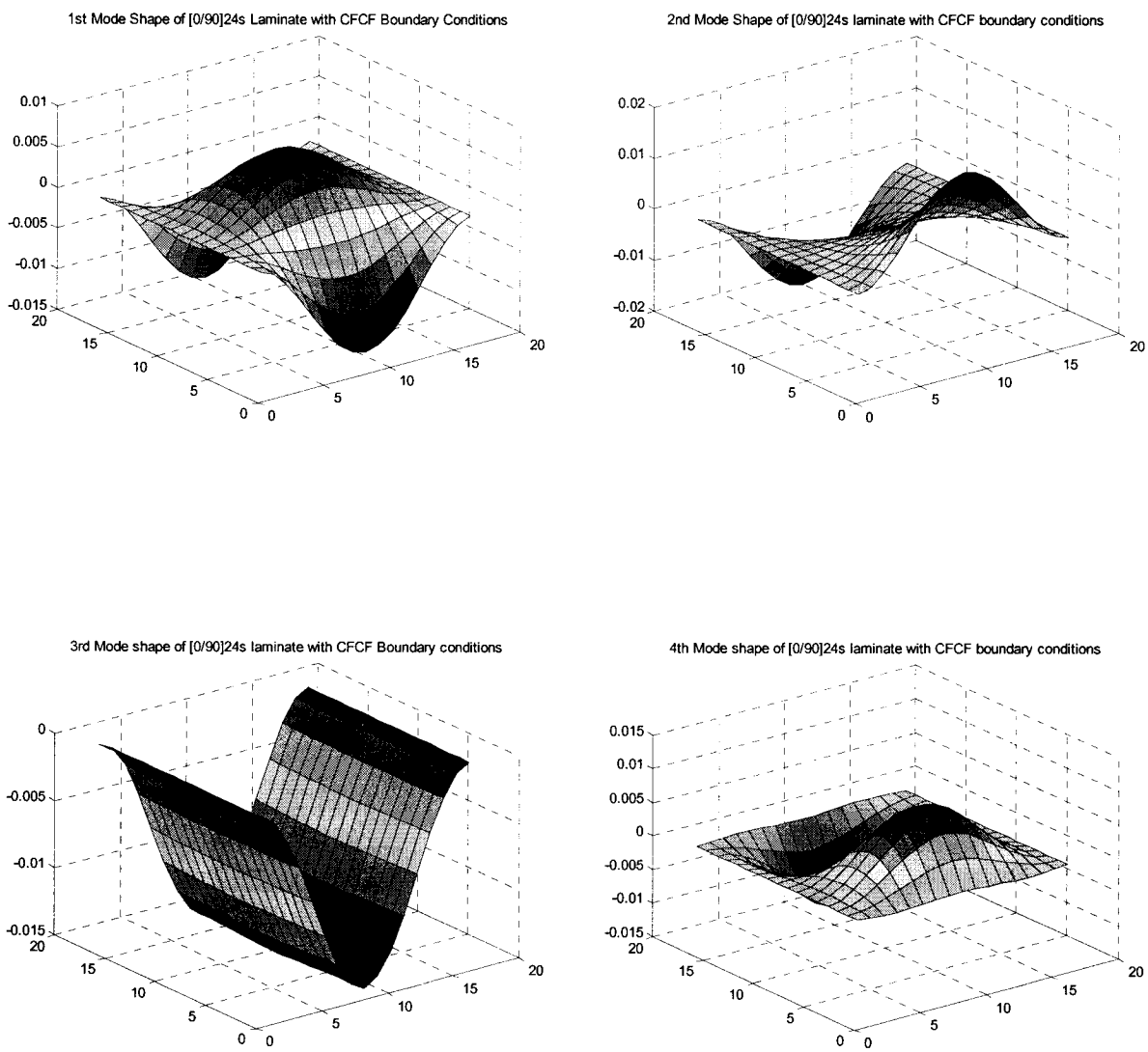

Figure 4.10 First four mode shapes of $[0/90]_{24s}$ laminate with CFCF boundary conditions

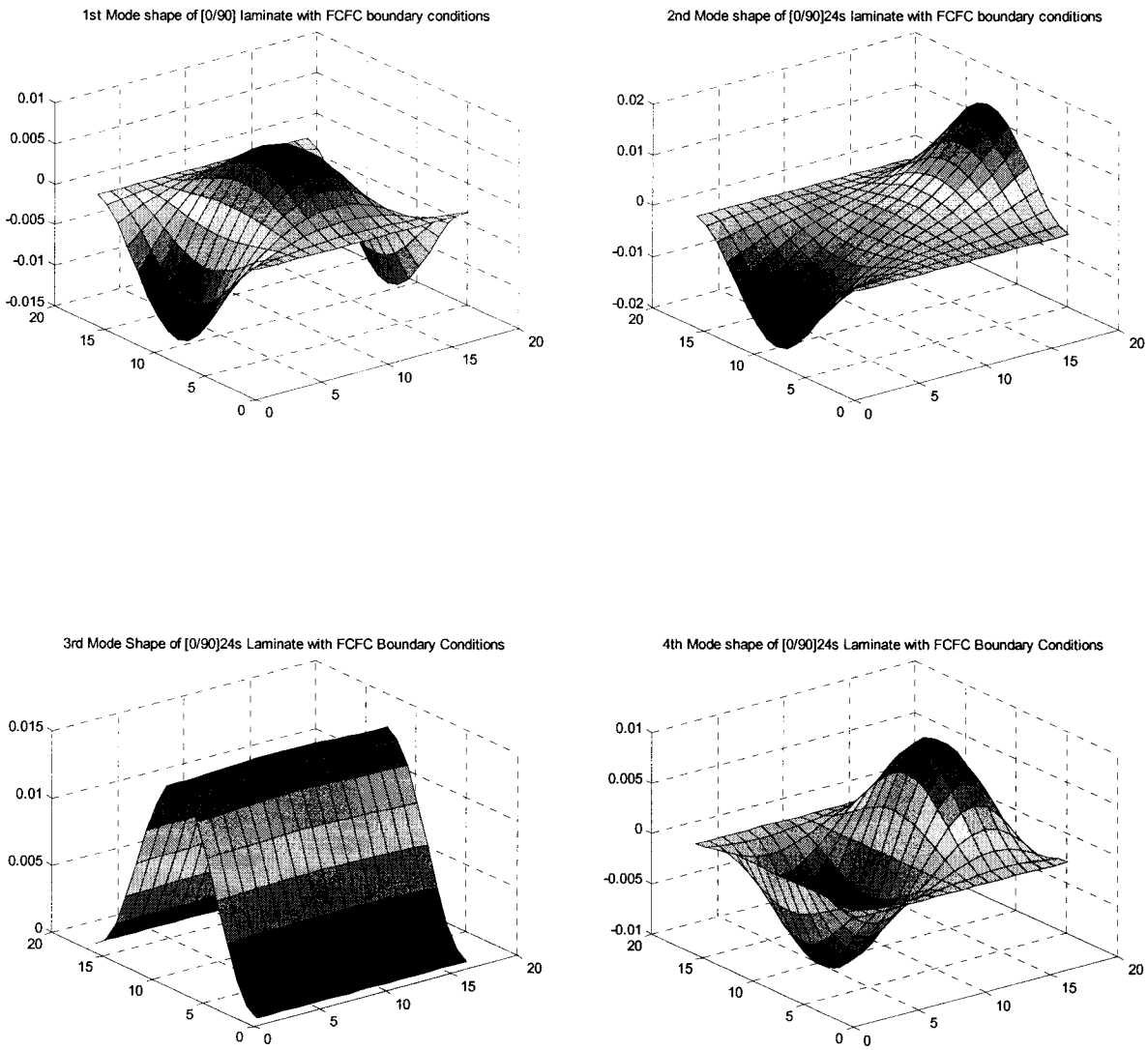

Figure 4.11 First four mode shapes of $[0/90]_{24s}$ laminate with FCFC boundary conditions

We will now see the effect of swapping the boundary conditions for $[0/90/\pm 45]_{12s}$ laminate. The frequencies corresponding to first four modes are as given below. As

expected the two sets of boundary conditions give different natural frequencies because of the anisotropic behavior of laminate.

Mode	CFCF	FCFC
1	196.658	194.842
2	202.474	202.444
3	244.385	240.544
4	288.254	290.209

Table 4.10 First four frequencies of $[0/90/\pm 45]_{12s}$ laminate with CFCF and FCFC boundary conditions

We will now observe the effect of swapping the boundary conditions as discussed before but on anti-symmetric laminate$[\pm 45]_{48}$. The corresponding table containing the frequencies for the first four modes is given below.

Mode	CFCF	FCFC
1	183.299	183.299
2	192.078	192.078
3	232.827	232.827
4	275.353	275.353

Table 4.11 First four frequencies of $[\pm 45]_{48}$ laminate with CFCF and FCFC boundary conditions

Clearly the swapping of the boundary conditions does not have any effect on $[+-45]_{48}$ laminate which is because of the special alignment of the fibers at + and - 45 degrees

which gives the laminate same stiffness in both x and y directions. It is very interesting to observe how the mode shapes of $[0/90/\pm 45]_{12s}$ and $[\pm 45]_{48}$ laminates change upon swapping the boundary conditions. The respective mode shapes are given in Appendix-II in Figure 4.10.1, Figure 4.10.2, and Figure 4.11.1and Figure 4.11.2.

4.4 The Effects of Boundary Conditions and Laminate Configurations

In this section the effect of different boundary conditions on the frequencies for different laminate configurations other than $[0/90]_{24s}$ is considered. The laminate configurations under study in this section are$[0/90/\pm 45]_{12s}$, $[\pm 45]_{24s}$ and $[\pm 45]_{48}$. The mode shapes for CCCC boundary condition are provided here along with the comparison graph for all the boundary conditions. The mode shapes for boundary conditions SSSS, CFFC and CFFF are shown in Figure 4.12.1, Figure 4.12.2, and Figure 4.12.3 respectively in Appendix-II.

Mode	CCCC	SSSS	CFFC	CFFF
1	2546.349	956.857	804.297	533.600
2	3434.591	1141.121	1281.203	733.016
3	3474.886	1152.725	1799.486	1237.817
4	4010.119	1186.488	2049.237	1567.964

Table 4.12 Natural frequencies (rad/s) for different boundary conditions for $[0/90/\pm 45]_{12s}$ laminate

It is interesting to observe from CCCC, CFFC and CFFF boundary conditions from Table 4.12 that the frequencies corresponding to first mode of $[0/90/\pm 45]_{12s}$ laminate decrease as the constraints on the edges are relaxed. Comparing the first four natural frequencies of CCCC, CFFC and CFFF boundary conditions from Table 4.6 with the corresponding values in Table 4.12, it is observed that the frequencies for $[0/90/\pm 45]_{12s}$ laminate are less than that of the $[0/90]_{24s}$ laminate which explains the little stiffness edge symmetric cross-ply laminate enjoys over symmetric quasi-isotropic laminate.

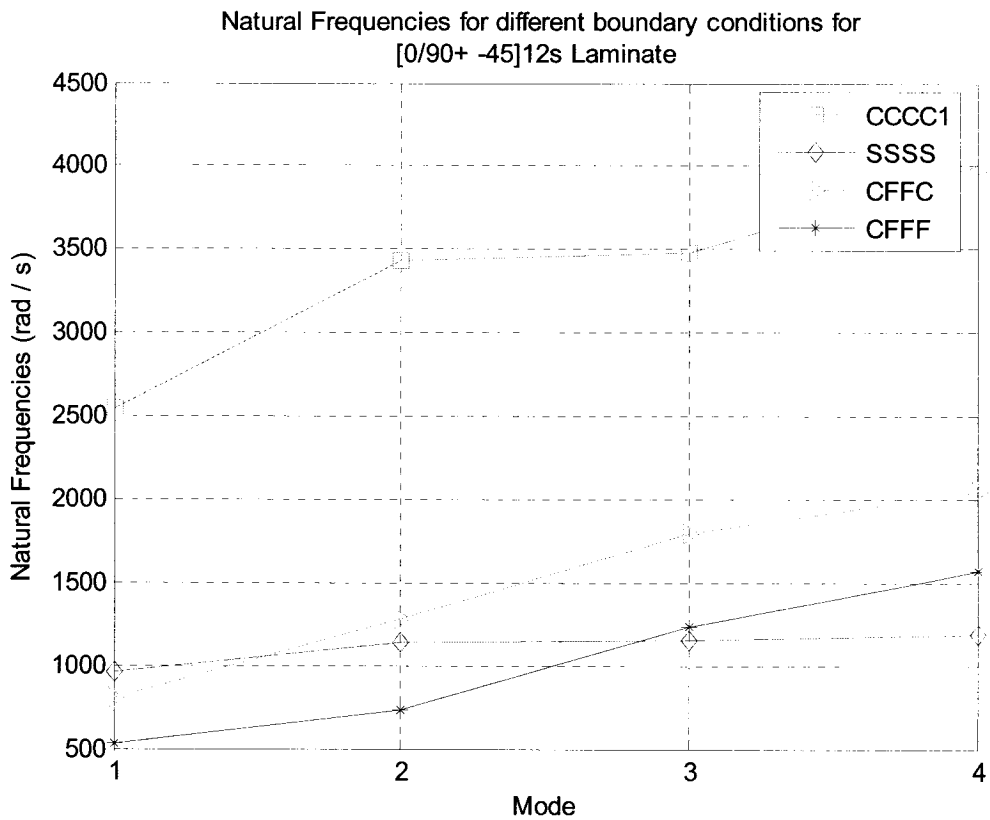

Figure 4.12 Natural frequencies of $[0/90/\pm 45]_{12s}$ laminate under different boundary conditions

Mode Shapes

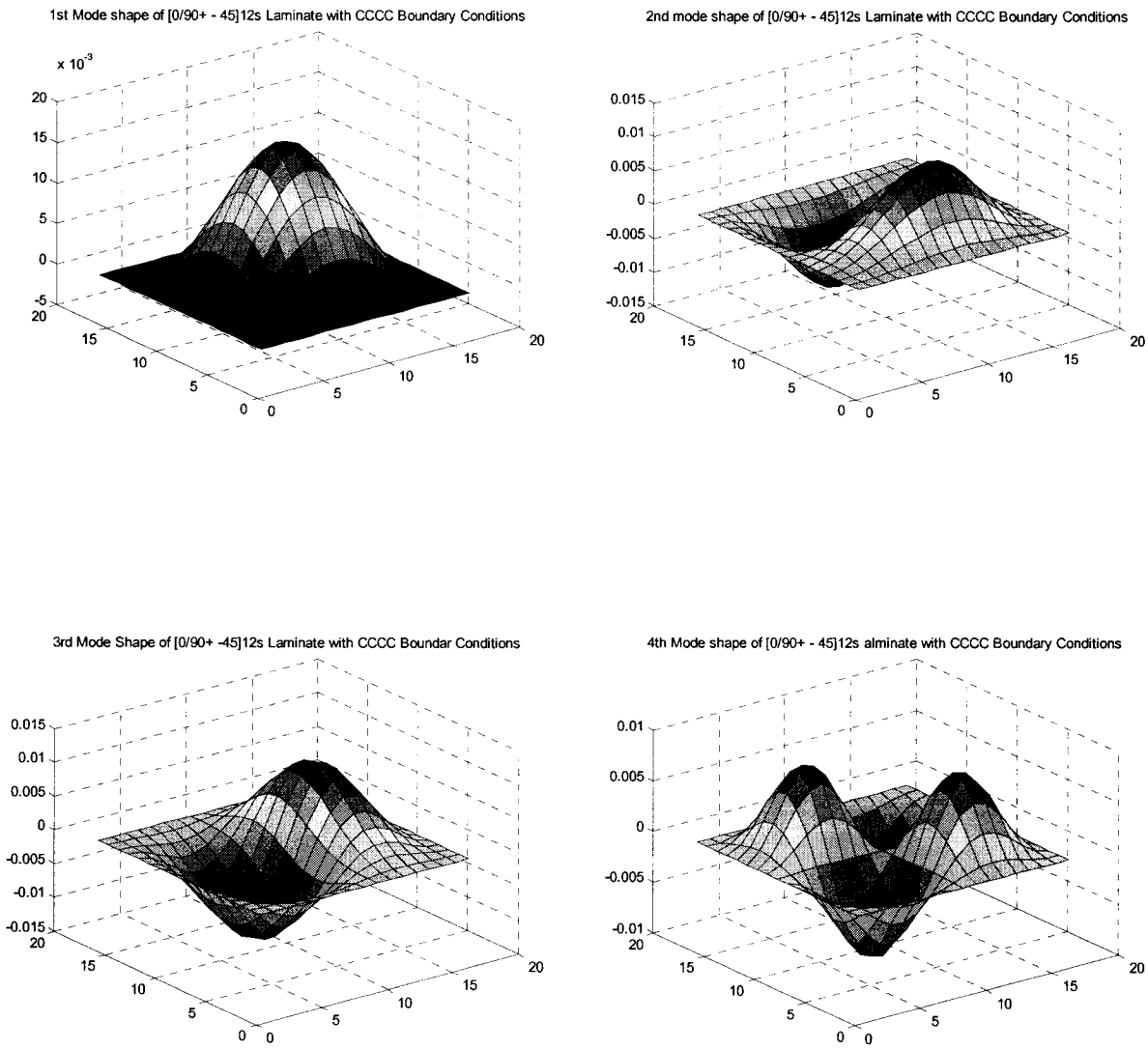

Figure 4.13 First four mode shapes of $[0/90/\pm 45]_{12s}$ laminate with CCCC boundary conditions

Mode	CCCC	SSSS	CFFC	CFFF
1	2499.218	450.746	890.815	391.884
2	3309.732	1113.572	1056.381	892.600
3	3341.601	1207.779	1738.643	997.687
4	4172.888	1213.406	2177.093	1499.352

Table 4.13 Natural frequencies (rad/s) for different boundary conditions for $[\pm 45]_{24s}$ laminate

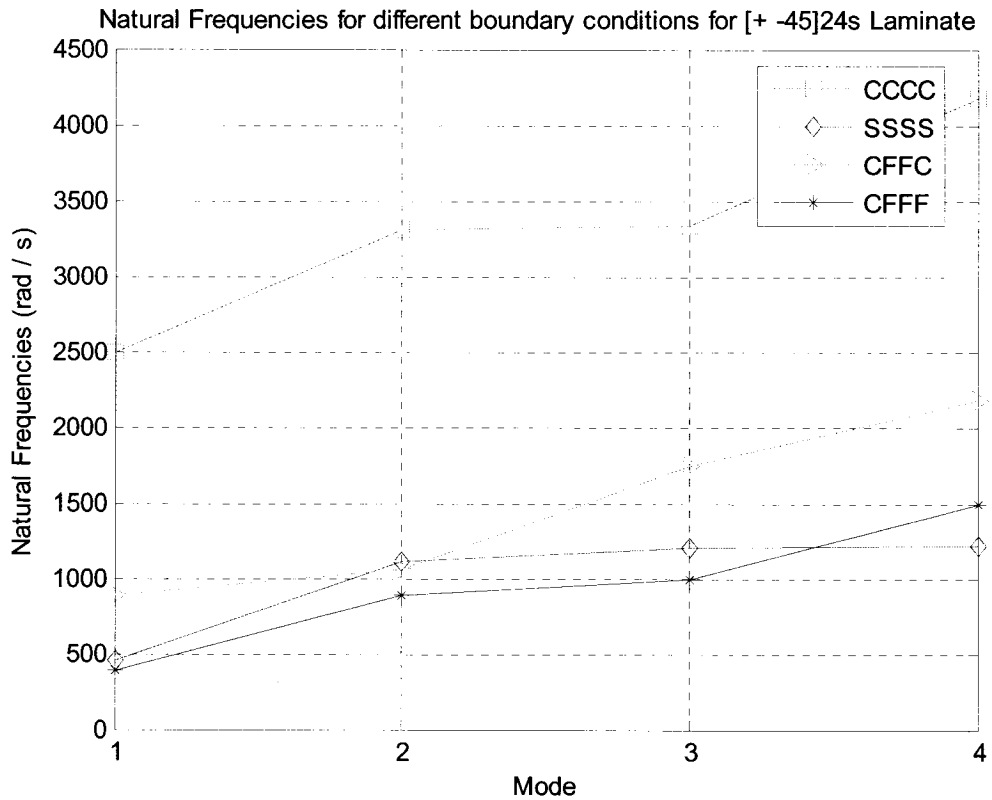

Figure 4.14 Natural frequencies of $[\pm 45]_{24s}$ laminate under different boundary conditions

Mode shapes

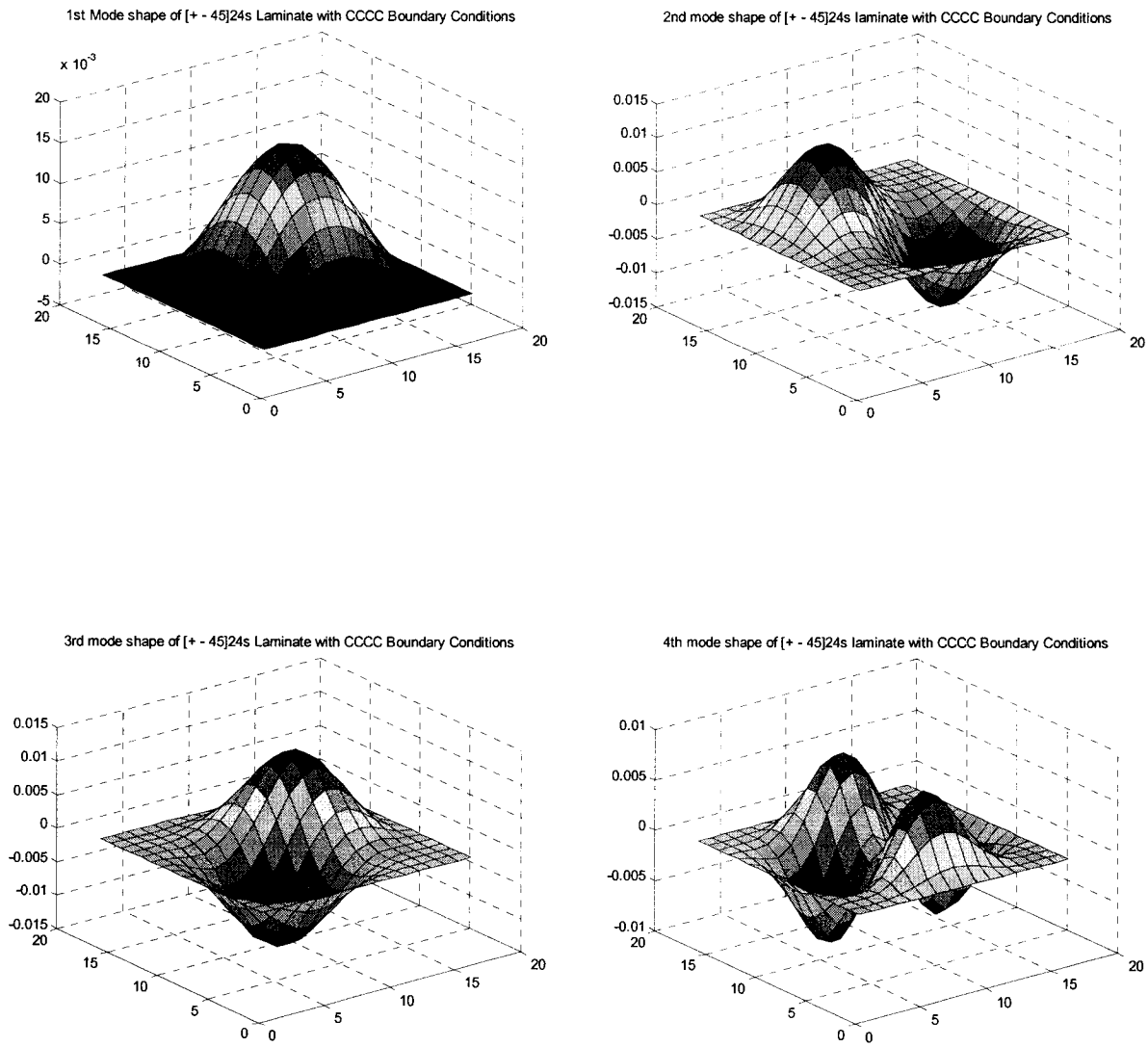

Figure 4.15 First four mode shapes of $[\pm 45]_{24s}$ laminate with CCCC boundary conditions

The mode shapes for boundary conditions SSSS, CFFC and CFFF are shown in Figure 4.13.1, Figure 4.13.2, and Figure 4.13.3 respectively in Appendix-II.

Mode	CCCC	SSSS	CFFC	CFFF
1	2499.569	450.751	896.952	391.941
2	3325.851	1113.621	1059.825	892.912
3	3325.851	1210.982	1746.548	997.714
4	4173.043	1210.982	2182.122	1502.156

Table 4.14 Natural frequencies (rad/s) for different boundary conditions for $[\pm 45]_{48}$ laminate

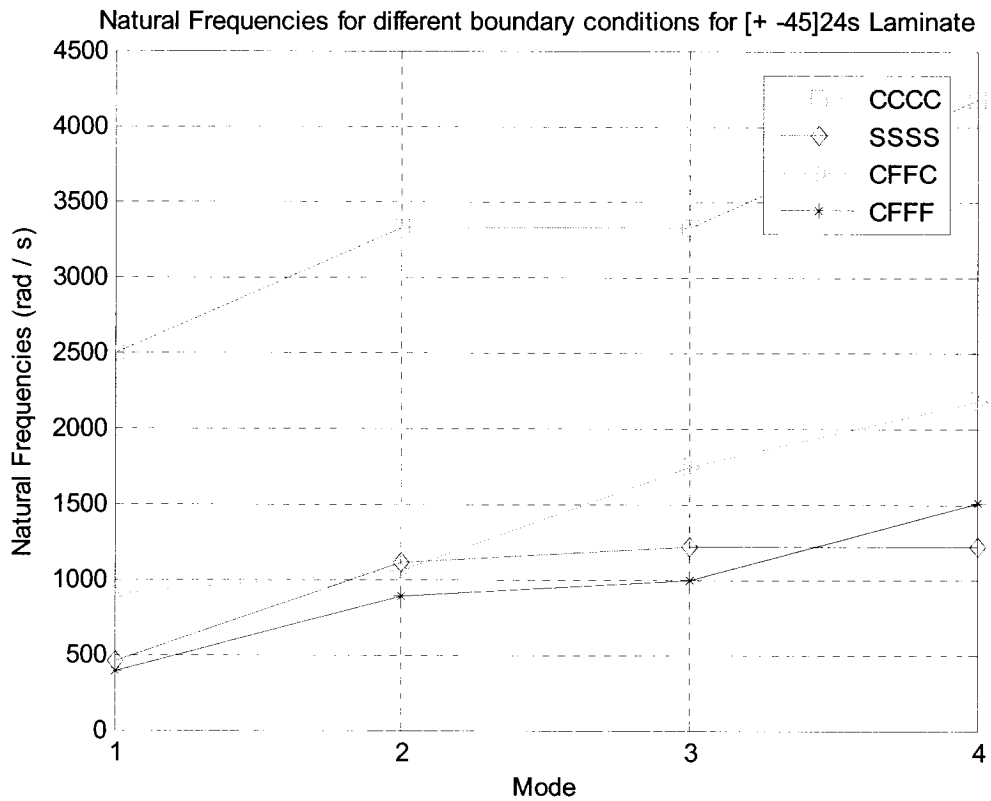

Figure 4.16 Natural frequencies of $[\pm 45]_{48}$ laminate under different boundary conditions

Mode Shapes

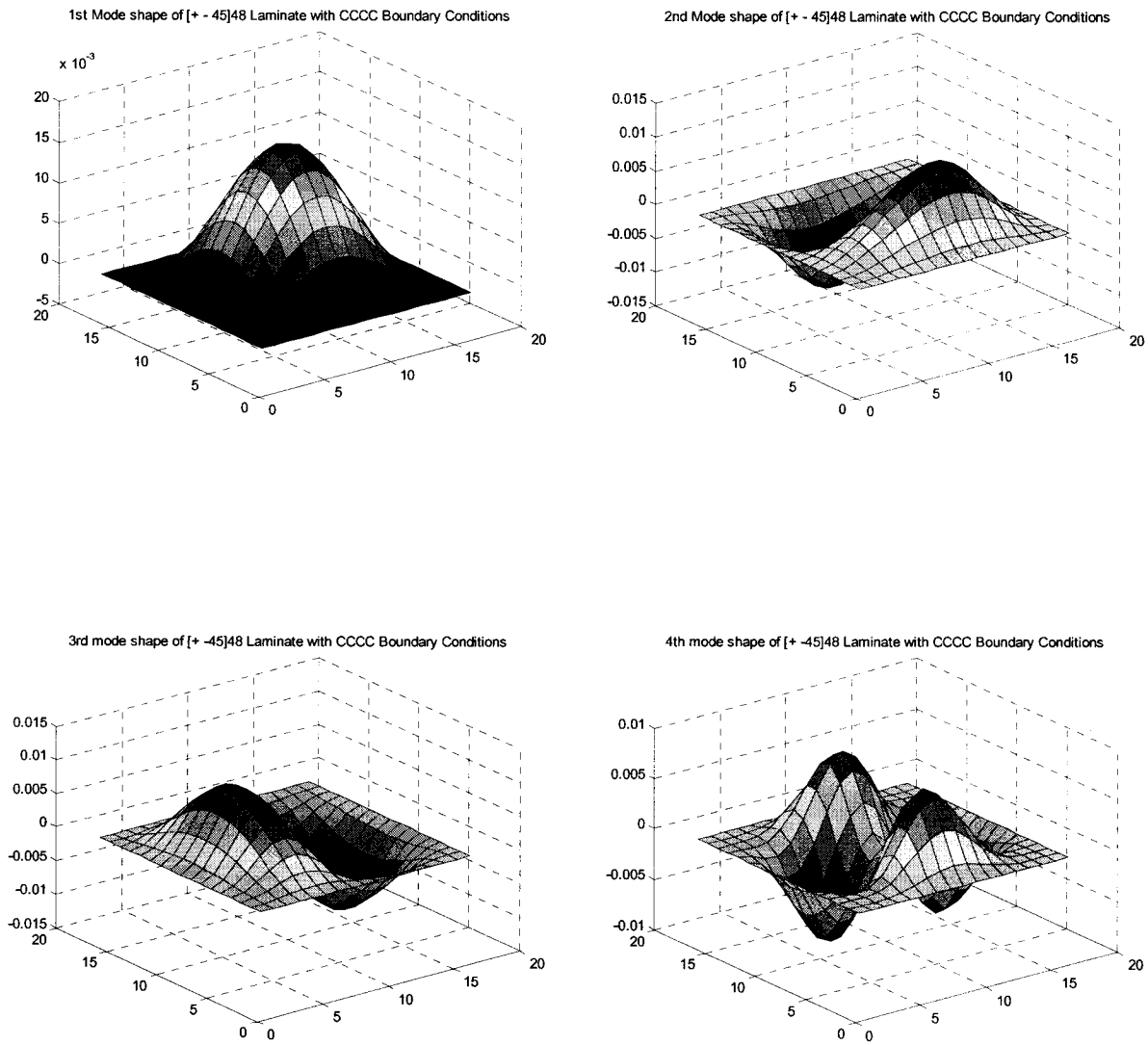

Figure 4.17 First four mode shapes of $[\pm 45]_{48}$ Laminate with CCCC boundary conditions

The mode shapes for boundary conditions SSSS, CFFC and CFFF are shown in Figure 4.14.1, Figure 4.14.2, and Figure 4.14.3 respectively in Appendix-II. From Tables 4.12, 4.13 and 4.14 and Figures 4.13, 4.15 and 4.17 we can see how the values and mode

shapes of first four natural frequencies change for plates under exactly same boundary conditions but with different laminate configurations. Under CCCC boundary condition, the plate with laminate configuration $[0/90/\pm 45]_{12s}$ has the highest value of first natural frequency followed by $[\pm 45]_{48}$ and $[\pm 45]_{24s}$.

4.5 The Effect of Fiber Orientations on Natural Frequencies

To see the effect of different fiber orientations on the natural frequencies of rectangular laminated composite plates, different laminate configurations are chosen for one particular boundary condition which in this case is CCCC i.e. all sides clamped. The lowest four natural frequencies are determined for the following types of laminates that have the following configurations: cross-ply $[0/90]_{24s}$, quasi-isotropic $[0/90/\pm 45]_{12s}$, symmetric angle-ply $[\pm 45]_{24s}$ and anti-symmetric angle-ply $[\pm 45]_{48}$ laminates.

Mode	$[0/90]_{24s}$	$[0/90/\pm 45]_{12s}$	$[\pm 45]_{24s}$	$[\pm 45]_{48}$
1	2578.262	2546.349	2499.218	2499.569
2	3508.950	3434.591	3309.732	3325.851
3	3575.024	3474.886	3341.601	3325.851
4	3847.203	4010.119	4172.888	4173.043

Table 4.15 Lowest four natural frequencies (rad/s) for different laminate configurations for laminates clamped at all sides (CCCC)

Clearly the symmetric cross-ply laminate has the highest first natural frequency and symmetric angle-ply laminate has the lowest. The variation of first four natural frequencies for different laminate configurations under CCCC boundary conditions is shown in graph below. The values are determined using polynomial hierarchical finite element formulation using only one element to model the plate. The element has 4 internal degrees of freedom in each direction which accounts to sixteen internal degrees of freedom.

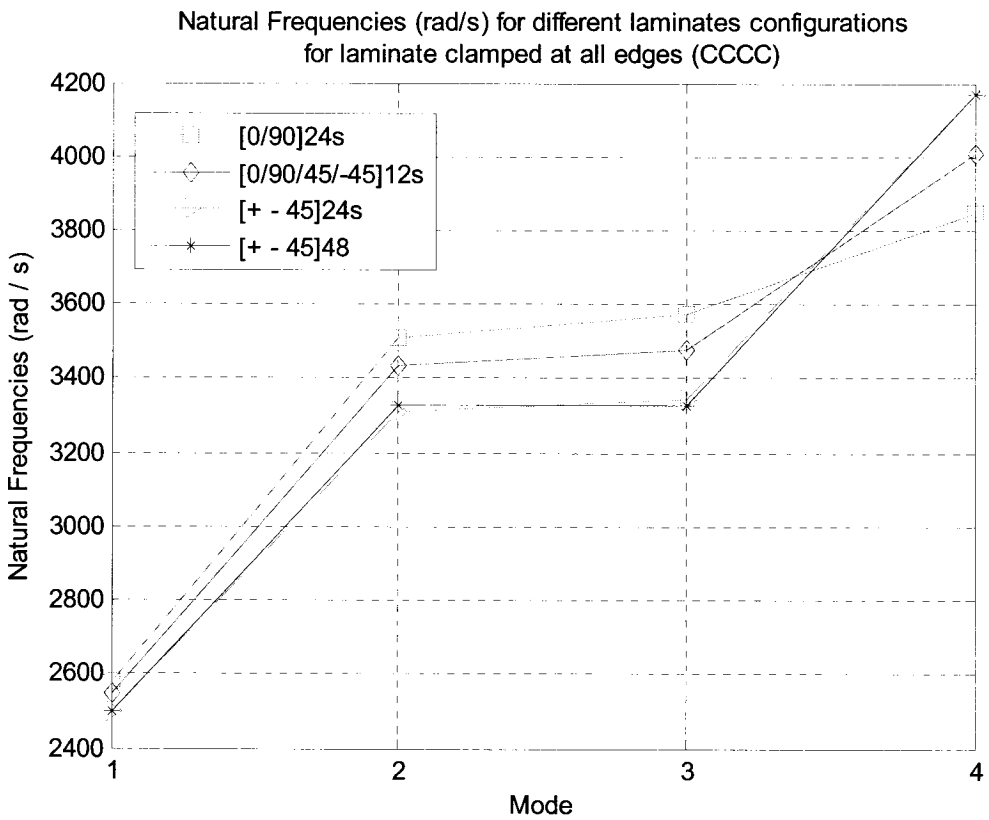

Fig 4.18 Natural frequencies of different laminate configurations under CCCC boundary condition

4.5 Effect of Aspect Ratio on Natural frequencies

In this section, the effect of changing the aspect ratio on natural frequencies is studied for different laminate configurations under a particular boundary condition (CCCC). It is also interesting to see the effect of changing aspect ratios for various laminate configurations under SSSS boundary conditions, as given in Tables 4.16.1, 4.17.1 and 4.18.1 in Appendix-II.

Firstly, the Boundary Condition of CCCC is applied to various laminate configurations with different aspect ratios as below and the values of first 4 natural frequencies are noted.

Mode	Aspect Ratio				
	R=0.25	R=0.5	R=1	R=2	R=4
1	2189.500	2254.687	2578.262	2237.851	2155.396
2	2193.062	2302.604	3508.950	2259.104	2164.001
3	2329.720	2611.719	3575.024	2623.965	2281.215
4	2354.455	3173.147	3847.203	3222.320	2343.248

Table 4.16 Natural frequencies (rad/s) for different aspect ratios for $[0/90]_{24s}$ laminate with CCCC boundary conditions

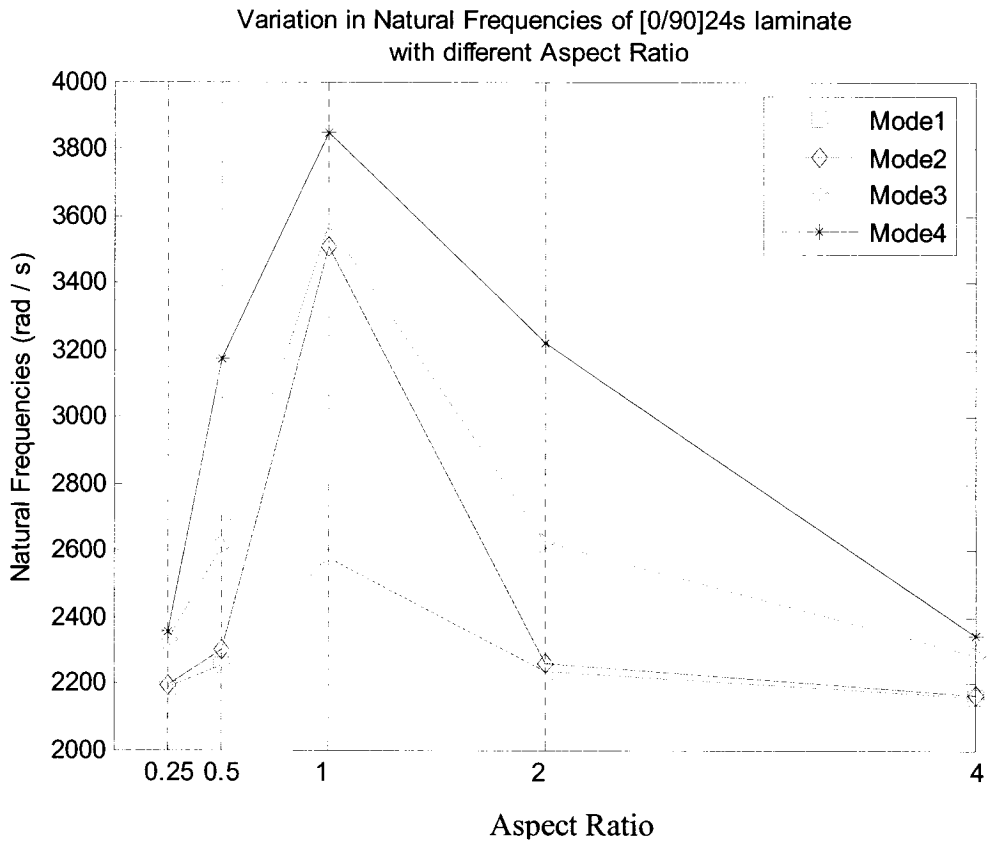

Figure 4.19 Variation of natural frequencies of $[0/90]_{24s}$ laminate with different aspect ratio values

It is observed that under CCCC boundary condition, the $[0/90]_{24s}$ laminate gives lower values of natural frequencies as the aspect ratio is either increased or decreased than 1. The maximum value for each mode is always reached when aspect ratio R=1.

Now we will observe the effect of aspect ratios on natural frequencies on $[0/90/\pm 45]_{12s}$ and $[\pm 45]_{24s}$ laminates under CCCC boundary condition. We observe that these two laminates also behave similar to $[0/90]_{24s}$ laminate as shown in Figures 4.20 and 4.21 and Tables 4.17 and 4.18.

Mode	Aspect Ratio				
	R=0.25	R=0.5	R=1	R=2	R=4
1	2168.961	2193.740	2546.349	2165.744	2140.090
2	2169.823	2294.864	3434.591	2285.920	2146.617
3	2213.178	2648.780	3474.886	2659.107	2179.453
4	2261.154	3176.280	4010.119	3201.601	2249.237

Table 4.17 Natural frequencies (rad/s) for different aspect ratio values for $[0/90/\pm 45]_{12s}$ laminate with CCCC boundary conditions

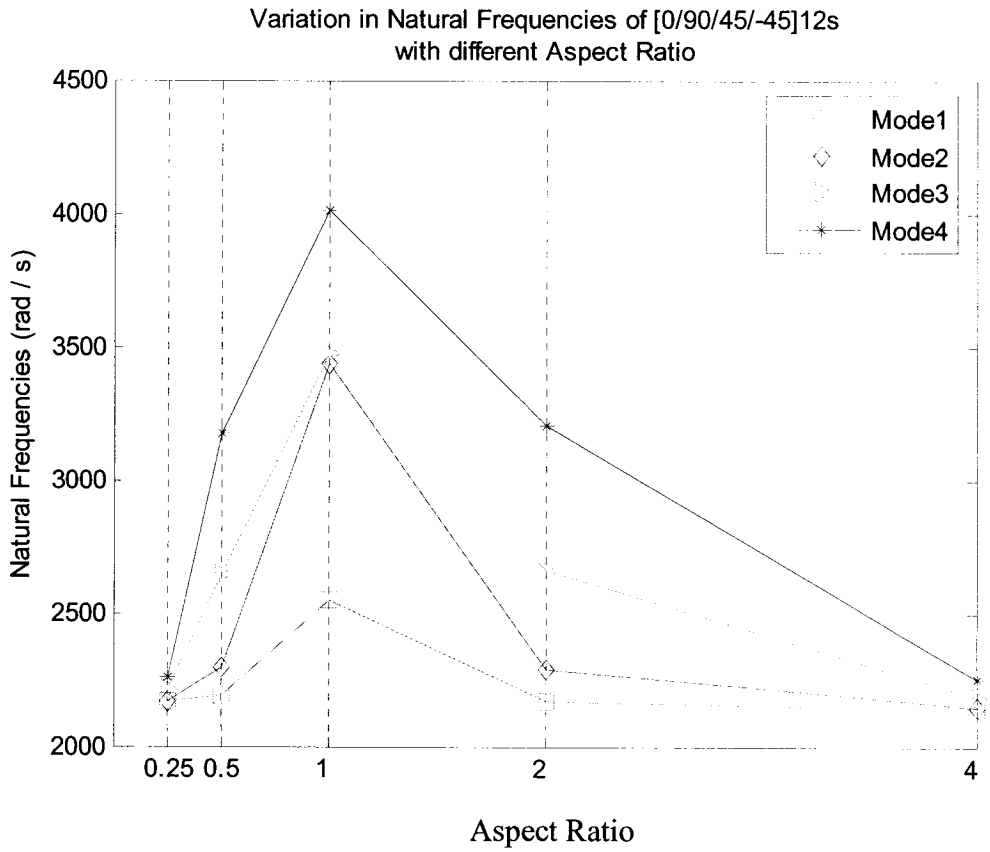

Figure 4.20 Variation in natural frequencies of $[0/90/\pm 45]_{12s}$ laminate with different aspect ratio values

Mode	Aspect Ratio				
	R=0.25	R=0.5	R=1	R=2	R=4
1	1907.860	2021.546	2499.218	2021.546	1907.860
2	1998.817	2324.935	3309.732	2324.935	1998.817
3	2129.860	2693.336	3341.601	2693.336	2129.860
4	2297.317	2872.568	4172.888	2872.568	2297.317

Table 4.18 Natural frequencies (rad/s) for different aspect ratio values for $[\pm 45]_{24s}$ laminate with CCCC boundary conditions

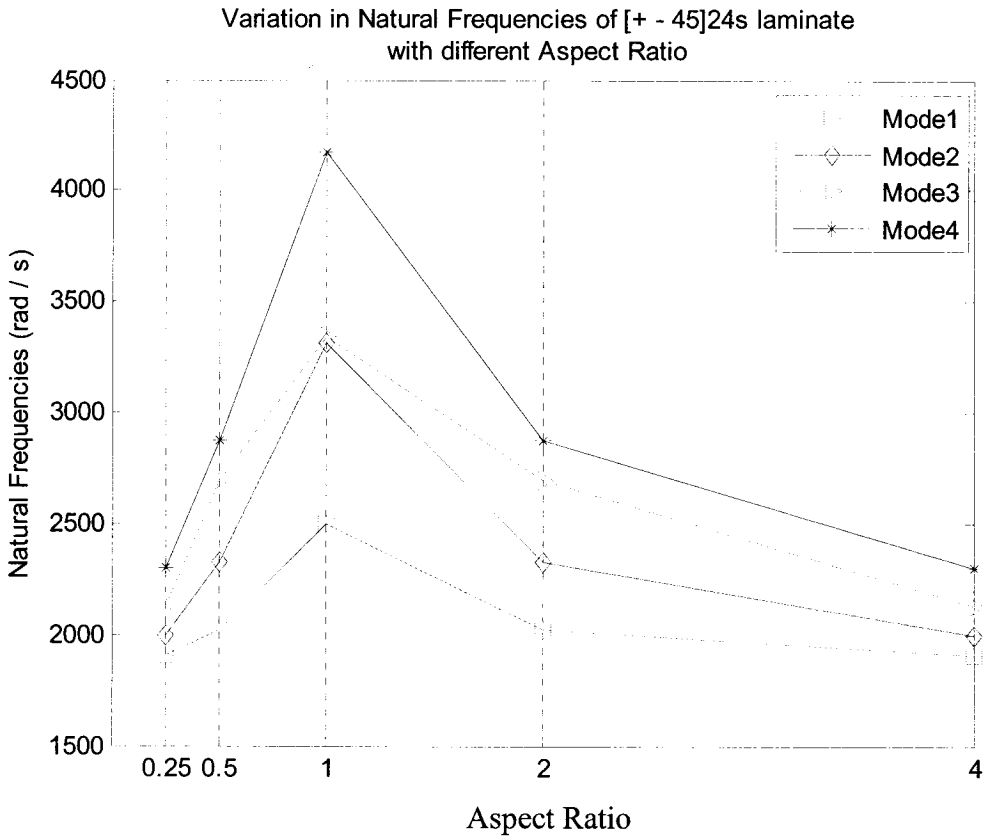

Figure 4.21 Variation in natural frequencies of $[\pm 45]_{24s}$ laminate with different aspect ratio values

4.7 Effect of Elastic Modulus to Shear Modulus (E/G) Ratio on Natural Frequencies

In this section the natural frequencies are calculated for different elastic to shear modulus (E/G) ratio values. The elastic modulus in transverse direction E_2 and shear modulus G_{12} are considered. The case of CCCC boundary conditions is considered. The results are tabulated below and comparison is plotted in Figure 4.22.

Mode	E/G Ratio				
	E/G=1/0.4	E/G=1/0.5	E/G=1/0.6	E/G=1/0.7	E/G=1/0.8
1	2544.683	2556.774	2568.772	2580.680	2592.499
2	3408.840	3424.025	3439.021	3453.837	3468.479
3	3470.135	3485.334	3500.333	3515.140	3529.764
4	3739.831	3770.214	3800.263	3829.988	3859.398

Table 4.19 Natural frequencies of $[0/90]_{24s}$ laminate under CCCC boundary conditions for different E/G ratio values

It is observed that as the E/G ratio decreases, the natural frequencies in all the first four modes increase for $[0/90]_{24s}$ laminate with CCCC boundary conditions. It is also interesting to note the variation of natural frequencies of plate under SSSS boundary conditions which behaves quite similar to the one under CCCC boundary conditions as shown in the following tables.

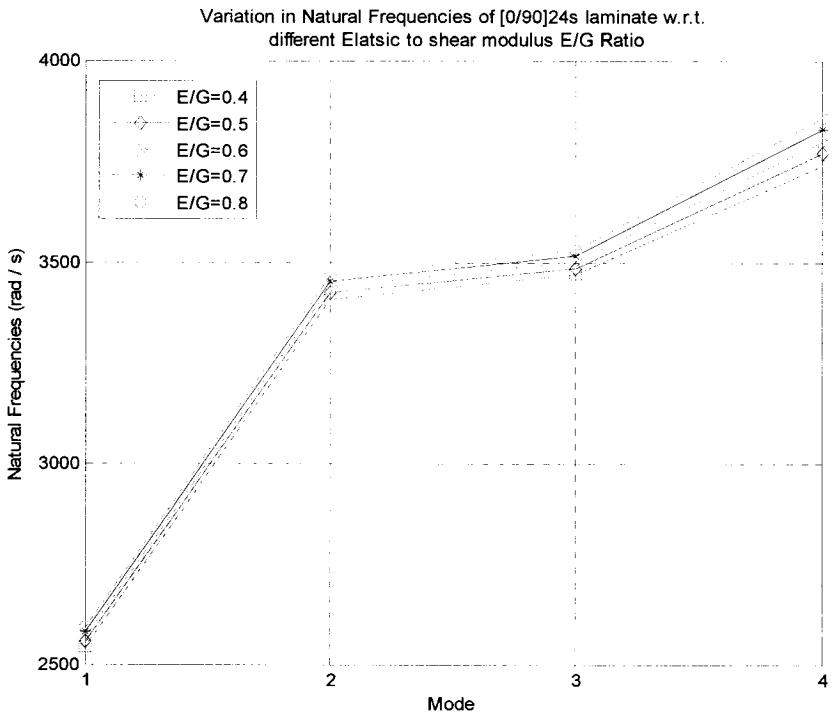

Figure 4.22 Variation in natural frequencies of $[0/90]_{24_s}$ laminate under CCCC boundary conditions for different E/G ratios

Mode	E/G Ratio				
	E/G=1/0.4	E/G=1/0.5	E/G=1/0.6	E/G=1/0.7	E/G=1/0.8
1	1325.068	1342.651	1360.001	1377.127	1394.037
2	2347.588	2363.849	2379.987	2396.004	2411.903
3	2398.239	2414.178	2430.000	2445.707	2461.302
4	2676.361	2711.591	2746.356	2780.675	2814.564

Table 4.20 Natural frequencies of $[0/90]_{24_s}$ laminate under SSSS boundary conditions for different E/G ratio values

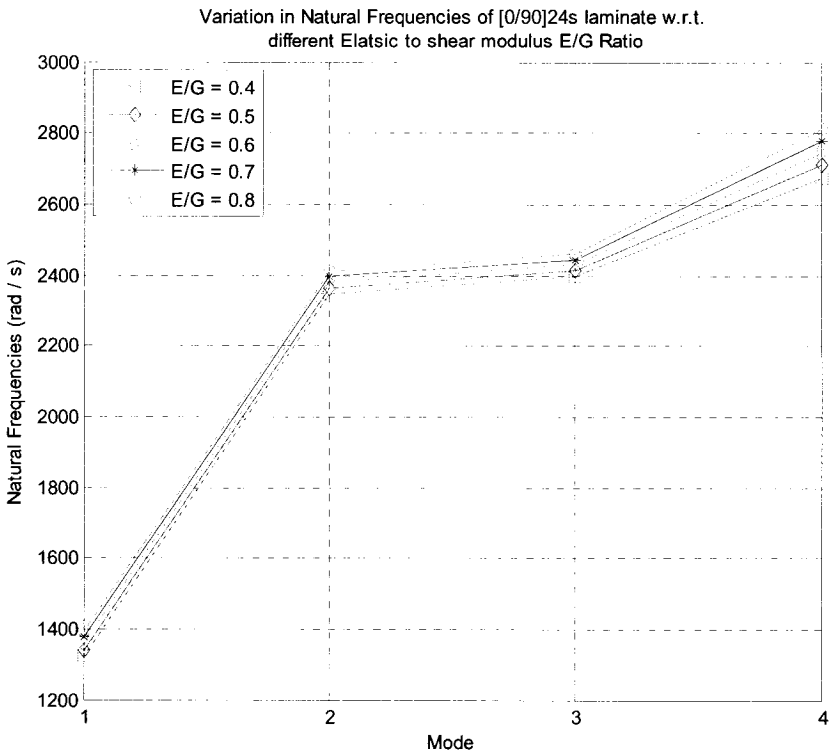

Figure 4.23a Variation in natural frequencies of $[0/90]_{24s}$ laminate under SSSS boundary conditions for different E/G ratio values

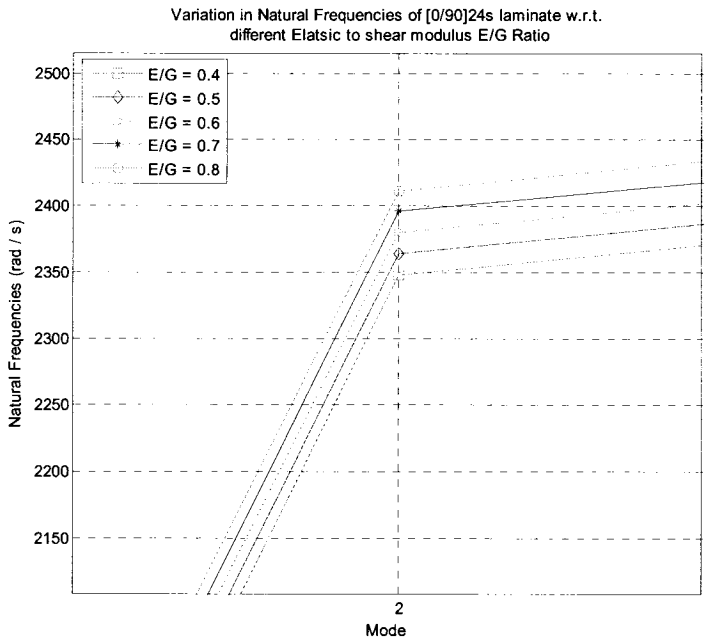

Figure 4.23b Variation in 2nd mode natural frequencies of $[0/90]_{24s}$ laminate under SSSS boundary conditions for different E/G ratio values

4.8 Conclusions

A detailed parametric study has been carried out using Conventional as well as Hierarchical FEM. A comparison study between the two methods has also been carried out and the superiority of HFEM over conventional FEM is proved. Effects of laminate parameters such as boundary conditions, ply configuration, Aspect Ratio and Elastic modulus to shear modulus (E/G) ratio are studied on the static deflection and natural frequencies of laminated composite plates. Mode shapes are plotted for all the cases and the change in their shapes is observed and compared under different laminate parameters as explained in previous sections.

Chapter 5

Conclusions and Recommendations

5.1 Conclusions

In the present thesis hierarchical finite element formulations have been developed for the analysis of laminated composite plates. Static and modal analyses of rectangular laminated plates have been conducted using the developed formulations.

Conventional finite element formulation is developed before introducing HFEM. Results from HFEM are compared with those from conventional FEM to state the efficiency and accuracy of HFEM. Conventional finite element modal is developed using Mindlin finite element consisting of nine nodes, where each node has five degrees of freedom. The hierarchical formulation improves the capabilities of the element by making the degree of approximating polynomial to tend to infinity. The shape functions of a bar element are retained and extra nodes are inserted with shape functions given by Legendre polynomials of Rodrigues form. Stiffness and mass matrices are developed using these shape functions.

The programming involved symbolic computation and is done using MATLAB software. The element properties such as stiffness and mass matrices have been computed numerically using individual sub-routines. The parametric study is performed on the laminated rectangular plates to see the effects of various changes in the laminate parameters on the static deflection and natural frequencies. The effects of aspect ratio, elastic modulus to shear modulus ratio, ply configurations and boundary conditions are considered in the parametric study. The work done in the present thesis has provided some conclusions on the performance of hierarchical finite element formulations based on first order shear deformation theory.

The important conclusions are:-

1) The accuracy can be obtained more efficiently and rapidly by increasing the degree of approximating polynomial than by increasing the number of elements. A comparison of the conventional and hierarchical FEM justifies this conclusion.

2) Simple structures like a rectangular plate can be modeled using only one element which completely eliminates the time and hassles involved in generating meshes and subsequently the need to satisfy inter element continuity.

3) Parametric study performed on various rectangular laminated plates gives a comprehensive understanding of their behavior under physical conditions. The values of natural frequencies and static deflections under different boundary

conditions and for different ply configurations provide useful contribution in developing an optimum design.

5.2 Contributions

The primary contributions have been mentioned in the previous chapters and are summarized below.

1) A set of polynomials has been proposed for polynomial hierarchical formulation which performs better than the conventional FEM formulation.
2) Stiffness and mass matrices are developed using hierarchical finite element formulation based on first-order shear deformation theory.

Besides above mentioned contributions, generalized programs are developed for conventional finite element formulation, Hierarchical finite element formulation and Rayleigh-Ritz Formulation based on first-order shear deformation theory for laminated composite plates.

5.3 Recommendations for Future Work

The modal analysis of rectangular laminated plates using hierarchical finite element formulation can be continued in the future based on following recommendations.

1) The hierarchical finite element formulation developed in the present thesis can be applied to the analysis of forced vibration response of different types of laminated plates.

2) The HFEM formulation can be extended for the analysis of tapered laminated composite plates.

3) Trigonometric functions could be used as approximating functions in HFEM for the analysis of laminated rectangular plates.

4) H-p adaptivity could be used by increasing the number of elements as well as by increasing the order of polynomial .The challenge here lies in developing the accurate element connectivity matrix.

5) The effect of damping could be included in the free and forced vibration analysis of laminated composite plates.

6) The HFEM could be extended by using second and third order shear deformation theories.

References

[1] Bertholet, J.M., *Composite Materials – Mechanical Behavior and Structural Analysis,* 1999, Springer Verlag, New York.

[2] Reddy, J.N., *Mechanics of Laminated Composite Plates – Theory and Analysis,* 1997, CRC Press, U.S.A.

[3] Leissa, A.W., "The Free Vibration of Rectangular Plates", Journal of Sound and Vibration, Vol. 31, 1973, pp.257-293.

[4] Dickinson, S.M. and Blasio, A.Di., "On the use of orthogonal polynomials in the Rayleigh-Ritz Method for the study of flexural vibration and buckling of isotropic and orthotropic rectangular plates", Journal of Sound and Vibration, Vol. 108, 1986, pp.51-62.

[5] Bhat, R.B., "Natural Frequencies of rectangular plates using characteristic orthogonal polynomials in the Rayleigh-Ritz Method", Journal of Sound and Vibration, Vol. 102, 1985, pp.493-499.

[6] Liew, K.M., Lam, K.Y., Chow, S.T., "Free vibration analysis of rectangular plates using orthogonal plate functions", Computers and Structures, Vol. 34, 1990, pp.79-85.

[7] Lin, C.C., King, W.W., "Free transverse vibration of rectangular un-symmetrically laminated plates", Journal of Sound and Vibration, Vol. 36, 1974, pp.91-103.

[8] Reissner,E., "On the bending of elastic plates", Quart. Appl. Math., Vol. 5, 1947, pp.55-68.

[9] Mindlin, R.D., "Influence of rotary inertia and shear on flexural motions of isotropic elastic plates", Journal of Applied Mechanics., Vol. 18, 1951, pp. 31-38.

[10] Stavsky, Y., "On the theory of symmetrically heterogeneous plates having the same thickness variation of the elastic moduli", Topics in Applied Mechanics., 1965, pp. 105.

[11] Yang, P.C., Norris, C.H., Stavsky, Y., "Elastic wave propagation in heterogeneous plates", International journal of solids and structures., Vol. 2, 1966, pp. 665-684.

[12] Ambantsumyan, S.A., "Theory of anisotropic shells", NASA Report., 1966, TTF-118.

[13] Whitney, J.M., Pagano, N.J., "Shear deformation in hetrogenous anisotropic plates", Journal of Applied Mechanics, Vol. 37, 1970, pp. 1031-1036.

[14] Whitney, J.M., "Stress analysis of thick laminated composite and sandwich plates", Journal of Composite materials, Vol. 6, 1972, pp. 426-440.

[15] Lo, K.H., Christensen, R.M., Wu, E.M. "A higher order theory of plates deformation. Part 1: Homogenous plates", Journal of Applied Mechanics, Vol. 44, 1977, pp. 663-668.

[16] Lo, K.H., Christensen, R.M., Wu, E.M. "A higher order theory of plates deformation. Part 2: Laminated plates", Journal of Applied Mechanics, Vol. 44, 1977, pp. 669-676.

[17] Kant, T., Owen, D.R.J., Zienkiewicz, O.C., "A refined higher order C^0 plate bending element", Computers and Structures, Vol. 15, 1982, pp. 177-183.

[18] Whitney, J.M., Sun, C.T., "A higher order theory for the tensional motion of laminated composites", Journal of sound and vibrations, Vol. 30, 1973, pp. 85-97.

[19] Nelson, R.B., Lorch, D.R., "A refine theory of laminated orthotropic plates", Journal of Applied Mechanics., Vol. 41, 1975, pp. 171-183.

[20] Lo, K.H., Christensen, R.M., Wu, E.M. "Stress Solution determination for higher order plate theory", International journal of solids and structures., Vol. 14, 1978, pp. 655-662.

[21] Reddy, J.N., "A simple higher order theory for laminated composite plates", Journal of Applied Mechanics., Vol. 51, 1989, pp. 745.

[22] Pagano, N.J., "On the calculation of inter-laminar normal stress in composite plates", Journal of Composite Materials., Vol. 8 1974, pp. 65-82.

[23] Srinivas, S., "A refined analysis of composite laminates", Journal of Sound and Vibrations., Vol. 30, 1973, pp. 495-507.

[24] Pagano, N.J., "Solution for composite laminate in cylindrical bending", Journal of composite materials., Vol. 3, 1969, pp. 398.

[25] Srinivas, S., Rao, A.K., "Bending vibration and buckling of simply supported thick orthotropic rectangular plates and laminates", International Journal of solids and structures., Vol. 6, 1970, pp.1463-1481.

[26] Reddy, J.N., "Free vibration of anti-symmetric, angle-ply laminated plates including transverse shear deformation by the finite element method", Journal of sound and vibrations, Vol. 66, 1979, pp. 565-576.

[27] Peano, A. G., "Hierarchies of Conforming Finite Elements for Plane Elasticity and Plate Bending", Computers and Mathematics with Applications, Vol. 2, 1976, pp. 211-224.

[28] Babuska, I., Szabo, B. A., and Katz, I. N., "The p-version of the Finite Element Method", SIAM Journal of Numerical Analysis, Vol. 18(3), 1981, pp. 515-545.

[29] Noor, A. K., Mathers, M.D., "Anisotropy and shear deformation in laminated composite plates", American institute of aeronautics and astronautics journal, Vol. 14, 1976, pp. 282-285.

[30] Noor, A. K., Mathers, M.D., "Finite element analysis of anisotropic plates", International journal for numerical methods in engineering, Vol. 11, 1977, pp. 289-307.

[31] Zienkiewicz, O. C., Irons, B. M., Scott, F. C., and Campbell, J., "Three Dimensional Stress Analysis", University of Liege Press, Proc. IUTAM Symp. On High Speed Computing of Elastic Structures, 1971, pp. 413-433.

[32] Zienkiewicz, O. C., Owen, D. R. J., Philips, D. W., and Nayak, G. C., "Finite Element Methods in the Analysis of Reactor Vessels", Nuclear Engineering Design, Vol. 20, 1972, pp. 507-541.

[33] Peano, A. G., "Hierarchies of Conforming Finite Elements for Plane Elasticity and Plate Bending", Computers and Mathematics with Applications, Vol. 2, 1976, pp. 211-224.

[34] Szabo, B. A., and Mehta, A. V., "P-Convergent Finite Element Approximations in Fracture Mechanics", International Journal of Numerical Methods in Engineering, Vol. 12, 1978, pp. 551-560.

[35] Basu, P. K., Szabo, B. A., and Taylor, B. D., "Theoretical Manual and Users Guide for Comet-XA. Rep. WV/CCM-79/2", Center for Computational Mechanics, Washington University, 1979.

[36] Zienkiewicz, O. C., Kelly, D. W., Gago, J. P. de S. R., and Babuska, I., "Hierarchical Finite Element Approaches, Adaptive refinement and Error Estimates", Proc. MAFELAP 1981.

[37] Szabo, B. A., "Mesh Design for the p-version of the Finite Element", Computer Methods in Applied Mechanics and Engineering, Vol. 55, 1986, pp. 181-197.

[38] Kelly, D. W., Gago, J. P. De S. R., Zienkiewicz, O. C., and Babuska, I., "A Posteriori Error Analysis and Adaptive Processes in the Finite Element Method: Part I – Error Analysis", International Journal of Numerical Methods in Engineering, Vol. 19, 1983, pp. 1593-1619.

[39] Gago, J. P. De S. R., Kelly, D. W., Zienkiewicz, O. C., and Babuska, I., "A Posteriori Error Analysis and Adaptive Processes in the Finite Element Method: Part II – Adaptive Mesh Refinement", International Journal of Numerical Methods in Engineering, Vol. 19, 1983, pp. 1621-1656.

[40] Han, W., and Petyt, M., "Linear Vibration Analysis of Laminated Rectangular Plates using the Hierarchical Finite Element Method – I: Free Vibration Analysis", Computers and Structures, Vol. 61, 1996, pp. 705-712.

[41] Han, W., and Petyt, M, "Linear Vibration Analysis of Laminated Rectangular Plates using the Hierarchical Finite Element Method – II: Forced Vibration Analysis", Computers and Structures, Vol. 61, 1996, pp. 713-724.

[42] Han, W., and Petyt, M., "Geometrically Non-Linear Vibration Analysis of Thin, Rectangular Plates using the Hierarchical Finite Element Method – I: The Fundamental Mode of Isotropic Plates", Computers and Structures, Vol. 63, 1997, pp. 295-308.

[43] Han, W., and Petyt, M., "Geometrically Non-Linear Vibration Analysis of Thin, Rectangular Plates using the Hierarchical Finite Element Method – II: 1st Mode of Laminated Plates and Higher Modes of Isotropic and Laminated Plates", Computers and Structures, Vol. 63, 1997, pp. 309-318.

[44] Bardell, N.S., "Free vibration analysis of a flat plate using the hierarchical finite element method", Journal of sound and vibrations, Vol. 151, 1991, pp. 263-289.

[45] Bardell, N. S., Dunsdon, J. M., and Langlay, R. S., "Free Vibration of Thin, Isotropic, Open, Conical Panels ", Journal of Sound and Vibration, Vol. 217, 1998, pp. 297-320.

[46] Han, W., Petyt, M., and Hsiao, K. M., "An Investigation into Geometrically Non-Linear Analysis of Rectangular Laminated Plates Using the Hierarchical Finite Element Method", Finite Element Analysis and Design, Vol. 18, 1994, pp. 273-288.

[47] Kowda, Vijay K., "Free-vibration and buckling of prismatic and thin-walled composite beam-columns with stochastic properties", M.A.Sc. Thesis, 2002, Concordia University.

General References

[48] Cook, R. D., Malkus, D. S., and Plesha, M. E., *Concepts and Applications of Finite Element Analysis,* 1989, New York, U. S. A., Wiley Publishing Company.

[49] Reddy, J. N., *An Introduction to Finite Element Method,* 1993, New York, U. S. A., McGraw-Hill Inc.

[50] Weaver, W. Jr., Timoshenko, S. P., and Young, D. H., *Vibration Problems in Engineering,* 1990, New York, U. S. A., Wiley Publishing Company.

[51] Yang, T. Y., *Finite Element Analysis of Structures,* 1985, New York, U. S. A., Wiley Inc.

[52] Paz, M, *Structural Dynamics – Theory and Computation,* 1997, New York, U. S. A., Chapman & Hall Inc.

[53] Kim, D. H., *Composite Structures for Civil and Architectural Engineering,* 1995, U. S. A., E & FN Spon.

[54] Hyer, M.W., *Stress Analysis of Fibre-Reinforced Composite Materials,* 1998, New York, U. S. A., McGraw-Hill Inc.

[55] Bathe, K. J., *Finite Element Procedures,* 1996, New Jersy, U. S. A., Princeton Hall.

[56] Whitney, J. M., and Ashton, J. E., *Structural Analysis of Laminated Anisotropic Plates*, 1987, Lancaster, Pa., U. S. A., Technomic Publishing Company.

[57] Nigam, Amit, "Dynamic Analysis of Composite Beams using Hierarchical Finite Element Method", M.A.Sc. Thesis, 2002, Concordia University.

Appendix-I

Term 5 to Term 16 of the Equation (2.11)

Term 5

$$2D_{12}\frac{\partial \psi_x}{\partial x}\frac{\partial \psi_y}{\partial y}$$

$$\text{Term 5} = 2D_{12}\sum_{m=1}^{M}\sum_{n=1}^{N}\sum_{i=1}^{M}\sum_{j=1}^{N}\left(B_{mn}C_{ij}\frac{dP_m}{dx}Q_n\frac{dT_j}{dy}S_i + B_{ij}C_{mn}\frac{dP_i}{dx}Q_j\frac{dT_n}{dy}S_m\right)$$

$$\frac{1}{2}\frac{\partial}{\partial A_{mn}}(Term5) = 0$$

$$\frac{1}{2}\frac{\partial}{\partial B_{mn}}(Term5) = D_{12}\sum_{i=1}^{M}\sum_{j=1}^{N}C_{ij}\frac{dP_m}{dx}Q_n\frac{dT_j}{dy}S_i$$

$$\frac{1}{2}\frac{\partial}{\partial C_{mn}}(Term5) = D_{12}\sum_{i=1}^{M}\sum_{j=1}^{N}B_{ij}\frac{dP_i}{dx}Q_j\frac{dT_n}{dy}S_m$$

Integration of non zero terms yields

$$\frac{1}{2}\int_{x=0}^{a}\int_{y=0}^{b}\frac{\partial}{\partial B_{mn}}(Term5)dxdy = D_{12}\sum_{i=1}^{M}\sum_{j=1}^{N}C_{ij}\int_{x=0}^{a}\frac{dP_m}{dx}S_i dx\int_{y=0}^{b}\frac{dT_j}{dy}Q_n dy$$

$$\frac{1}{2}\int_{x=0}^{a}\int_{y=0}^{b}\frac{\partial}{\partial C_{mn}}(Term5)dxdy = D_{12}\sum_{i=1}^{M}\sum_{j=1}^{N}B_{ij}\int_{x=0}^{a}\frac{dP_i}{dx}S_m dx\int_{y=0}^{b}\frac{dT_n}{dy}Q_j dy$$

Term 6

$$2D_{66}\frac{\partial \psi_x}{\partial y}\frac{\partial \psi_y}{\partial x}$$

$$\text{Term 6} = 2D_{66}\sum_{m=1}^{M}\sum_{n=1}^{N}\sum_{i=1}^{M}\sum_{j=1}^{N}\left(B_{mn}C_{ij}\frac{dQ_n}{dy}P_m\frac{dS_i}{dx}T_j + B_{ij}C_{mn}\frac{dQ_j}{dy}P_i\frac{dS_m}{dx}T_n\right)$$

$$\frac{1}{2}\frac{\partial}{\partial A_{mn}}(Term6) = 0$$

$$\frac{1}{2}\frac{\partial}{\partial B_{mn}}(Term6) = D_{66}\sum_{i=1}^{M}\sum_{j=1}^{N}C_{ij}\frac{dQ_n}{dy}P_m\frac{dS_i}{dx}T_j$$

$$\frac{1}{2}\frac{\partial}{\partial C_{mn}}(Term6) = D_{66}\sum_{i=1}^{M}\sum_{j=1}^{N}B_{ij}\frac{dQ_j}{dy}P_i\frac{dS_m}{dx}T_n$$

Integration of non zero terms yields

$$\frac{1}{2}\int_{x=0}^{a}\int_{y=0}^{b}\frac{\partial}{\partial B_{mn}}(Term6)dxdy = D_{66}\sum_{i=1}^{M}\sum_{j=1}^{N}C_{ij}\int_{x=0}^{a}\frac{dS_i}{dx}P_m dx\int_{y=0}^{b}\frac{dQ_n}{dy}T_j dy$$

$$\frac{1}{2}\int_{x=0}^{a}\int_{y=0}^{b}\frac{\partial}{\partial C_{mn}}(Term6)dxdy = D_{66}\sum_{i=1}^{M}\sum_{j=1}^{N}B_{ij}\int_{x=0}^{a}\frac{dS_m}{dx}P_i dx\int_{y=0}^{b}\frac{dQ_j}{dy}T_n dy$$

Term 7

$$A_{44}\left(\frac{\partial w}{\partial y}\right)^2$$

$$\text{Term 7} = A_{44}\sum_{m=1}^{M}\sum_{n=1}^{N}\sum_{i=1}^{M}\sum_{j=1}^{N}A_{mn}A_{ij}X_m\frac{dY_n}{dy}X_i\frac{dY_j}{dy}$$

$$\frac{1}{2}\frac{\partial}{\partial A_{mn}}(Term7) = A_{44}\sum_{i=1}^{M}\sum_{j=1}^{N}A_{ij}X_m\frac{dY_n}{dy}X_i\frac{dY_j}{dy}$$

$$\frac{1}{2}\frac{\partial}{\partial B_{mn}}(Term7) = 0$$

$$\frac{1}{2}\frac{\partial}{\partial C_{mn}}(Term7) = 0$$

Integration of non zero term yields

$$\frac{1}{2}\int_{x=0}^{a}\int_{y=0}^{b}\frac{\partial}{\partial A_{mn}}(Term7)dxdy = A_{44}\sum_{i=1}^{M}\sum_{j=1}^{N}A_{ij}\int_{x=0}^{a}X_m X_i dx\int_{y=0}^{b}\frac{dY_n}{dy}\frac{dY_j}{dy}dy$$

Term 8

$$A_{55}\left(\frac{\partial w}{\partial x}\right)^2$$

$$\text{Term 8} = A_{55}\sum_{m=1}^{M}\sum_{n=1}^{N}\sum_{i=1}^{M}\sum_{j=1}^{N}A_{mn}A_{ij}\frac{dX_m}{dx}Y_n\frac{dX_i}{dx}Y_j$$

$$\frac{1}{2}\frac{\partial}{\partial A_{mn}}(Term8) = A_{55}\sum_{i=1}^{M}\sum_{j=1}^{N}A_{ij}\frac{dX_m}{dx}Y_n\frac{dX_i}{dx}Y_j$$

$$\frac{1}{2}\frac{\partial}{\partial B_{mn}}(Term8) = 0$$

$$\frac{1}{2}\frac{\partial}{\partial C_{mn}}(Term8) = 0$$

Integration of non zero term yields

$$\frac{1}{2}\int_{x=0}^{a}\int_{y=0}^{b}\frac{\partial}{\partial A_{mn}}(Term8)dxdy = A_{55}\sum_{i=1}^{M}\sum_{j=1}^{N}A_{ij}\int_{x=0}^{a}\frac{dX_m}{dx}\frac{dX_i}{dx}dx\int_{y=0}^{b}Y_n Y_j dy$$

Term 9

$$A_{44}(\psi_y)^2$$

$$\text{Term 9} = A_{44}\sum_{m=1}^{M}\sum_{n=1}^{N}\sum_{i=1}^{M}\sum_{j=1}^{N}C_{mn}C_{ij}S_m T_n S_i T_j$$

$$\frac{1}{2}\frac{\partial}{\partial A_{mn}}(Term9) = 0$$

$$\frac{1}{2}\frac{\partial}{\partial B_{mn}}(Term9) = 0$$

$$\frac{1}{2}\frac{\partial}{\partial C_{mn}}(Term9) = A_{44}\sum_{i=1}^{M}\sum_{j=1}^{N} C_{ij} S_m T_n S_i T_j$$

Integration of non zero term yields

$$\frac{1}{2}\int_{x=0}^{a}\int_{y=0}^{b}\frac{\partial}{\partial C_{mn}}(Term9)dxdy = A_{44}\sum_{i=1}^{M}\sum_{j=1}^{N} C_{ij}\int_{x=0}^{a} S_m S_i dx \int_{y=0}^{b} T_n T_j dy$$

Term 10

$$A_{55}(\psi_x)^2$$

$$\text{Term } 10 = A_{55}\sum_{m=1}^{M}\sum_{n=1}^{N}\sum_{i=1}^{M}\sum_{j=1}^{N} B_{mn} B_{ij} P_m Q_n P_i Q_j$$

$$\frac{1}{2}\frac{\partial}{\partial A_{mn}}(Term10) = 0$$

$$\frac{1}{2}\frac{\partial}{\partial B_{mn}}(Term10) = A_{55}\sum_{i=1}^{M}\sum_{j=1}^{N} B_{ij} P_m Q_n P_i Q_j$$

$$\frac{1}{2}\frac{\partial}{\partial C_{mn}}(Term10) = 0$$

Integration of non zero term yields

$$\frac{1}{2}\int_{x=0}^{a}\int_{y=0}^{b}\frac{\partial}{\partial B_{mn}}(Term10)dxdy = A_{55}\sum_{i=1}^{M}\sum_{j=1}^{N} B_{ij}\int_{x=0}^{a} P_m P_i dx \int_{y=0}^{b} Q_n Q_j dy$$

Term 11

$$2A_{45}\frac{\partial w}{\partial x}\frac{\partial w}{\partial y}$$

$$\text{Term 11} = 2A_{45}\sum_{m=1}^{M}\sum_{n=1}^{N}\sum_{i=1}^{M}\sum_{j=1}^{N}A_{mn}A_{ij}\left(X_m\frac{dY_n}{dy}\frac{dX_i}{dx}Y_j + X_i\frac{dY_j}{dy}\frac{dX_m}{dx}Y_n\right)$$

$$\frac{1}{2}\frac{\partial}{\partial A_{mn}}(Term11) = A_{45}\sum_{i=1}^{M}\sum_{j=1}^{N}A_{ij}\left(X_m\frac{dY_n}{dy}\frac{dX_i}{dx}Y_j + X_i\frac{dY_j}{dy}\frac{dX_m}{dx}Y_n\right)$$

$$\frac{1}{2}\frac{\partial}{\partial B_{mn}}(Term11) = 0$$

$$\frac{1}{2}\frac{\partial}{\partial C_{mn}}(Term11) = 0$$

Integration of non zero term yields

$$\frac{1}{2}\int_{x=0}^{a}\int_{y=0}^{b}\frac{\partial}{\partial A_{mn}}(Term11)dxdy =$$

$$A_{45}\sum_{i=1}^{M}\sum_{j=1}^{N}A_{ij}\left(\int_{x=0}^{a}X_m\frac{dX_i}{dx}dx\int_{y=0}^{b}\frac{dY_n}{dy}Y_j dy + \int_{x=0}^{a}X_i\frac{dX_m}{dx}dx\int_{y=0}^{b}\frac{dY_j}{dy}Y_n dy\right)$$

$$\frac{1}{2}\int_{x=0}^{a}\int_{y=0}^{b}\frac{\partial}{\partial B_{mn}}(Term11)dxdy = 0$$

$$\frac{1}{2}\int_{x=0}^{a}\int_{y=0}^{b}\frac{\partial}{\partial C_{mn}}(Term11)dxdy = 0$$

Term 12

$$2A_{45}\frac{\partial w}{\partial y}\psi_x$$

$$\text{Term } 12 = 2A_{45}\sum_{m=1}^{M}\sum_{n=1}^{N}\sum_{i=1}^{M}\sum_{j=1}^{N}\left(A_{mn}B_{ij}\frac{dY_n}{dy}X_mP_iQ_j + A_{ij}B_{mn}\frac{dY_j}{dy}X_iP_mQ_n\right)$$

$$\frac{1}{2}\frac{\partial}{\partial A_{mn}}(Term12) = A_{45}\sum_{i=1}^{M}\sum_{j=1}^{N}B_{ij}\frac{dY_n}{dy}X_mP_iQ_j$$

$$\frac{1}{2}\frac{\partial}{\partial B_{mn}}(Term12) = A_{45}\sum_{i=1}^{M}\sum_{j=1}^{N}A_{ij}\frac{dY_j}{dy}X_iP_mQ_n$$

$$\frac{1}{2}\frac{\partial}{\partial C_{mn}}(Term12) = 0$$

Integration of non zero terms yields

$$\frac{1}{2}\int_{x=0}^{a}\int_{y=0}^{b}\frac{\partial}{\partial A_{mn}}(Term12)dxdy = A_{45}\sum_{i=1}^{M}\sum_{j=1}^{N}B_{ij}\int_{x=0}^{a}X_mP_idx\int_{y=0}^{b}\frac{dY_n}{dy}Q_jdy$$

$$\frac{1}{2}\int_{x=0}^{a}\int_{y=0}^{b}\frac{\partial}{\partial B_{mn}}(Term12)dxdy = A_{45}\sum_{i=1}^{M}\sum_{j=1}^{N}A_{ij}\int_{x=0}^{a}P_mX_idx\int_{y=0}^{b}\frac{dY_j}{dy}Q_ndy$$

Term 13

$$2A_{44}\frac{\partial w}{\partial y}\psi_y$$

$$\text{Term } 13 = 2A_{44}\sum_{m=1}^{M}\sum_{n=1}^{N}\sum_{i=1}^{M}\sum_{j=1}^{N}\left(A_{mn}C_{ij}\frac{dY_n}{dy}X_mS_iT_j + A_{ij}C_{mn}\frac{dY_j}{dy}X_iS_mT_n\right)$$

$$\frac{1}{2}\frac{\partial}{\partial A_{mn}}(Term13) = A_{44}\sum_{i=1}^{M}\sum_{j=1}^{N}C_{ij}\frac{dY_n}{dy}X_mS_iT_j$$

$$\frac{1}{2}\frac{\partial}{\partial B_{mn}}(Term13) = 0$$

$$\frac{1}{2}\frac{\partial}{\partial C_{mn}}(Term13) = A_{44}\sum_{i=1}^{M}\sum_{j=1}^{N}A_{ij}\frac{dY_j}{dy}X_iS_mT_n$$

Integration of non zero terms yields

$$\frac{1}{2}\int_{x=0}^{a}\int_{y=0}^{b}\frac{\partial}{\partial A_{mn}}(Term13)dxdy = A_{44}\sum_{i=1}^{M}\sum_{j=1}^{N}C_{ij}\int_{x=0}^{a}X_m S_i dx\int_{y=0}^{b}\frac{dY_n}{dy}T_j dy$$

$$\frac{1}{2}\int_{x=0}^{a}\int_{y=0}^{b}\frac{\partial}{\partial C_{mn}}(Term13)dxdy = A_{44}\sum_{i=1}^{M}\sum_{j=1}^{N}A_{ij}\int_{x=0}^{a}S_m X_i dx\int_{y=0}^{b}\frac{dY_j}{dy}T_n dy$$

Term 14

$$2A_{45}\frac{\partial w}{\partial x}\psi_y$$

$$\text{Term 14} = 2\ A_{45}\sum_{m=1}^{M}\sum_{n=1}^{N}\sum_{i=1}^{M}\sum_{j=1}^{N}(A_{mn}C_{ij}\frac{dX_m}{dx}Y_n S_i T_j + A_{ij}C_{mn}\frac{dX_i}{dx}Y_j S_m T_n)$$

$$\frac{1}{2}\frac{\partial}{\partial A_{mn}}(Term14) = A_{45}\sum_{i=1}^{M}\sum_{j=1}^{N}C_{ij}\frac{dX_m}{dx}Y_n S_i T_j$$

$$\frac{1}{2}\frac{\partial}{\partial B_{mn}}(Term14) = 0$$

$$\frac{1}{2}\frac{\partial}{\partial C_{mn}}(Term14) = A_{45}\sum_{i=1}^{M}\sum_{j=1}^{N}A_{ij}\frac{dX_i}{dx}Y_j S_m T_n$$

Integration of non zero terms yields

$$\frac{1}{2}\int_{x=0}^{a}\int_{y=0}^{b}\frac{\partial}{\partial A_{mn}}(Term14)dxdy = A_{45}\sum_{i=1}^{M}\sum_{j=1}^{N}C_{ij}\int_{x=0}^{a}\frac{dX_m}{dx}S_i dx\int_{y=0}^{b}Y_n T_j dy$$

$$\frac{1}{2}\int_{x=0}^{a}\int_{y=0}^{b}\frac{\partial}{\partial C_{mn}}(Term14)dxdy = A_{45}\sum_{i=1}^{M}\sum_{j=1}^{N}A_{ij}\int_{x=0}^{a}S_m\frac{dX_i}{dx}dx\int_{y=0}^{b}Y_j T_n dy$$

Term 15

$$2A_{55}\frac{\partial w}{\partial x}\psi_x$$

$$\text{Term } 15 = 2A_{55}\sum_{m=1}^{M}\sum_{n=1}^{N}\sum_{i=1}^{M}\sum_{j=1}^{N}(A_{mn}B_{ij}\frac{dX_m}{dx}Y_nP_iQ_j + A_{ij}B_{mn}\frac{dX_i}{dx}Y_iP_mQ_n)$$

$$\frac{1}{2}\frac{\partial}{\partial A_{mn}}(Term15) = A_{55}\sum_{i=1}^{M}\sum_{j=1}^{N}B_{ij}\frac{dX_m}{dx}Y_nP_iQ_j$$

$$\frac{1}{2}\frac{\partial}{\partial B_{mn}}(Term15) = A_{55}\sum_{i=1}^{M}\sum_{j=1}^{N}A_{ij}\frac{dX_i}{dx}Y_iP_mQ_n$$

$$\frac{1}{2}\frac{\partial}{\partial C_{mn}}(Term15) = 0$$

Integration of non zero terms yields

$$\frac{1}{2}\int_{x=0}^{a}\int_{y=0}^{b}\frac{\partial}{\partial A_{mn}}(Term15)dxdy = A_{55}\sum_{i=1}^{M}\sum_{j=1}^{N}B_{ij}\int_{x=0}^{a}\frac{dX_m}{dx}P_idx\int_{y=0}^{b}Y_nQ_jdy$$

$$\frac{1}{2}\int_{x=0}^{a}\int_{y=0}^{b}\frac{\partial}{\partial B_{mn}}(Term15)dxdy = A_{55}\sum_{i=1}^{M}\sum_{j=1}^{N}A_{ij}\int_{x=0}^{a}P_m\frac{dX_i}{dx}dx\int_{y=0}^{b}Y_jQ_ndy$$

Term 16

$$2A_{45}\psi_x\psi_y$$

$$\text{Term } 16 = 2A_{45}\sum_{m=1}^{M}\sum_{n=1}^{N}\sum_{i=1}^{M}\sum_{j=1}^{N}(B_{mn}C_{ij}P_mQ_nT_jS_i + B_{ij}C_{mn}P_iQ_jT_nS_m)$$

$$\frac{1}{2}\frac{\partial}{\partial A_{mn}}(Term16) = 0$$

$$\frac{1}{2}\frac{\partial}{\partial B_{mn}}(Term16) = A_{45}\sum_{i=1}^{M}\sum_{j=1}^{N} C_{ij}P_mQ_nT_jS_i$$

$$\frac{1}{2}\frac{\partial}{\partial C_{mn}}(Term16) = A_{45}\sum_{i=1}^{M}\sum_{j=1}^{N} B_{ij}P_iQ_jT_nS_m$$

Integration of non zero terms yields

$$\frac{1}{2}\int_{x=0}^{a}\int_{y=0}^{b}\frac{\partial}{\partial B_{mn}}(Term16)dxdy = A_{45}\sum_{i=1}^{M}\sum_{j=1}^{N} C_{ij}\int_{x=0}^{a}P_mS_i dx\int_{y=0}^{b}T_jQ_n$$

$$\frac{1}{2}\int_{x=0}^{a}\int_{y=0}^{b}\frac{\partial}{\partial C_{mn}}(Term16)dxdy = A_{45}\sum_{i=1}^{M}\sum_{j=1}^{N} B_{ij}\int_{x=0}^{a}P_iS_m dx\int_{y=0}^{b}T_nQ_j dy$$

Appendix-II

Mode Shapes of various laminate configurations with different boundary conditions and variation of natural frequencies of various laminate configurations with respect to aspect ratio values with SSSS boundary conditions.

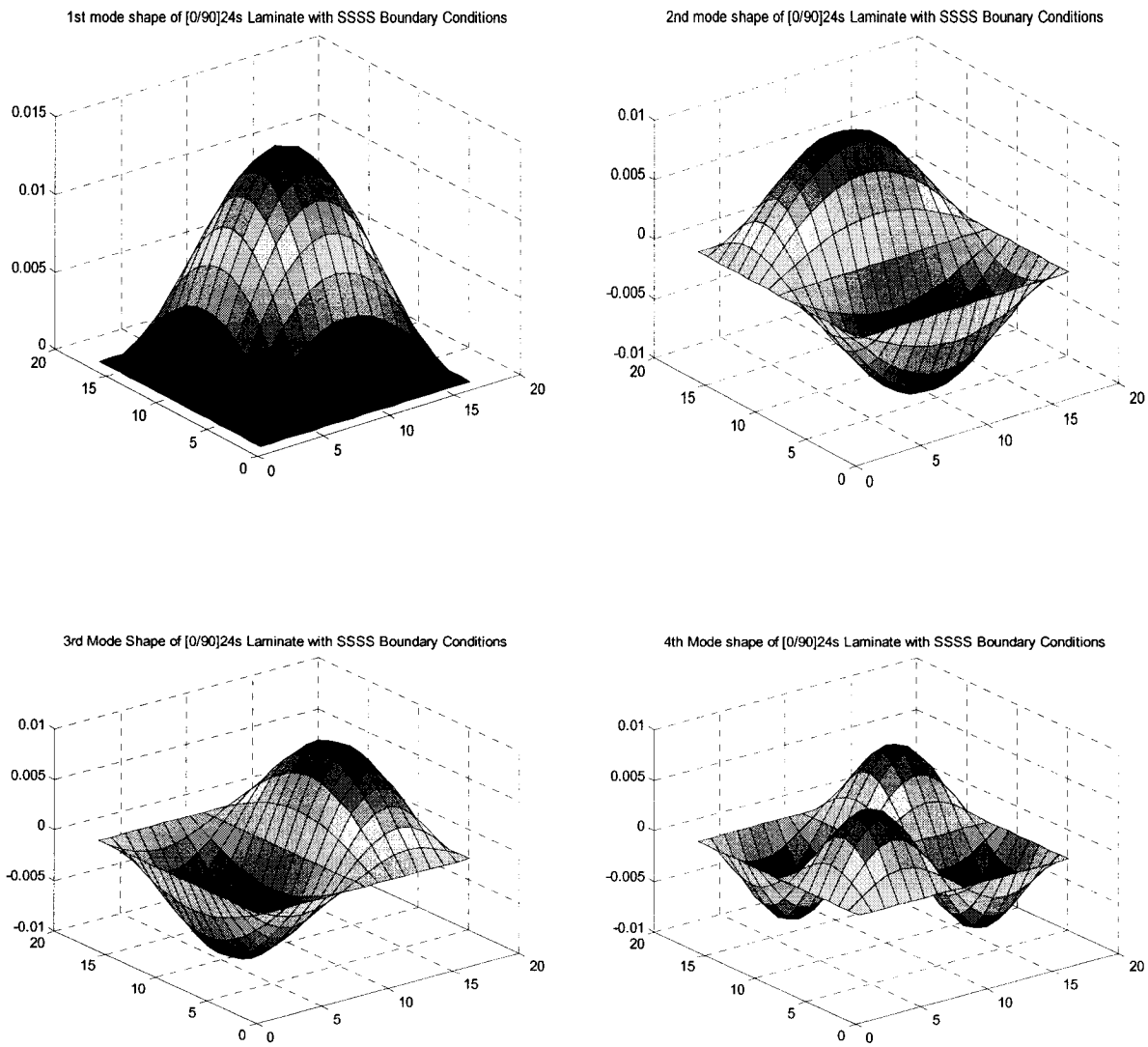

Figure 4.9.1 First four mode shapes of $[0/90]_{24s}$ laminate with SSSS boundary conditions

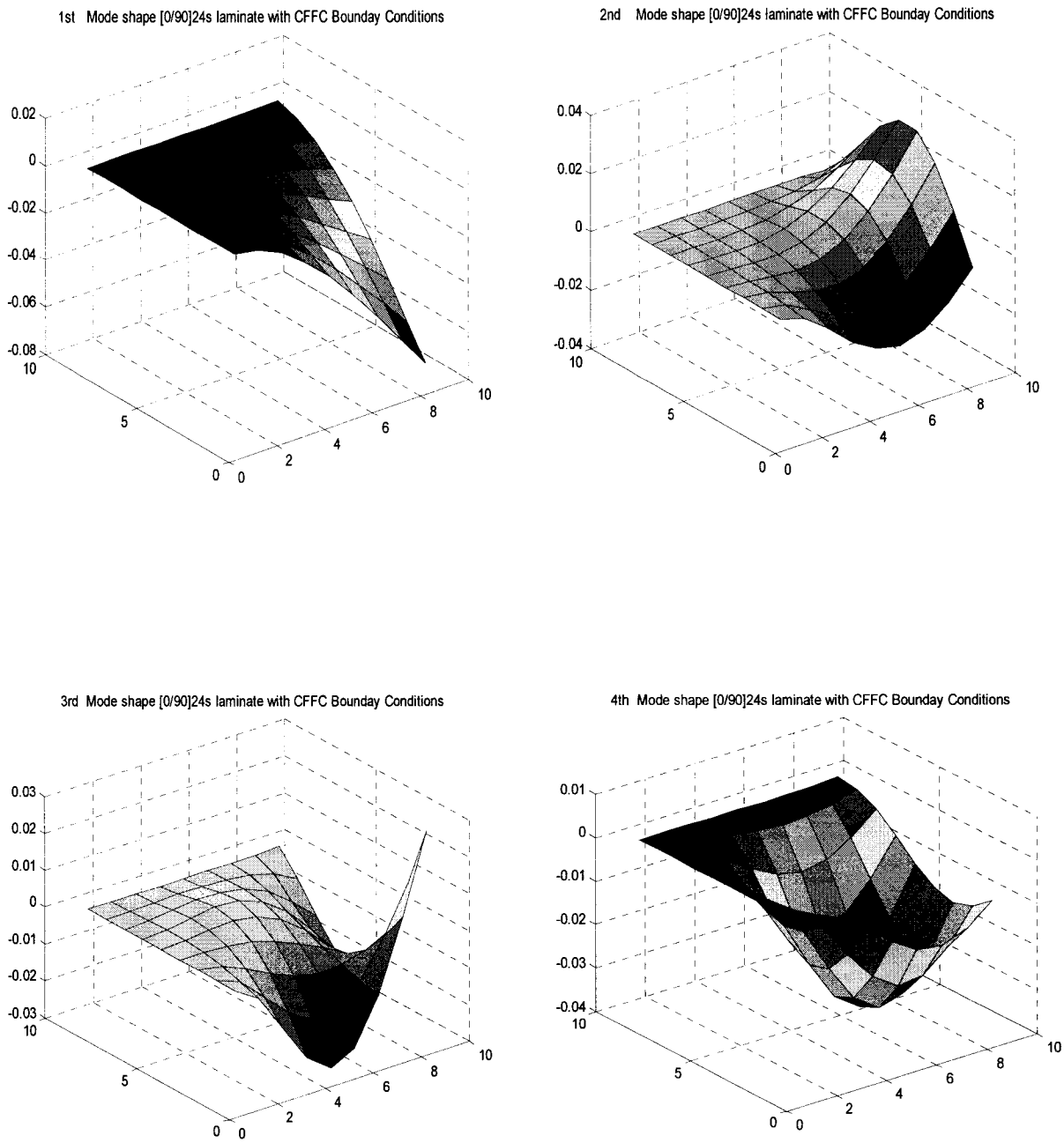

Figure 4.9.2 First four mode shapes of $[0/90]_{24s}$ laminate with CFFC boundary conditions

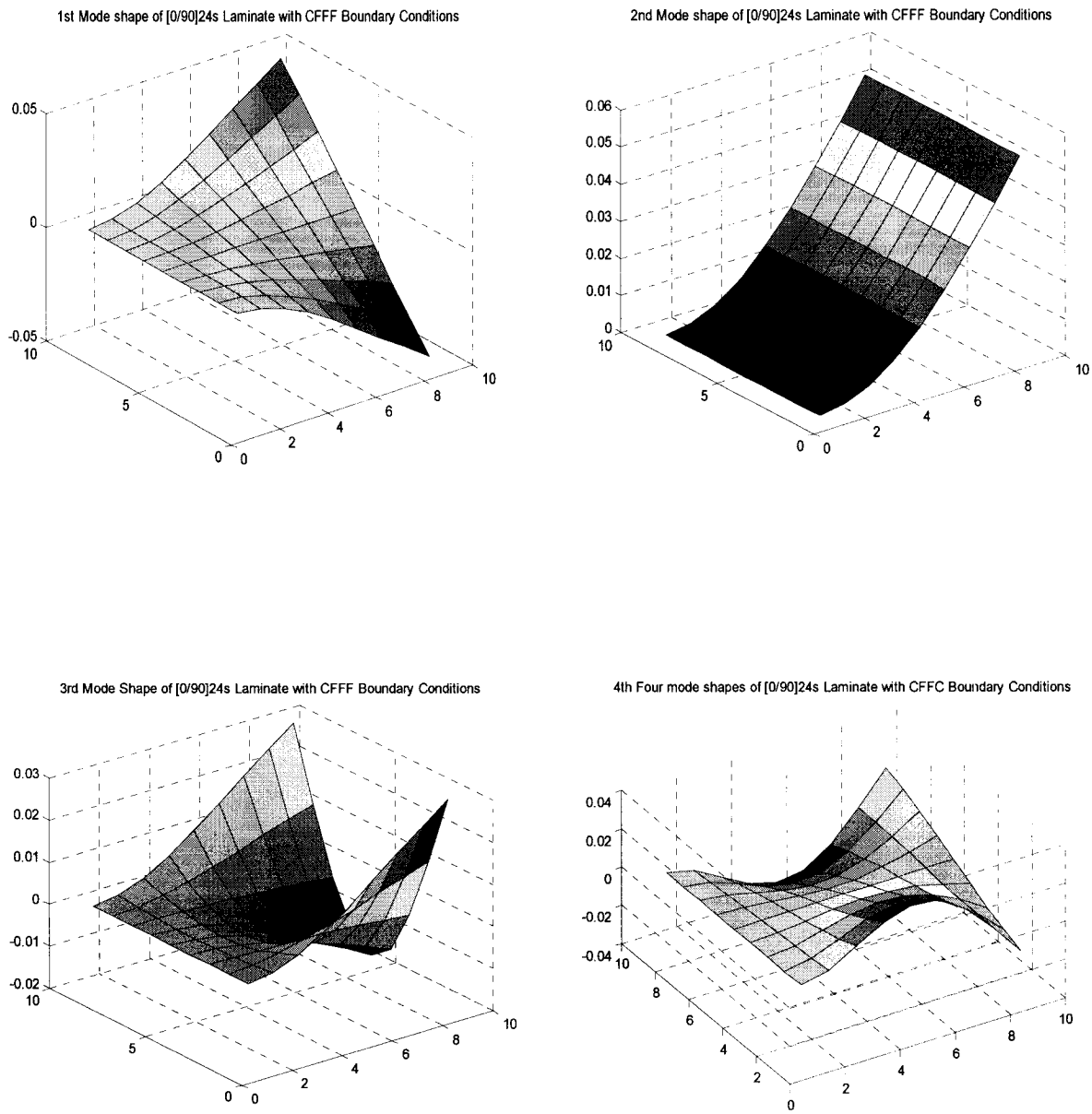

Figure 4.9.3 First four mode shapes of $[0/90]_{24s}$ laminate with CFFC boundary conditions

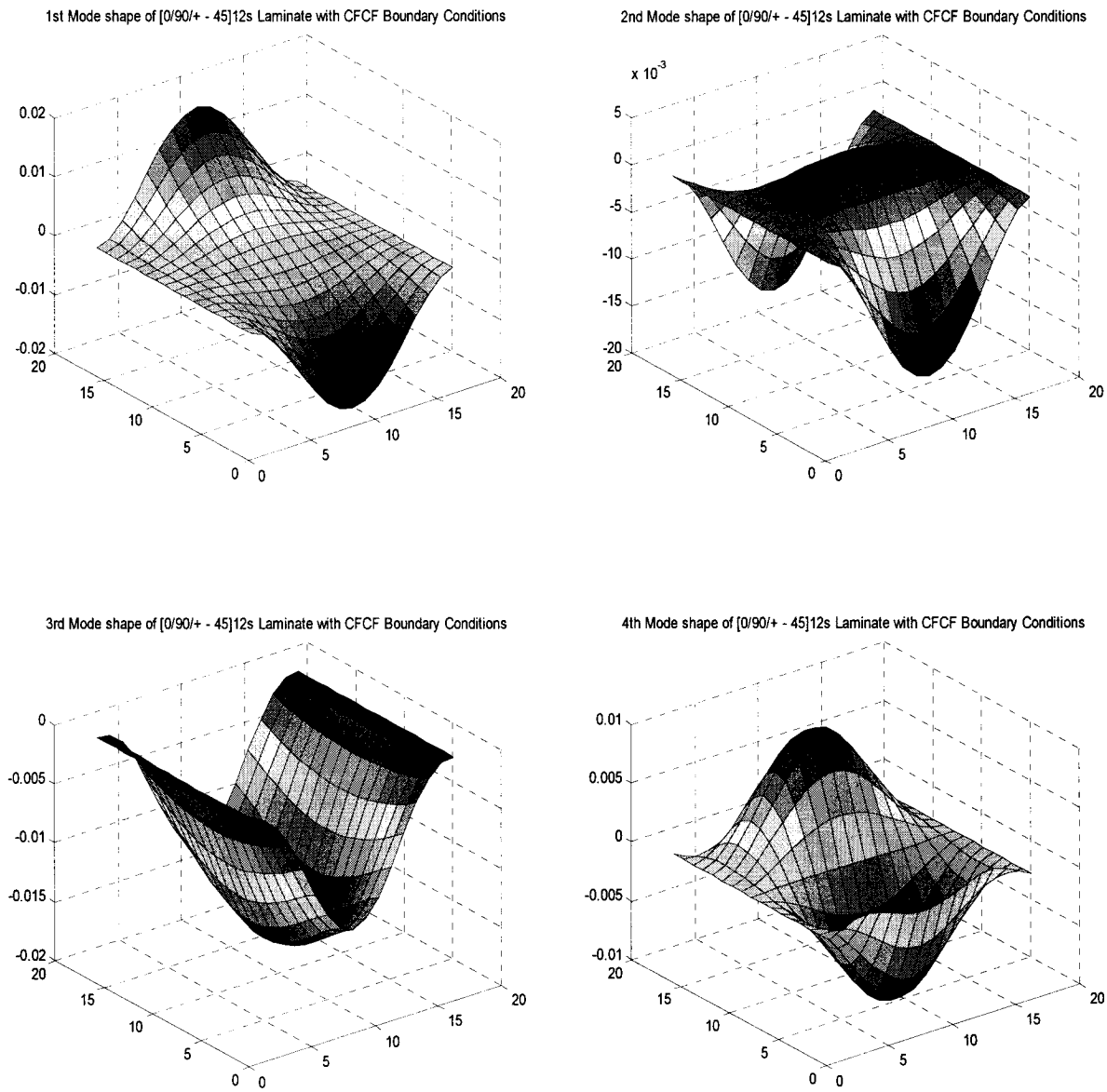

Figure 4.10.1 First four mode shapes of $[0/90/\pm 45]_{12s}$ laminate with CFCF boundary conditions

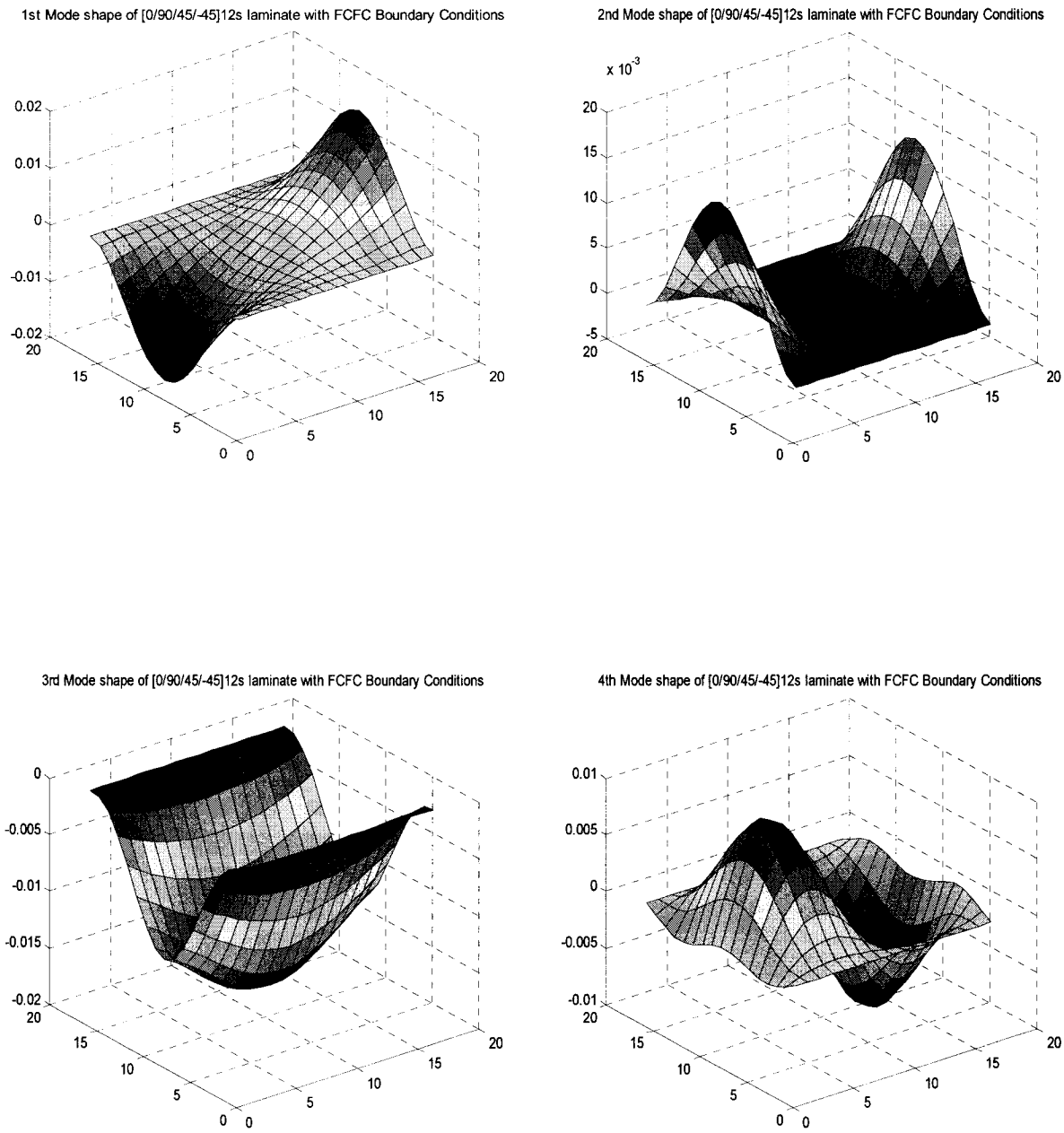

Figure 4.10.2 First four mode shapes of $[0/90/\pm 45]_{12s}$ laminate with FCFC boundary conditions

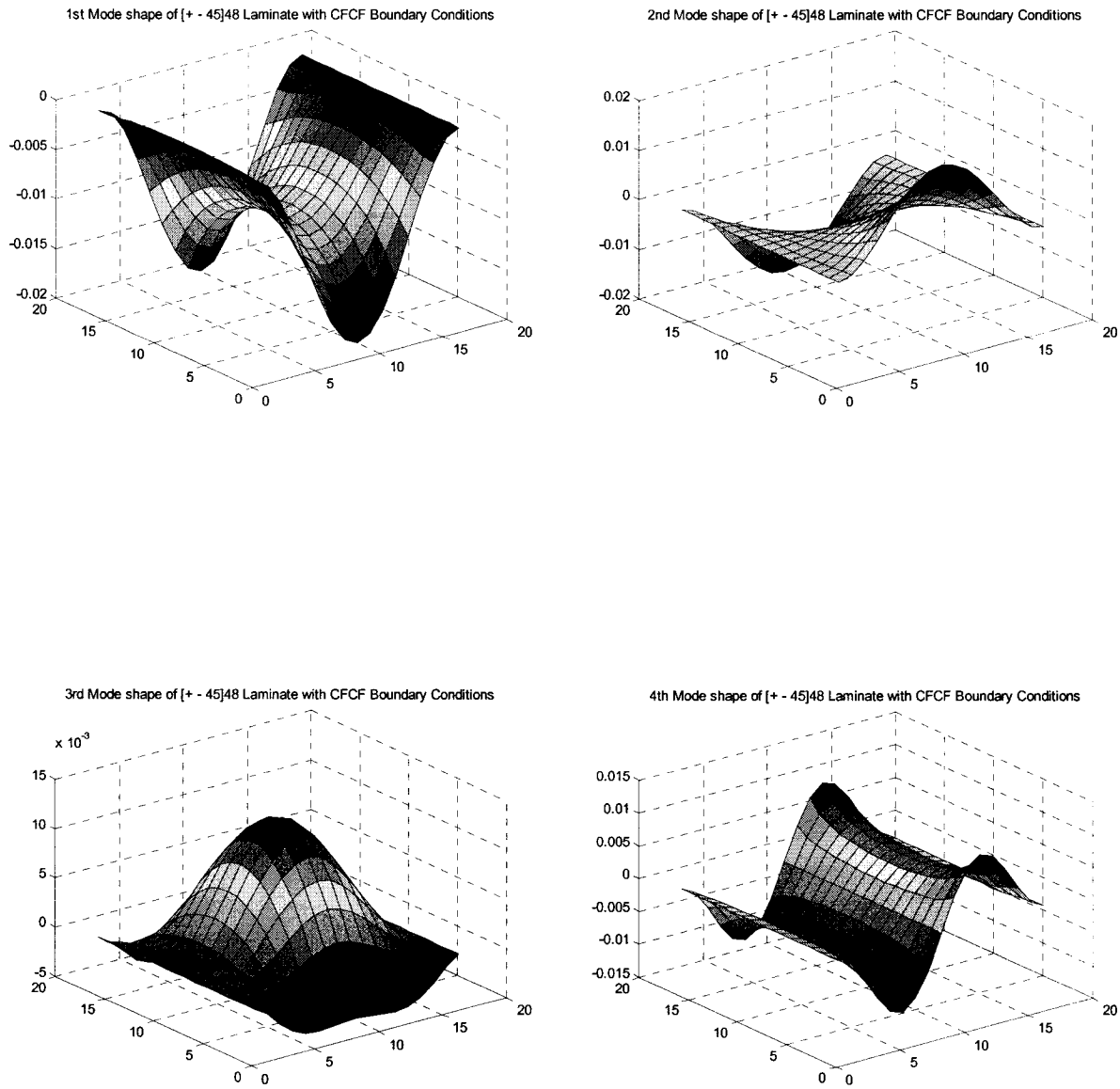

Figure 4.11.1 First four mode shapes of $[\pm 45]_{48}$ laminate with CFCF boundary conditions

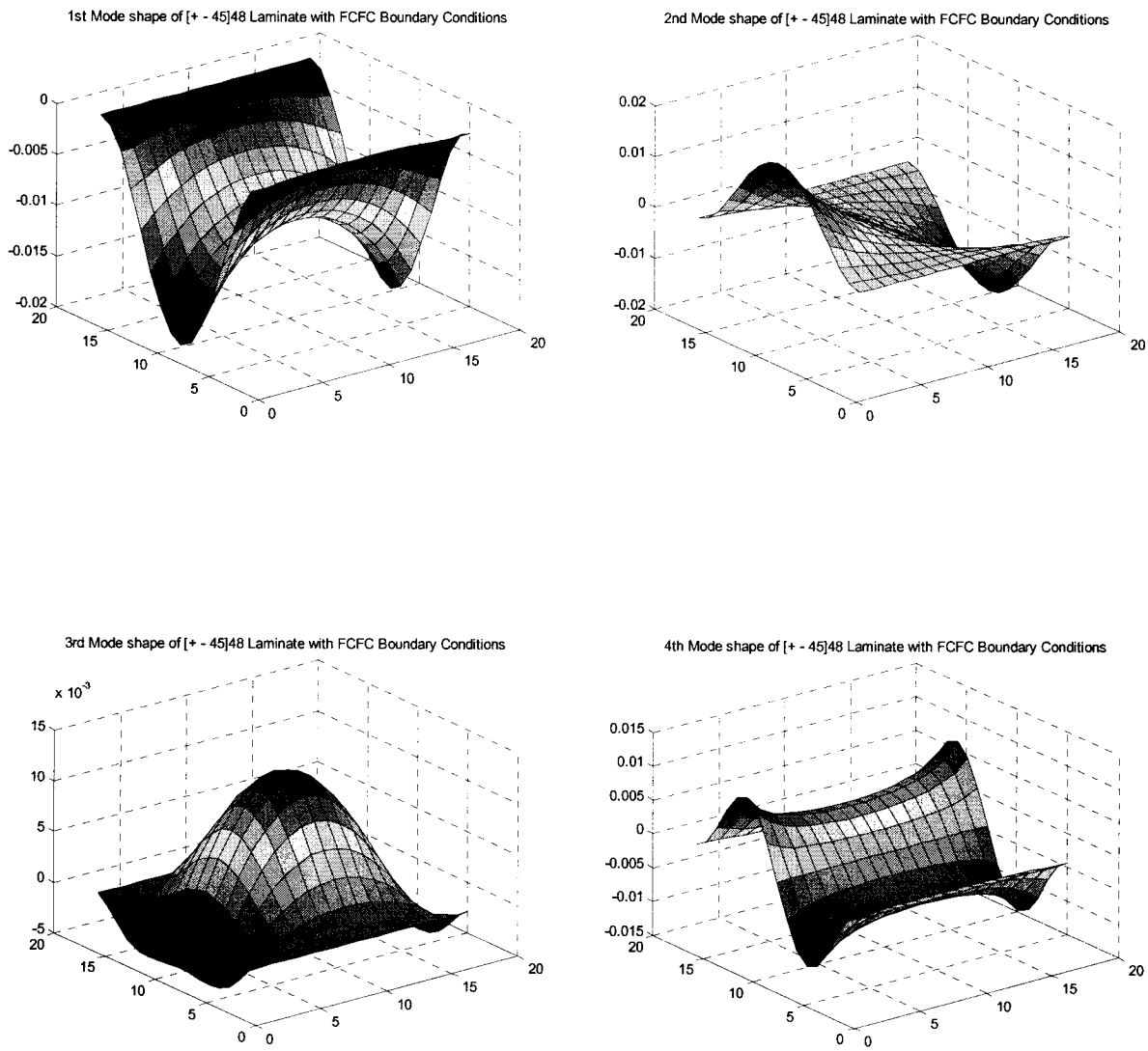

Figure 4.11.2 First Four mode shapes of $[\pm 45]_{48}$ Laminate with FCFC Boundary Conditions

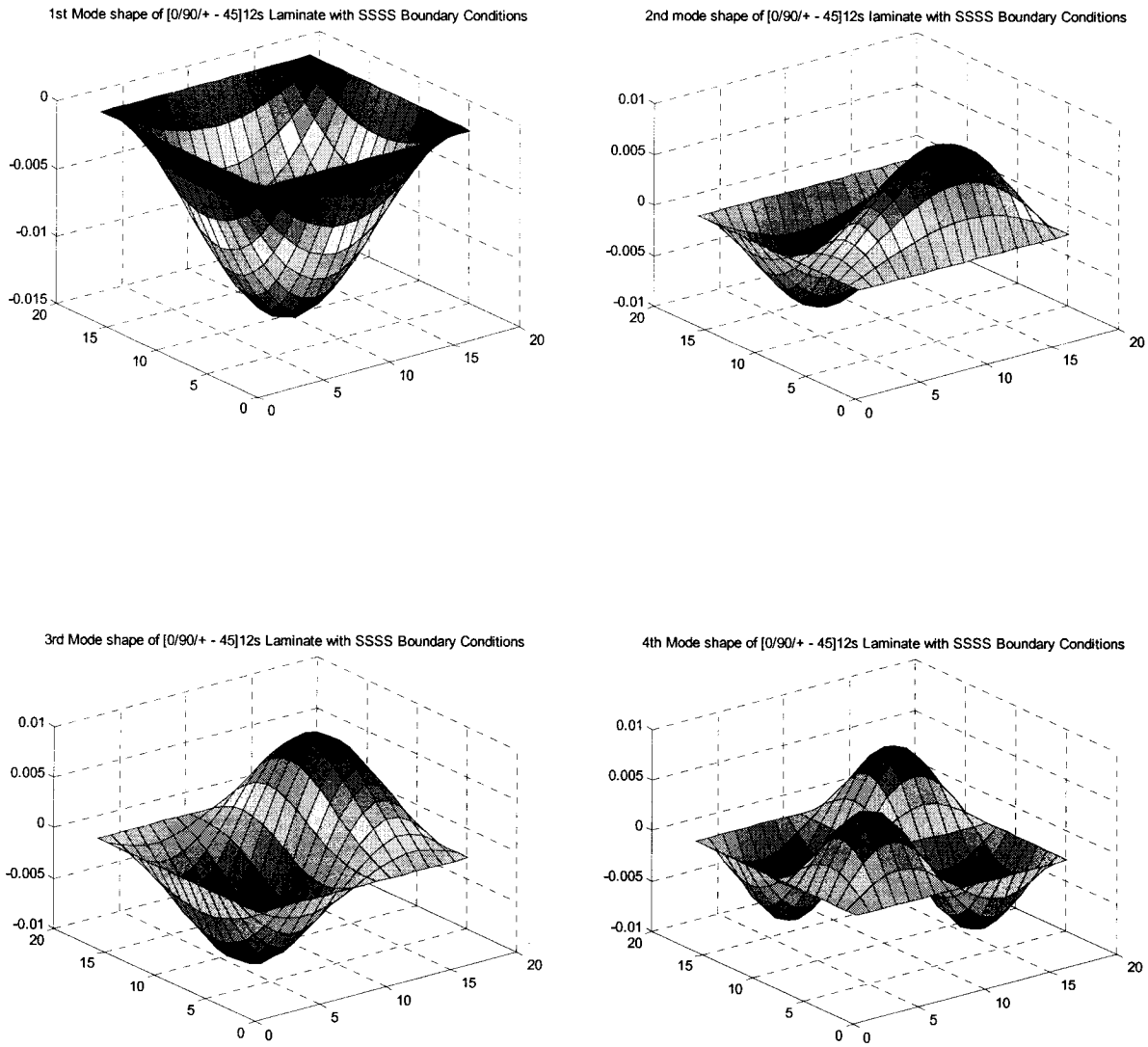

Figure 4.12.1 First four mode shapes of $[0/90/\pm 45]_{12s}$ laminate with SSSS boundary conditions

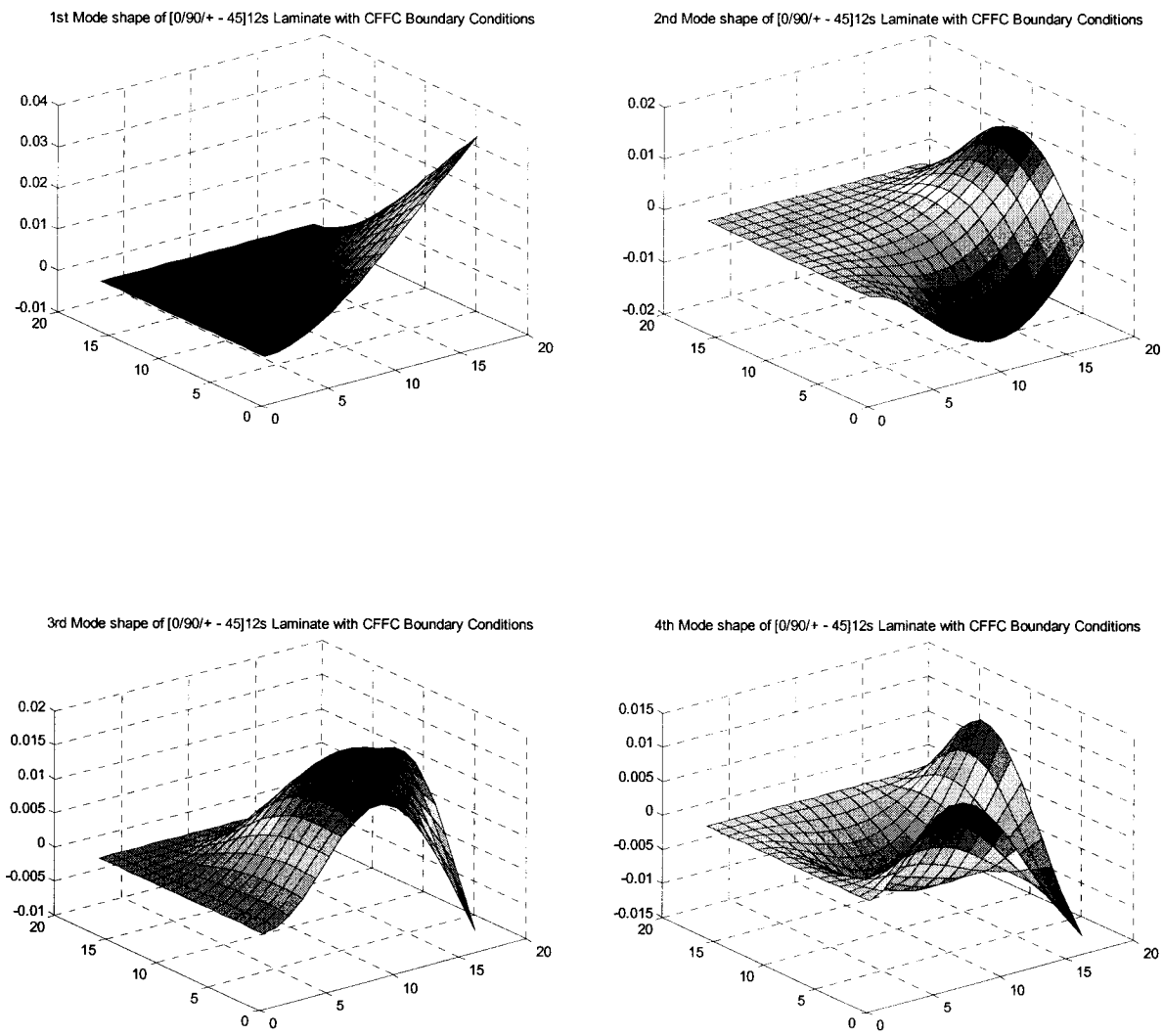

Figure 4.12.2 First four mode shapes of $[0/90/\pm 45]_{12s}$ laminate with CFFC boundary conditions

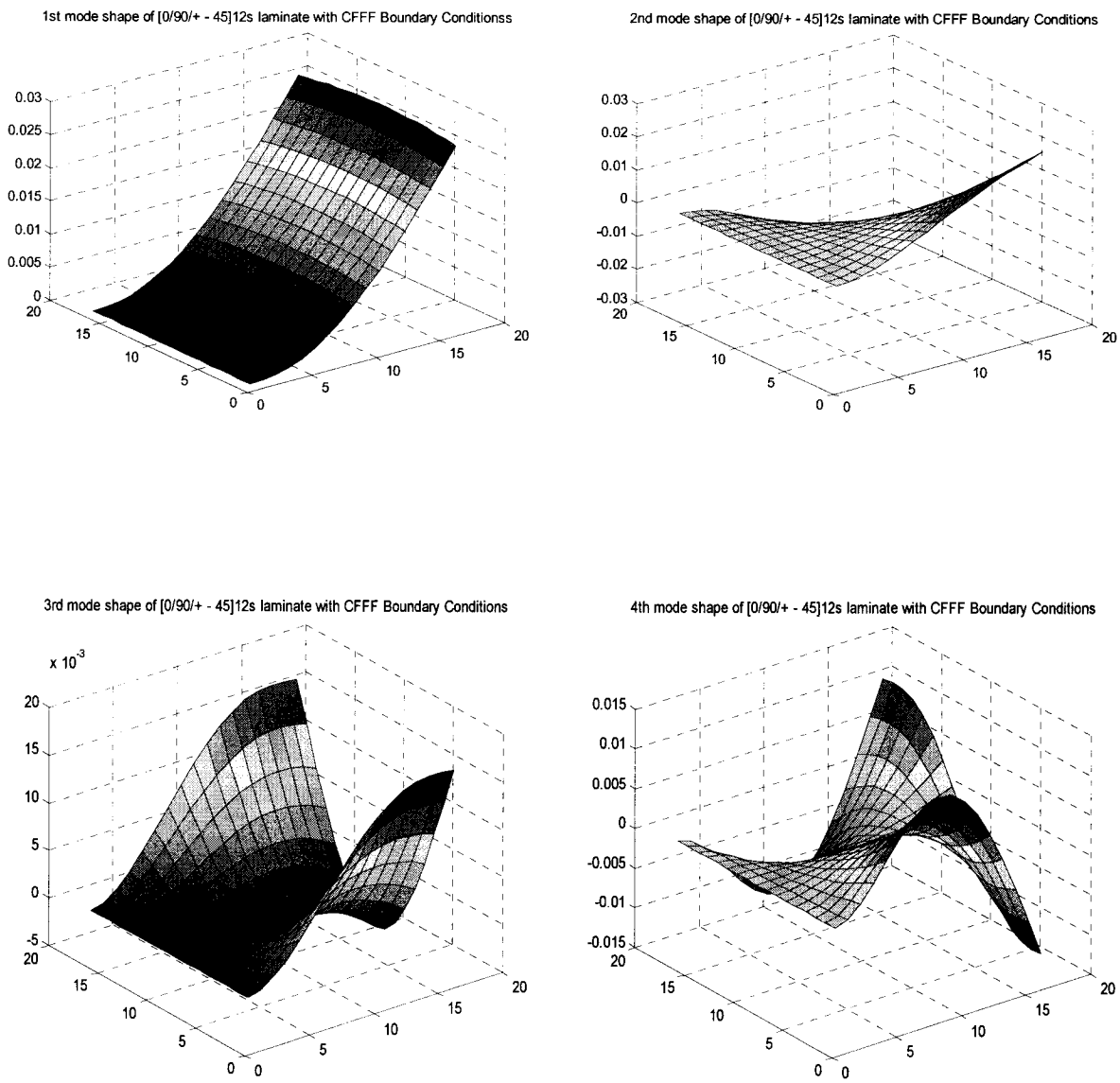

Figure 4.12.3 First four mode shapes of $[0/90/\pm 45]_{12s}$ laminate with CFFF boundary conditions

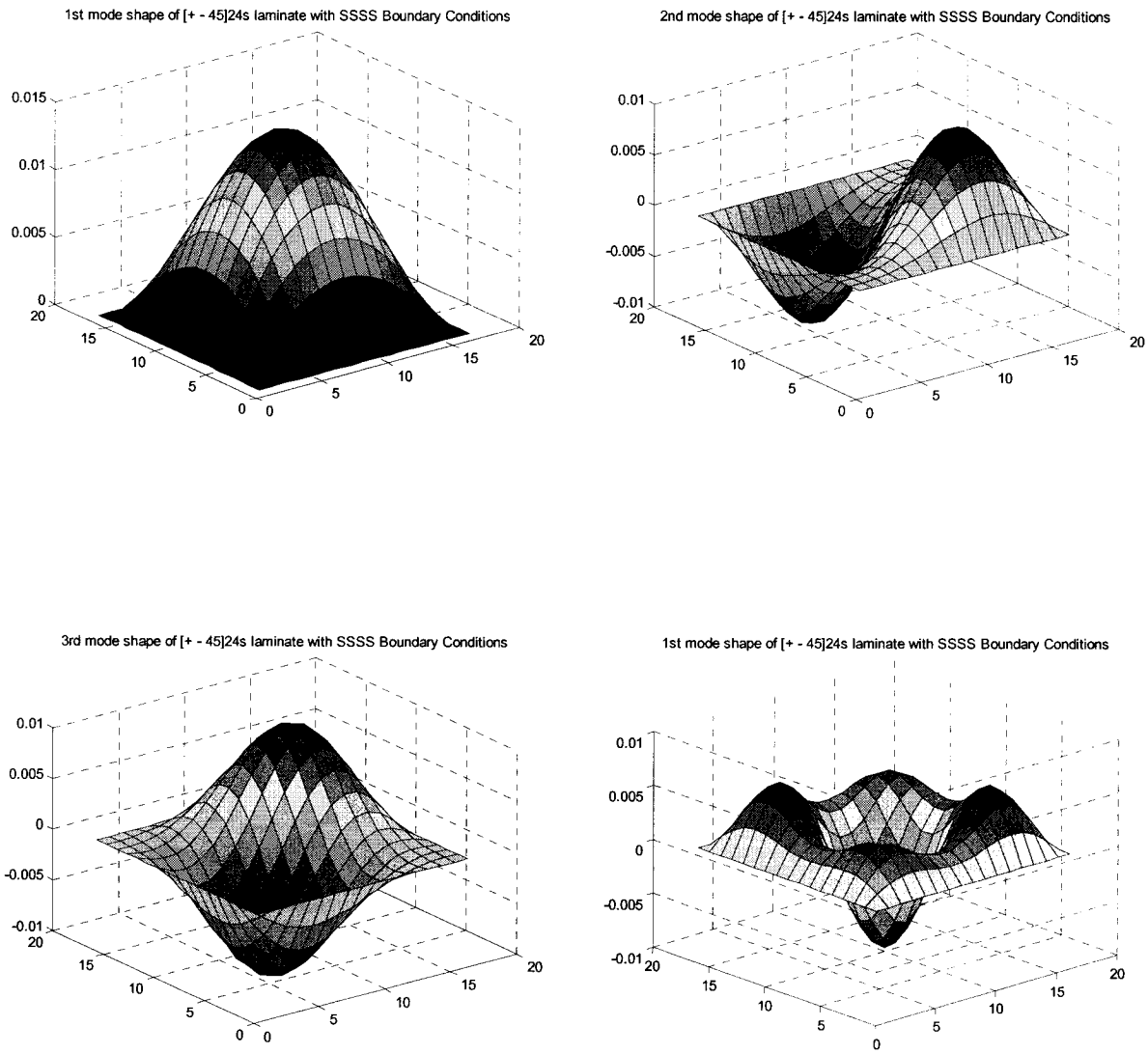

Figure 4.13.1 First four mode shape of $[\pm 45]_{24s}$ laminate with SSSS boundary conditions

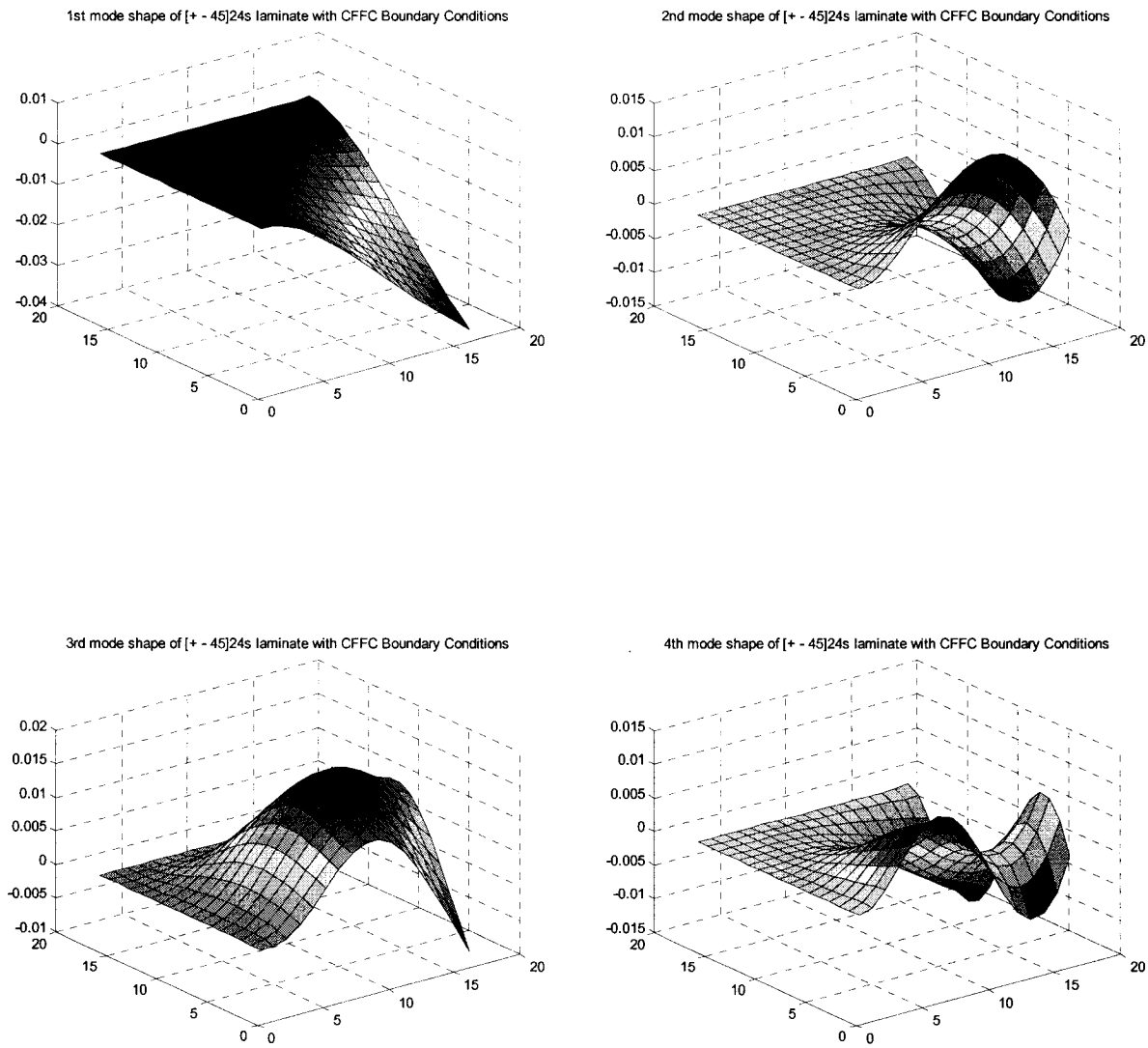

Figure 4.13.2 First four mode shape of $[\pm 45]_{24s}$ laminate with CFFC boundary conditions

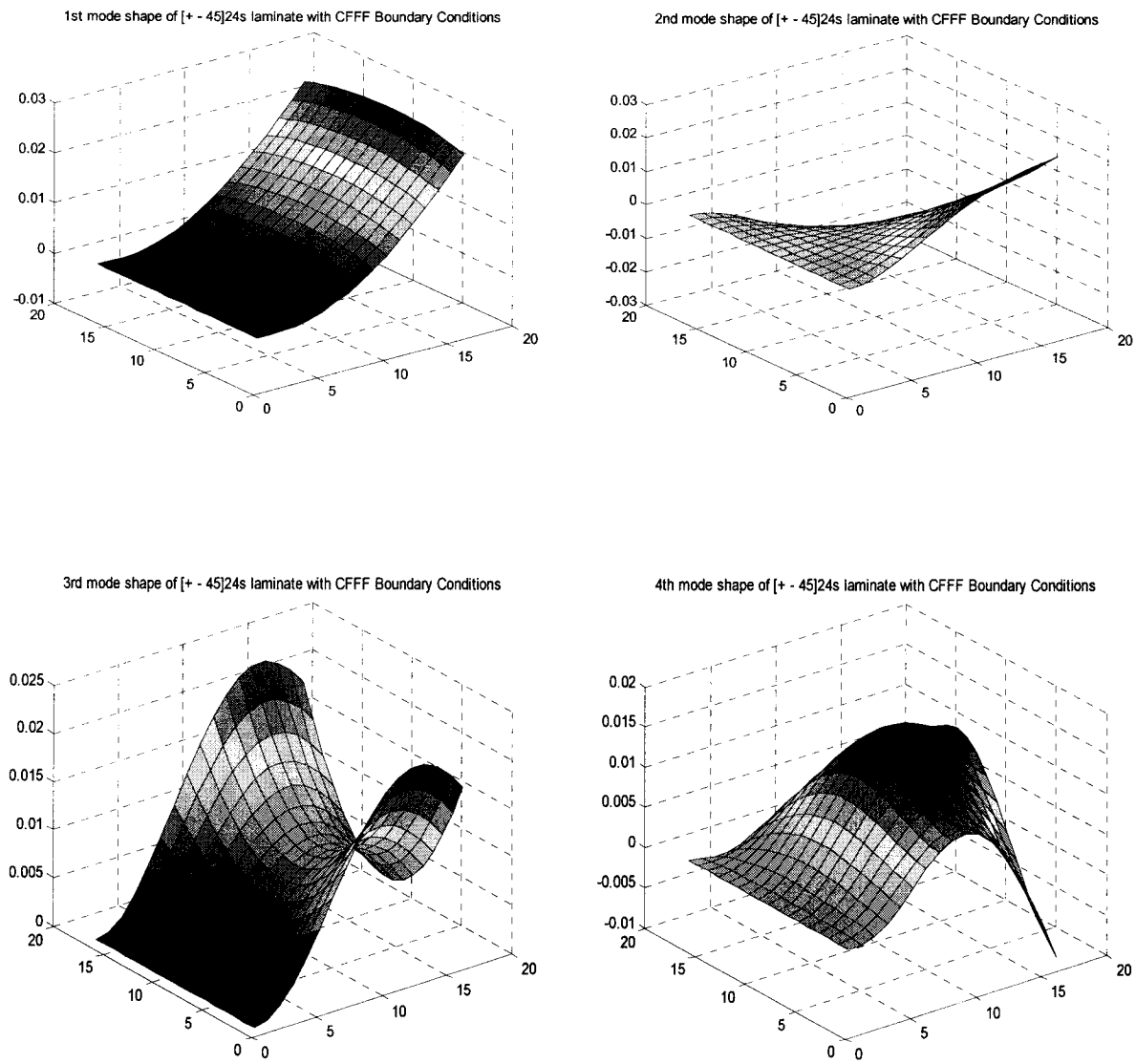

Figure 4.13.3 First four mode shapes of $[\pm 45]_{24s}$ laminate with CFFF boundary conditions

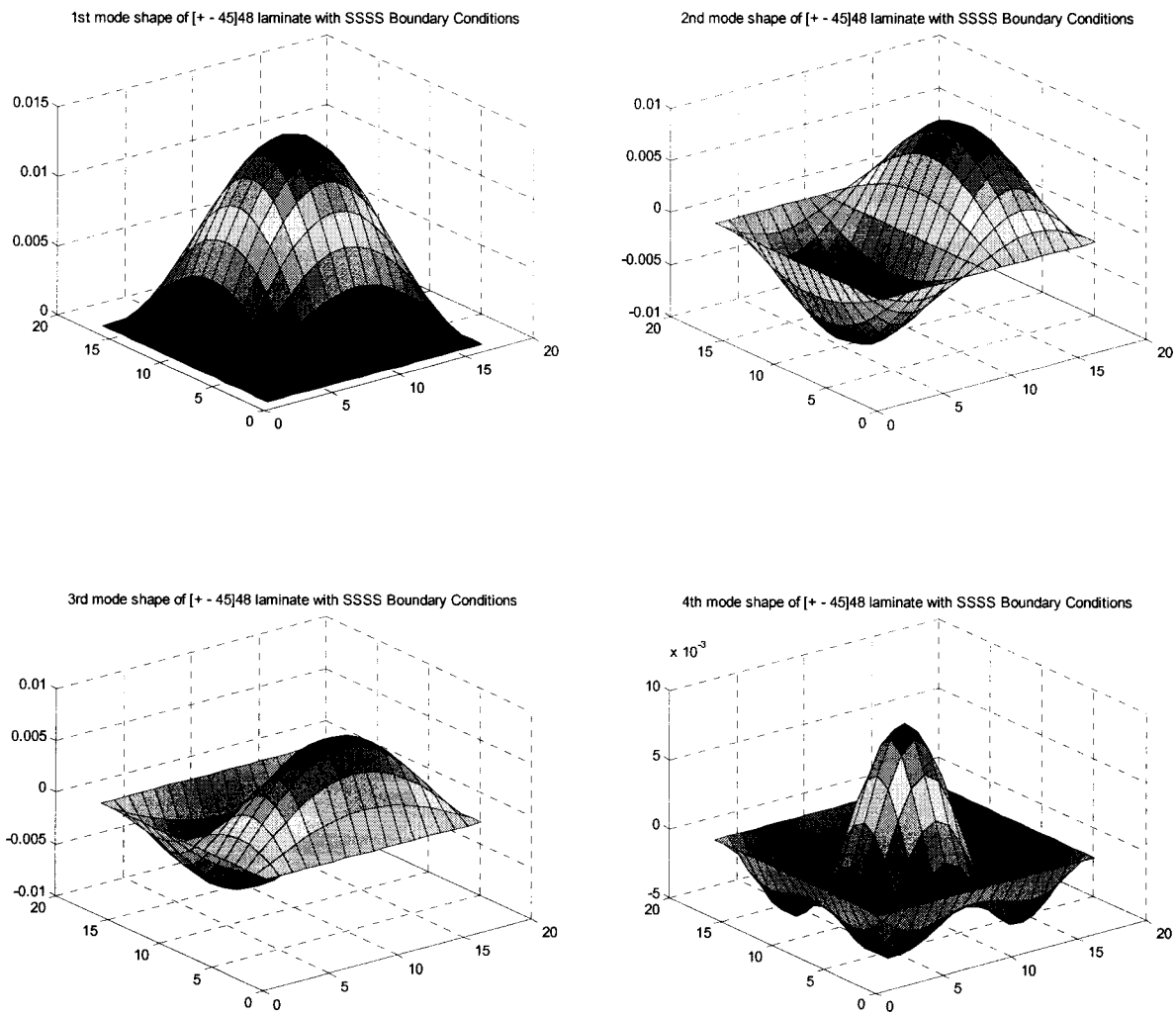

Figure 4.14.1 First four mode shapes of $[\pm 45]_{48}$ laminate with SSSS boundary conditions

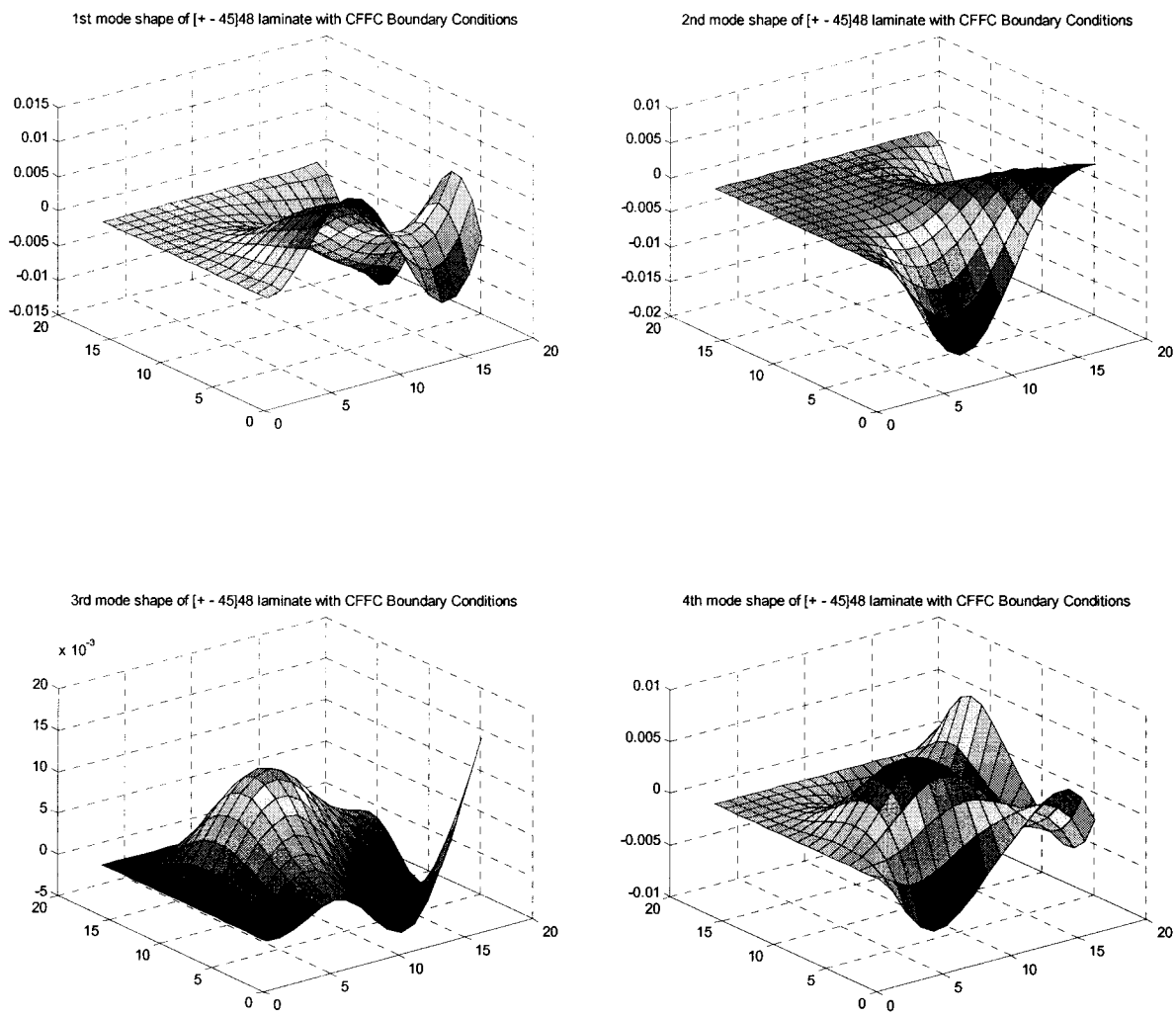

Figure 4.14.2 First four mode shapes of $[\pm 45]_{48}$ laminate with CFFC boundary conditions

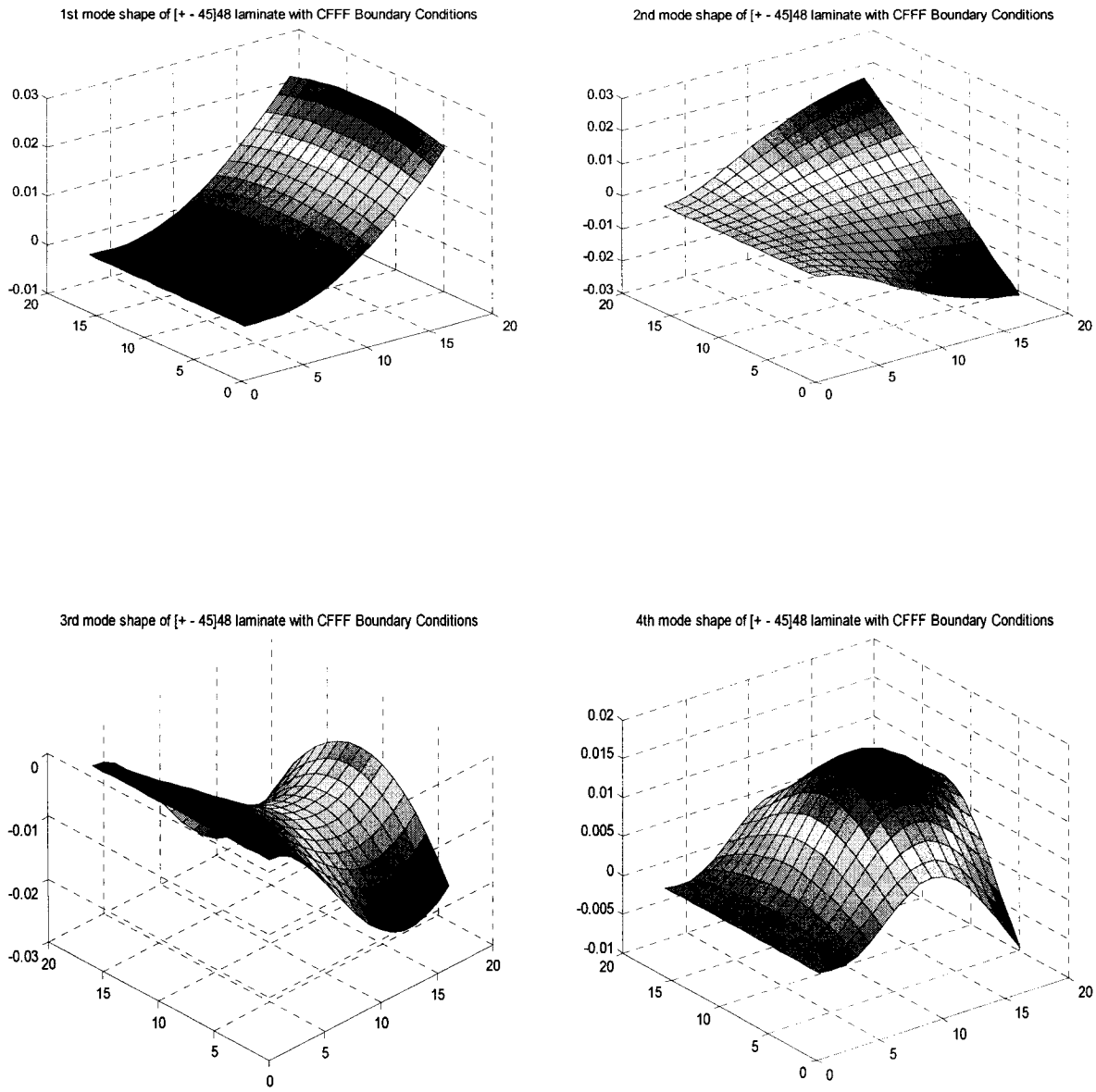

Figure 4.14.3 First four mode shapes of $[\pm 45]_{48}$ laminate with CFFF boundary conditions

Mode	Aspect Ratio				
	R=0.25	R=0.5	R=1	R=2	R=4
1	1183.304	1182.186	908.920	1156.794	1157.983
2	1216.473	1326.976	925.980	1327.154	1185.750
3	1216.568	1804.598	1203.932	1833.204	1202.631
4	1368.822	2394.942	1235.984	2344.225	1371.007

Table 4.16.1 Natural frequencies (rad/s) of $[0/90]_{24s}$ laminate under SSSS boundary conditions for different aspect ratio values

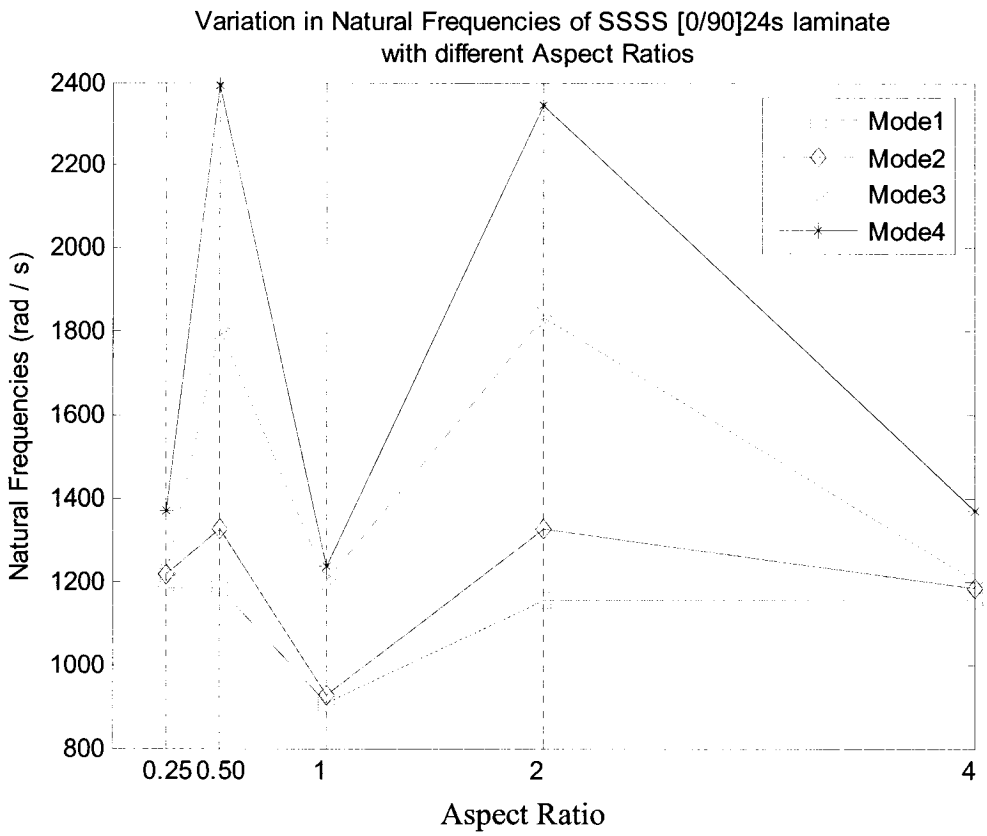

Figure 4.16.1 Variation of natural frequencies (rad/s) of $[0/90]_{24s}$ laminate under SSSS boundary conditions for different aspect ratio values

Mode	Aspect Ratio				
	R=0.25	R=0.5	R=1	R=2	R=4
1	1133.651	1220.175	956.857	1207.001	1116.332
2	1221.200	1537.657	1141.121	1536.899	1207.894
3	1365.990	1990.699	1152.725	2003.449	1358.548
4	1569.371	2302.848	1186.488	2267.983	1568.964

Table 4.17.1 Natural frequencies (rad/s) of $[0/90/\pm 45]_{12s}$ laminate under SSSS boundary conditions for different aspect ratio values

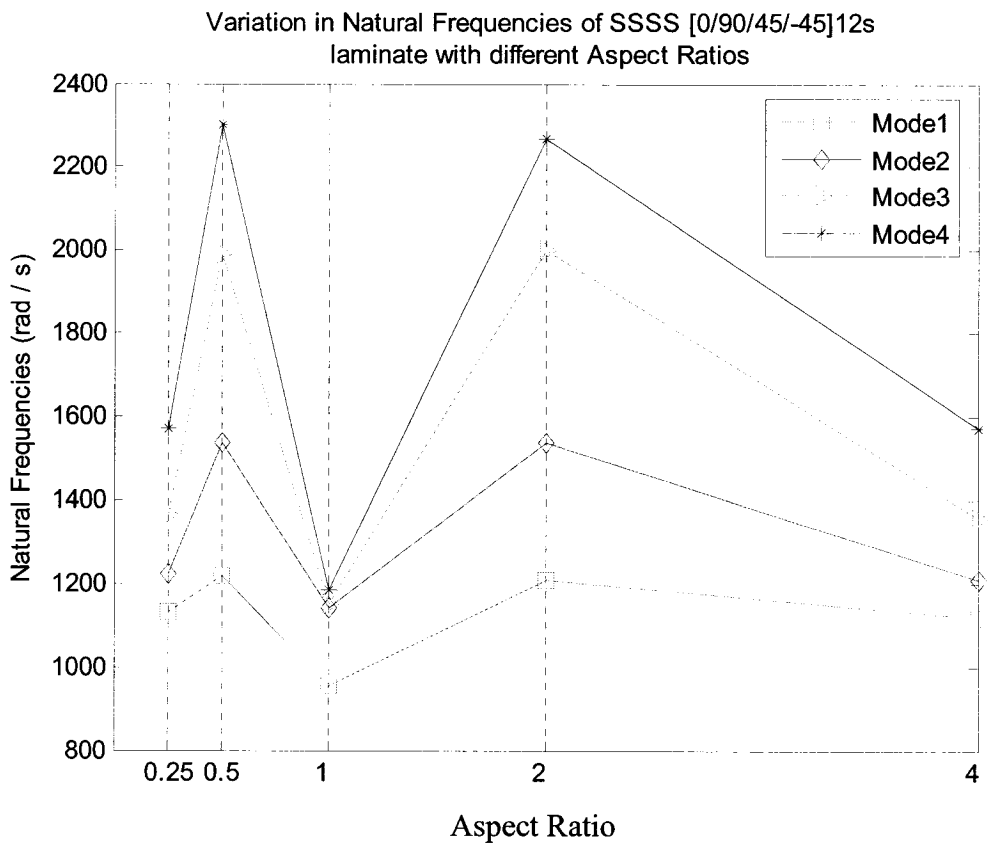

Figure 4.17.1 Variation of natural frequencies (rad/s) of $[0/90/\pm 45]_{12s}$ laminate under SSSS boundary conditions for different aspect ratio values

Mode	Aspect Ratio				
	R=0.25	R=0.5	R=1	R=2	R=4
1	1031.467	1261.084	450.746	1259.883	1030.906
2	1262.092	1745.135	1113.572	1742.710	1260.386
3	1517.116	2094.766	1207.779	2093.931	1514.186
4	1768.484	2179.095	1213.406	2175.990	1764.321

Table 4.18.1 Natural frequencies (rad/s) of $[\pm 45]_{24s}$ laminate under SSSS boundary conditions for different aspect ratio values

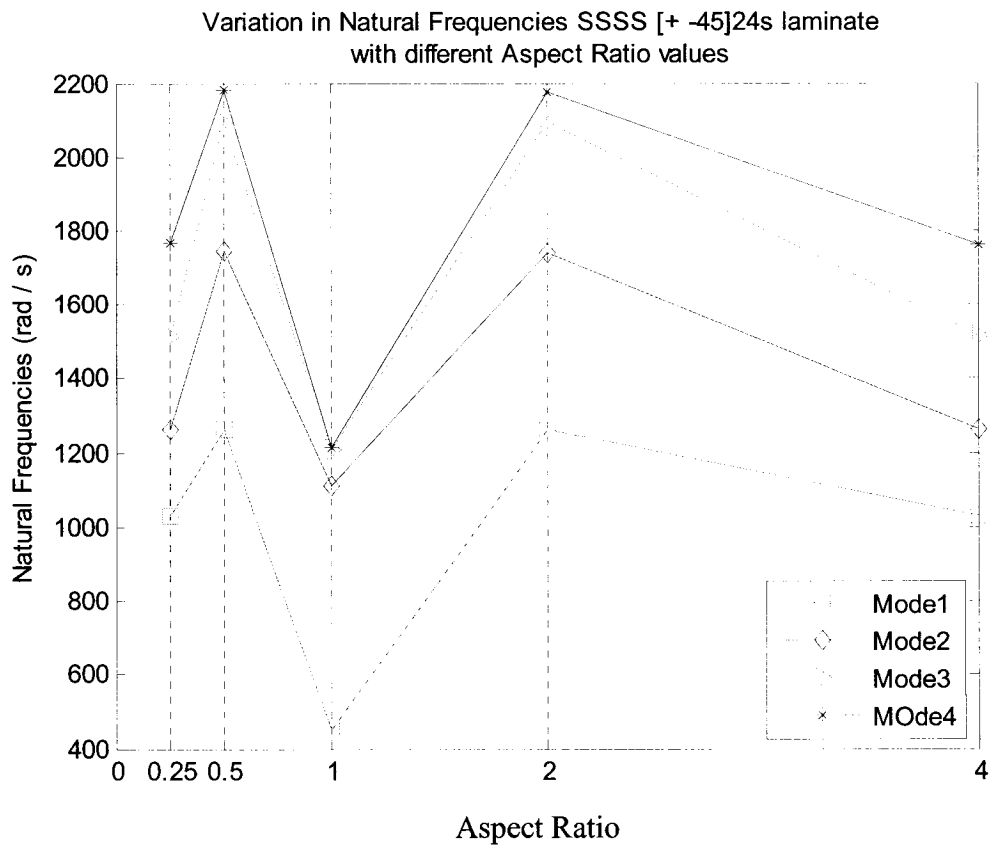

Figure 4.18.1 Variation of natural frequencies (rad/s) of $[\pm 45]_{24s}$ laminate under SSSS boundary conditions for different aspect ratio values

Appendix-III

The Comparison of times the MATLAB program takes for Hierarchical FEM and Conventional FEM.

The comparison of times is done by considering a 96 ply symmetric cross-ply rectangular laminate $[0/90]_{24s}$ of dimensions 0.55 by 0.55 meters with all sides fully clamped (CCCC). The material used is NCT-301 graphite/epoxy.

In the MATLAB program for Hierarchical FEA in which the hierarchical shape functions are determined, the symbolic variables and hence the symbolic integration were used. The symbolic calculations consume the majority of the program execution time. So the shape functions and their derivatives are calculated for 1 element with 36 hierarchical shape functions in a separate sub-routine and are used in the main program. This avoids the need to use symbolic variables and hence the symbolic integration for this particular case. In this specific case, the time taken by Hierarchical FEM with 1 element and 36 shape functions with 4 hierarchical shape functions in each of the x and y directions is compared with that of the conventional FEM, using a mesh of 100 elements.

Static Analysis: Comparison is done for the bending analysis of the above laminate subjected to 1KPa uniform surface load. The program is run five times for each method and average of the times taken is compared as given in Table 4.19.1.

Trial number for the MATLAB program execution	Time taken by Conventional FEM using 100 elements and 2205 degrees of freedom	Time taken by HFEM using 1 element and 180 degrees of freedom
1st	18.1169 s	0.7483s
2nd	17.9760s	0.6958s
3rd	17.9601s	0.6459s
4th	17.9875s	0.6489s
5th	17.9608s	0.7212s
Average	**18.0002s**	**0.6920s**

Table 4.19.1 Comparison of times the MATLAB program takes for HFEM and Conventional FEM for static analysis of $[0/90]_{24s}$ laminate under CCCC boundary conditions subjected to 1KPa uniform surface load

Modal Analysis: Comparison is done for the modal analysis of the above laminate. The program is run five times for each method and average of the times taken is compared as given in Table 4.19.2.

Trial number for the MATLAB program execution	Time taken by Conventional FEM using 100 elements with 2205 degrees of freedom	Time taken by HFEM using 1 element with 180 degrees of freedom
1st	169.1434s	0.8067s
2nd	172.1939s	0.7676s
3rd	175.9138s	0.7762s
4th	174.3612s	0.7741s
5th	170.0850s	0.7784s
Average	**172.3394s**	**0.7806s**

Table 4.19.2 Comparison of times the MATLAB program takes for HFEM and Conventional FEM for modal analysis of $[0/90]_{24s}$ laminate under CCCC boundary conditions.